PERMANENT MAGNET ASSISTED SYNCHRONOUS RELUCTANCE MACHINE (PMA-SYNRM) DESIGN AND PERFORMANCE ANALYSIS FOR FAN AND PUMP APPLICATIONS

A Dissertation

by

ROBERT VARTANIAN

Submitted to the Office of Graduate and Professional Studies of
Texas A&M University
in partial fulfillment of the requirements for the degree of

DOCTOR OF PHILOSOPHY

Chair of Committee,	Hamid A. Toliyat
Committee Members,	Prasad Enjeti
	Shankar P. Bhattacharyya
	Won-Jong Kim
Head of Department,	Chanan Singh

August 2014

Major Subject: Electrical Engineering

ABSTRACT

One of the major industrial applications of electric machines is driving fans and pumps. According to the pump and fan affinity laws, decreasing the speed of the load can reduce the power consumption on the load significantly. Therefore, a variable speed drive offers reduction in energy consumption of the induction motor driving those types of loads. As an alternative, synchronous machines can be used for this application to get the benefit of higher efficiency. In this work, the performance of an optimized permanent magnet assisted synchronous reluctance machine (PMa-SynRM) with a NEMA standard stator has been studied for fan and pump applications. The effect of using different quantities of the permanent magnet in this machine is studied experimentally. In addition, the performance of the PMa-SynRM is compared with a standard general purpose induction machine for the same loading condition. This work presents the comparison of the energy consumption and performance of the machines under the fan and pump type loads operating on specific typical duty cycles.

ACKNOWLEDGEMENTS

I would like to thank my advisor, Prof. Hamid A. Toliyat. His enthusiasm for electric machine design and control convinced me to pursue my doctorate, and his guidance over my graduate career has helped me to complete this dissertation and gain invaluable knowledge and skills.

My sincere gratitude also goes to the members of my graduate study committee: Prof. Prasad Enjeti, Prof. Shankar Bhattacharyya, and Prof. Wong Jon Kim for their valuable advice and help through the years I spent at Texas A&M University. Also I thank Prof. Datta for attending my final exam and dissertation presentation.

I would like to acknowledge the Department of Electrical and Computer Engineering at Texas A&M University for providing an excellent academic environment. Special thanks go to Ms. Tammy Carda, Ms. Jeanie Marshall, Ms. Janice Allen, Ms. Anni Brunker, Ms. Claudia Samford, Mr. Henry Gongora, Mr. Wayne Matous, Ms. Eugenia Costea, Ms. Linda Currin, Ms. Gayle Travis, Prof. Scott Miller, and Prof. Krishna Narayanan for all their efforts.

Finally, thanks to my family for their encouragement and support.

NOMENCLATURE

B_m	Amplitude of the AC flux density component
E_{pm}	Peak phase voltage induced in the stator winding
f	frequency
i_a, i_b	Phase A and B currents
i_d, i_q	Currents on the rotating reference frame
i_s	Stator line current
i_α, i_β	Currents on the stationary reference frame
k_c	Eddy-current core loss coefficient
k_e	Excess core loss coefficient
k_h	Hysteresis core loss coefficient
L_d	d-axis static inductance
L_q	q-axis static inductance
P	differential operator
P	Number of machine pole par
P	pole pair number of the machine
R_s	Stator resistance
T_e	Electric developed torque
THD	Total Harmonic Distortion
V_d, V_q	Voltages on the rotating reference frame
V_α, V_β	Voltages on the stationary reference frame

γ	Current angle leading d-axis
δ	Voltage angle
θ_e	Rotor position at electrical angle
λ_{pm}	Magnetic flux linkage
ω_e	Angular velocity at electrical angle (rad/s)
ω_r	Angular velocity at mechanical speed (rad/s)
ω_{ref}	Reference angular velocity at mechanical angle (rad/s)

TABLE OF CONTENTS

Page

Page

Page

LIST OF FIGURES

Page

Page

Page

Page

Page

Page

Page

LIST OF TABLES

Page

Page

CHAPTER I

INTRODUCTION*

IA. Overview

According to the "United States Industrial Electric Motor Systems Market Opportunities Assessment" in 1994, about 23 percent of the electric energy sold in the United States was consumed by the industry sector, and the process motor system energy accounts for about 63 percent of consumed electric energy in industry [1]. The same research indicates that about 30 percent of the motors in the industry are used for fan and pump drive and those account for about 40 percent of energy consumption in industry. Fig. 1-1 shows the distribution of the motors in industry and energy consumption estimation based on [1]. In the majority of these applications to control the process, flow control is required. In fan and pump applications, the flow control can be done by typical forms shown in Fig. 1-2. This control can be done by controlling the motor speed using Variable Frequency Drives (VFDs). VFDs are used in order to adjust speed to meet the speed requirement in some applications or reduce energy consumption in others [2, 3].

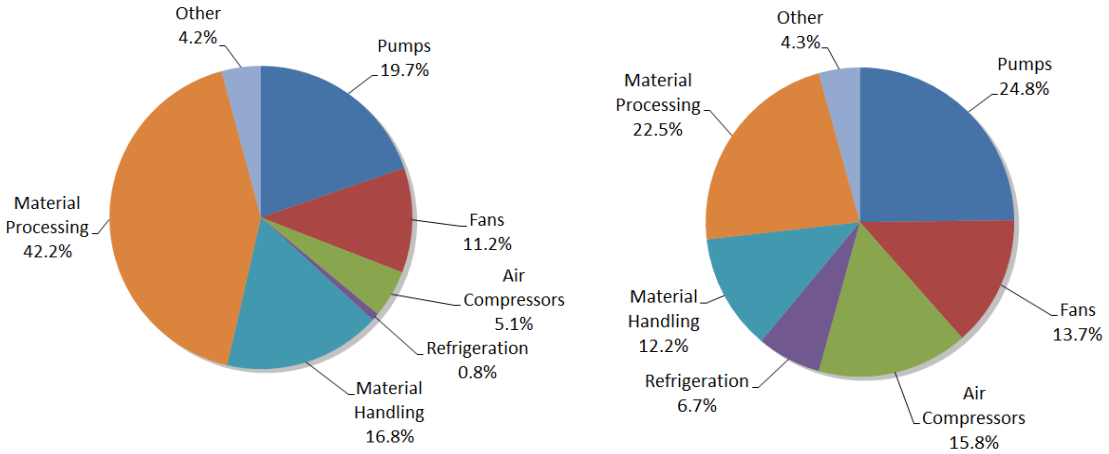

(a) (b)

Fig 1-1: Distribution of motors in industry by: (a) population and (b) energy system.

Using variable speed control in motor drive system with fan and pump type load has some advantages such as controlled and soft start with less current and disturbances on the power source, less mechanical stress on the motor and mechanical weariness of piping, higher reliability and energy efficiency on motor drive systems, and accurate process control based on the load demand [4].

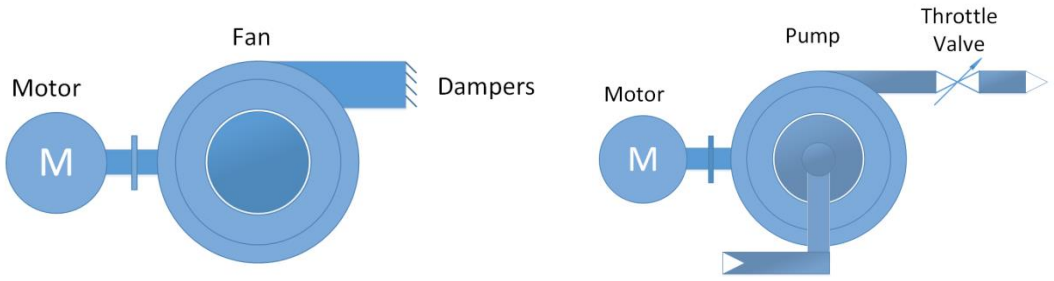

(a) (b)

Fig 1-2: Flow control in: (a) Fan application using dampers, (b) Pump application using throttle valve.

Fans and pumps Affinity law shows that the flow is proportional to the speed by.(1-1) and the torque is proportional to the square of the speed expressed by (1-2). Also, the power demand of the load is proportional to the cube of the shaft speed according to (1-3) [2, 3].

$$\frac{Q_1}{Q_2} = \left(\frac{N_1}{N_2}\right) \tag{1-1}$$

$$\frac{T_1}{T_2} = \left(\frac{N_1}{N_2}\right)^2 \tag{1-2}$$

$$\frac{P_1}{P_2} = \left(\frac{N_1}{N_2}\right)^3 \tag{1-3}$$

Fig. 1-3 shows the relationship between the physical quantities of the load versus speed. It can be seen that the reduction of the speed to the half of the full speed results in 87.5% reduction in the power while the flow rate is reduced only by 50%. This means the reduction of the speed in fan and pump has a significant effect on the energy consumption of the machine.

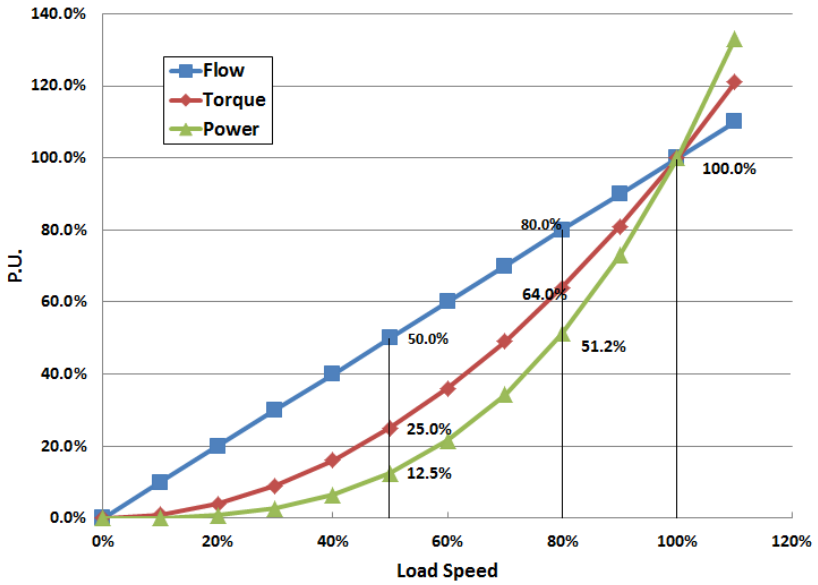

Fig 1-3: Effect of load speed on flow, torque, and power of the centrifugal fan and pump.

On the other hand, in the lifetime of the fan and pump energy system the energy cost accounts for up to 90% of the cost. This means using energy efficient machine to drive the load can save significant energy and cost. Fig. 1-4 illustrates the share cost of the system.

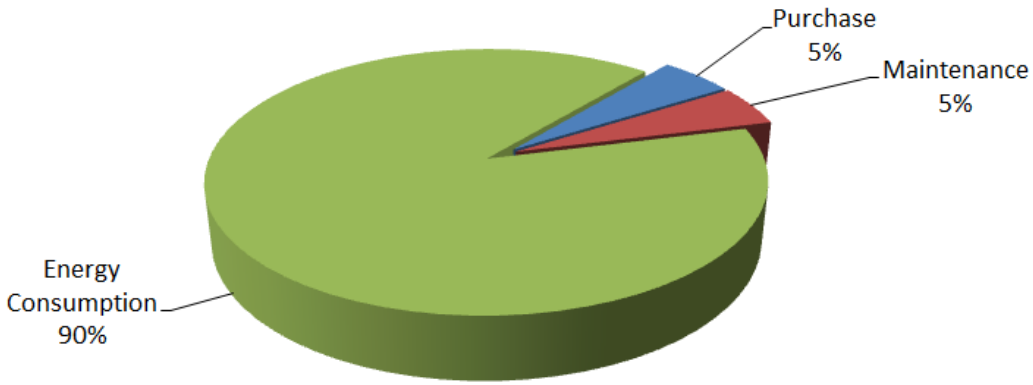

Fig 1-4: Typical life cost of a pump driven by electric motor [5]

IB. Fan and Pump Drivers

Induction machines are common type electric machines widely used to drive fan and pumps loads. However, induction machines show low efficiency at lower speed and lighter load especially running fan and pump loads [6]. There are other solutions to decrease the machine power consumption such as using synchronous machines instead of induction machines. Fig. 1-5 shows different types of a synchronous machine.

Permanent magnet machines have high torque and power density in comparison with the induction machines but they contain a significant amount of permanent magnets. Manufacturing a less expensive electric motor with acceptable performance has become a challenge. In addition, it is desired to avoid using rare earth permanent magnets or at least reducing the amount of this type of permanent magnets in the design as much as possible. PMSMs present high torque and power density in comparison with induction machines but the quantity of the permanent magnets used in the machine is significant. Moreover, PMSMs have efficiency drop in high speed applications such as air compressors because of the exposure of the permanent magnets to the magnetic flux in the air gap [7]. IPM machines have high power factor and torque density; but the developed torque in this machine is mostly magnet torque and it utilizes less reluctance torque. Presenting a low saliency ratio (L_d/L_q) for wide speed range operation, the IPM machine needs to operate in field weakening region [8-19]. Axially laminated synchronous reluctance machine presents a high saliency ration and torque density but the fabrication process is costly due to the bending and assembling the laminations on the shaft axially[11, 20-22].

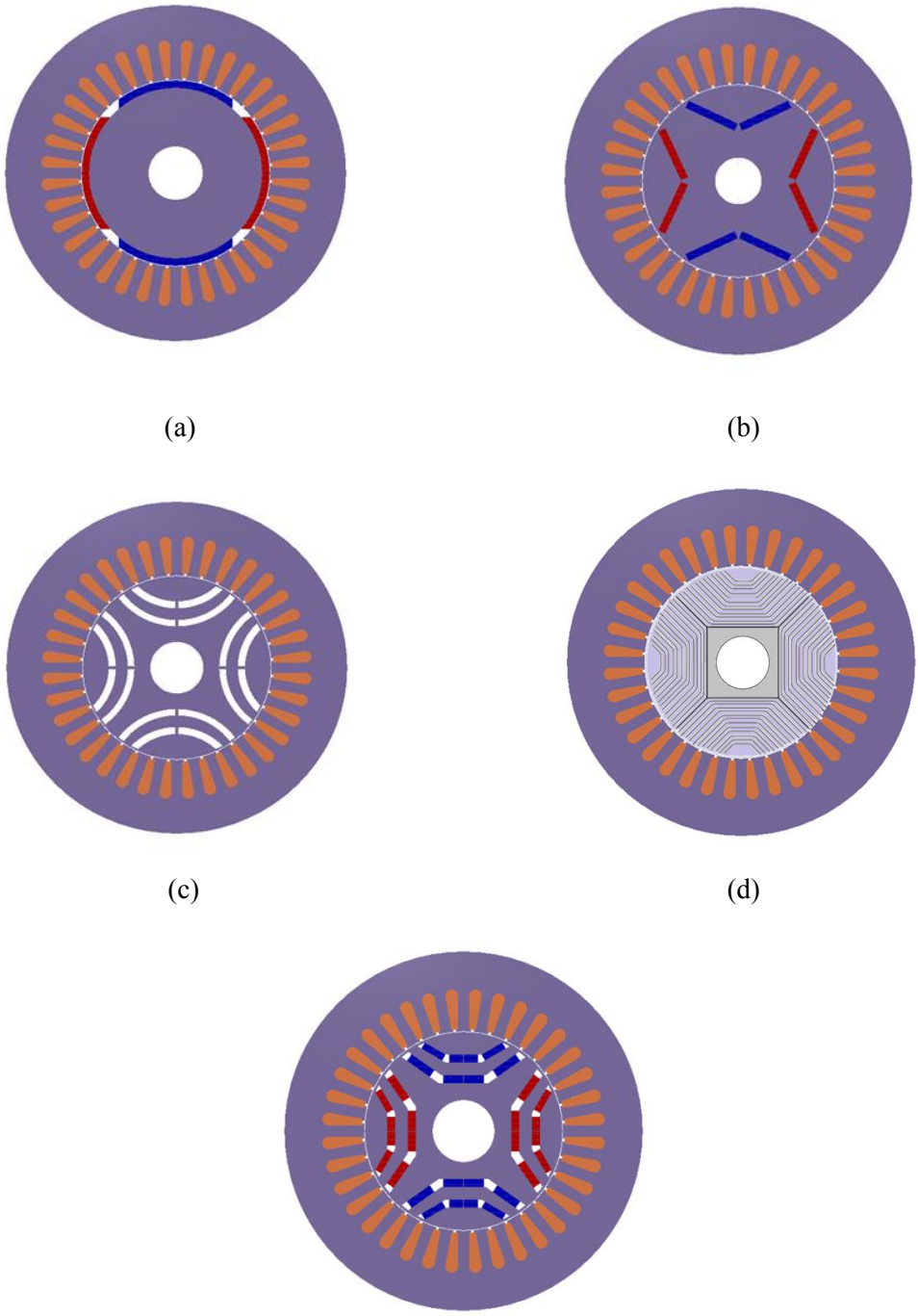

Fig 1-5: Different synchronous machines: (a) Permanent Magnet Synchronous Machine (PMSM), (b) Interior Permanent Magnet (IPM), (c) Synchronous Reluctance Machine (SynRM), (d) Axially Laminated Synchronous Reluctance Machine, (e) Permanent Magnet assisted SynRM.

IC. SynRM and PMa-SynRM

Design of the energy efficient electric machines with a reasonable cost has become a challenge. Machines with high torque density such as PMSMs and IPM are efficient but expensive. PMa-SynRM like SynRM has lower cost and rigid structure in comparison with the other PM machines and can be employed in a wide range of the applications. High performance PMa-SynRM is achievable by optimization of the magnet size and rotor geometry for a variety of applications [17, 23-32].

In this machine, the reluctance torque is the major component of the developed torque, but the type and quantity of the permanent magnets inside the rotor can change the performance of the machine by affecting the torque and power factor. The permanent magnets create the flux linkage (λ_{pm}), which contributes by generating the magnet torque and improving the torque performance of the machine. Moreover, the generated flux linkage improves the power factor resulting in a higher power factor than SynRM machine. Therefore, the quantity of the permanent magnet and its remanent flux density has an effect on the performance of the PMa-SynRM significantly.

SynRM has lower torque density and produces only reluctance torque. Because of the absence of a magnetic field source in the rotor, SynRM presents low power factor. However, it has been shown that with a high saliency ratio the power factor improves.

Fig. 1-6 shows the effect of saliency ratio on the power factor of the SynRM. This relation is expressed in (1-4). During the SynRM development, different rotor core structures have been presented. Fig. 1-7 shows some of the variations of the rotor core for a four-pole SynRM. Some of the models presented a higher saliency ratio such as

"Isolated Segmental", "Transversally Laminated", and "Axially Laminated" rotors. In SynRM increasing the torque density and power factor is possible by designing a rotor core with higher saliency ratio [20-22, 33-50]. In the same power level, a transversally laminated SynRM can be even cheaper than induction machine and more efficient because of elimination of the copper or aluminum bars from the rotor and the related energy losses. This type of machine could be a proper replacement for the induction machine but the low power factor of the machine is another problem, which has to be considered.

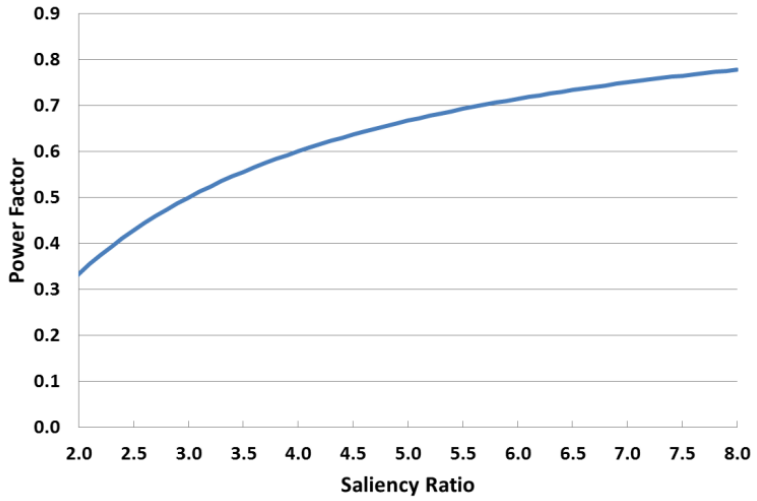

Fig 1-6: Power factor of a synchronous machine (SynRM).

$$pf = \left(\frac{L_d}{L_q} - 1\right) \Big/ \left(\frac{L_d}{L_q} + 1\right) \tag{1-4}$$

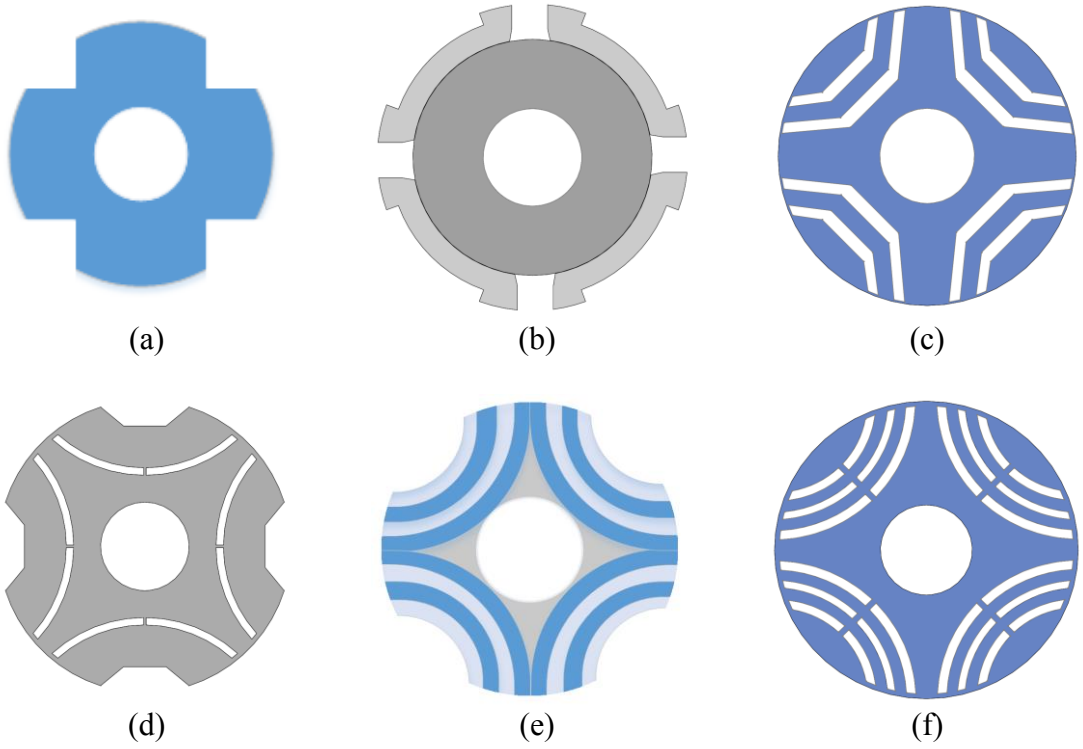

Fig 1-7: SynRM different rotors: (a) Conventional Salient Pole (b) Isolated Segmental, (c) Transversally Laminated, (d) Double Barrier, (e) Axially Laminated, (f) Modern Transversally Laminated [51].

There are some methods to increase the power factor of the SynRM, which will effectively reduce drive size of the machine and increase efficiency at the same time. Increasing the saliency ratio and/or adding permanent magnet to the rotor core with a proper design will increase the power factor and torque density of the machine (shown in Fig. 1-8). This machine, called Permanent Magnet Assisted Synchronous Reluctance Machine (PMa-SynRM), can utilize both reluctance and magnet torque and in comparison with the SynRM core results in higher power factor and torque density (based on the magnets type and quantity used in the machine)[17, 23-26, 52-54].

Some of the features of a PMa-SynRM are as following:

- Medium saliency ratio.
- Medium power factor.
- High power density by utilizing both reluctance and magnetic torque.
- Low cost.
- High reliability and robustness due to embedding magnets in rotor core.
- Less expensive construction compared to PMSM and IPM.

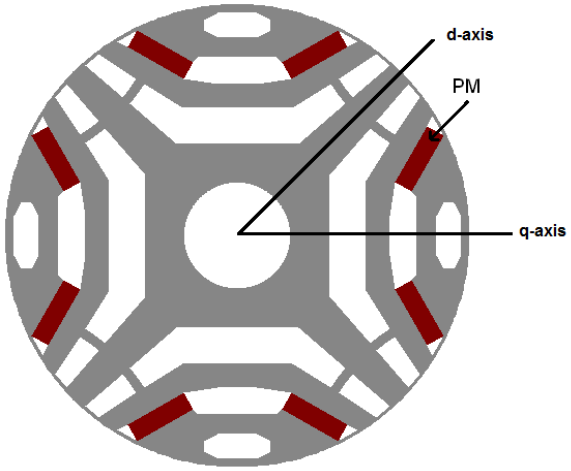

Fig 1-8: PMa-SynRM rotor core based on transversal lamination[51].

Although the reluctance torque is the major component of the developed torque in this machine, the permanent magnets inside the rotor can create additional magnet torque and improve the power factor of the machine. A low cost permanent magnet machine such as PMa-SynRM can be a proper replacement for variable speed applications such as fan

and constant speed-variable torque loads especially when an induction machine with variable frequency drive (VFD) is considered.

ID. Research Objectives

The objective of this research has been designing a PMa-SynRM using stator and winding of a NEMA standard induction machine. This design approach makes it possible to compare the performance of both machines while the input current and stator copper loss is the same or the load condition is the same. The performance of both induction and PMa-SynRM machines has been analyzed with the fan (pump) load applied to the machines using the dynamometer on a proper test bed. To compare the machines energy consumption, the electric power consumed by the machines has been measured for typical running cycles.

IE. Thesis Outline

This dissertation is organized as follows:

Chapter one covers the main reasons and objectives of this research. Chapter II discusses the induction machine structure and performance. The stator of a NEMA standard general purpose induction machine is analyzed and studied and the benefits of using this stator and its performance effects on the design of the PMa-SynRM is discussed.

In Chapter III the structure of the PMa-SynRM is described and studies. The key performances, which need to be optimized during the design, are identified in this chapter. The design optimization procedure based on performance post processing using

computer aid design with an FEA tool is considered and the design procedure flowchart is presented. Some variation of the rotor core geometry such as magnet location and barrier and rib thickness sizes used in other works are studied in this chapter and are compared. Finally, an optimized rotor for the selected stator is presented in this chapter. Some solutions for performance improvement such as rotor skewing are studied in this chapter. The use of different types of magnets is considered in the design of the machine and the effect of using different types of magnets on the performance of the machine is studied. Also, the demagnetization possibility and the effect of the temperature on the magnets under rated condition are studied. Moreover, the material consumption of the optimized PMa-SynRM with the induction machine is compared as a part of design criteria.

Chapter IV reviews the considered control method for the designed PMa-SynRM and derives the equations and parameters that are necessary for the control development in the digital processing unit. In addition, the PMa-SynRM parameter measurement method used in this study with the results is presented in this chapter.

For the designed PMa-SynRM the torque performance of the machine is obtained and compared with the reference induction machine. The same comparison is done by changing the magnet type and quantity, and the effect of the magnet type on the torque performance of the machine is studied.

In Chapter V the efficiency and energy consumption of the designed PMa-SynRM with all rotor variation with different magnet type and quantity are compared with the reference induction machine. The load of the machines is a fan and pump type load

simulated by the dynamometer under a certain load profile. To evaluate the designed PMa-SynRM for fan and pump applications some other machine performances such as power factor, input power, apparent power and current are compared in this chapter.

Chapter VI studies the effect of magnet quantity on the low power PMa-SynRM and compares the energy consumption and efficiency of the machine with another general purpose induction machine running the same load profile.

Based on the results obtained in this research, the conclusion is presented in the last chapter. Also, suggestions for further research and extension are offered.

CHAPTER II

STANDARD INDUCTION MACHINE STUDY AS THE NEMA FRAME REFERENCE MACHINE*

IIA. Introduction

The stator of an induction machine generates a sinusoidal magneto-motive force (MMF) in the air gap using distributed winding in the stator slots. This causes a high fundamental MMF existence in the air gap, which can develop a high torque. In this chapter the stator and winding structure of a standard induction machine is studied to use in the PMa-SynRM design. Also, the magnetic flux density in stator yoke and teeth and the performance of the machine at rated current are studied.

IIB. Reference Induction Machine

The reliability of the induction machine as an electromechanical conversion system is proven over a century. This machine has been optimized and improved significantly because of to the material improvement and the geometry design optimization especially using computer aid. The winding configuration and the lamination geometry have been optimized to increase the performance of the machine and decrease the cost of material as the most attractive design criteria. To ease the machine selection by the users, the

* © 2009 IEEE. Reprinted in part with permission from "Design and comparison of an optimized permanent magnet-assisted synchronous reluctance motor (PMa-SynRM) with an induction motor with identical NEMA Frame stators," by R. Vartanian and H. A. Toliyat, in Electric Ship Technologies Symposium, 2009. ESTS 2009. IEEE, 2009, pp. 107-112. 2977-2984.

characteristics of the induction machine have been standardized by National Electrical Manufacturing Association (NEMA). Parameter such as the frame size makes it easier to find the proper option for fan and pump applications. The requirement of manufacturing low cost electric machines leads to using available machine components. On the other hand, because of using distributed winding type in the induction machine stator, there are some benefits, which increases the performance of a synchronous machine if the same stator is used such as [55-57]:

- High fundamental MMF component due to the distributed winding configuration
- High Reluctance torque due to the higher inductance of the machine
- Sinusoidal MMF distribution in the air gap (less harmonics), which reduces the core losses (eddy and hysteresis losses) and less torque ripple
- Less harmonic in Back-EMF, which results in higher flux linkage (more torque and power for the PMa-SynRM machine)
- Higher winding factor is achievable resulting in higher electric torque
- Sensorless control development is feasible due to the sinusoidal back-EMF

Therefore, in this work a stator of a general purpose NEMA frame induction machine is selected to use in the PMa-SynRM design. Also, the side by side performance comparison between the PMa-SynRM and the induction machine will be possible. A major benefit of such consideration will be employing the same stator and machine housing fabrication process from the induction machine manufacturers. Another benefit will be the existence of a reference machine for comparison with designed PMa-SynRM.

For this purpose, a 7.5 HP, 4 poles, 3-phase squirrel cage induction motor has been selected. The NEMA frame of this motor is C213T. Table 2-1 includes the specifications of the motor with stator main information coming from the manufacturer's data sheet and from experiments. The stator lamination of this induction motor is used in the design of the PMa-SynRM. The selected induction machine is a general purpose standard NEMA213 frame induction machine shown in Fig. 2-1. Using the stator of this machine will allow direct comparison with the PMa-SynRM performance by keeping the stator copper loss the same in the rated excitation current condition. The machine stator and rotor geometry information is included in Appendix A.

Table 2-1: Induction machine parameters.

Machine Parameters	Measurement
Number of poles	4
Rated Power	7.5 (HP)
Rated Voltage	230(V)
Rated Speed	1730(RPM)
Rated Torque	30 (N.m)
Rated Current	21(A)
Rated Efficiency	89.1(%)
Rated PF	0.81
Minimum Air Gap	0.016(inch)

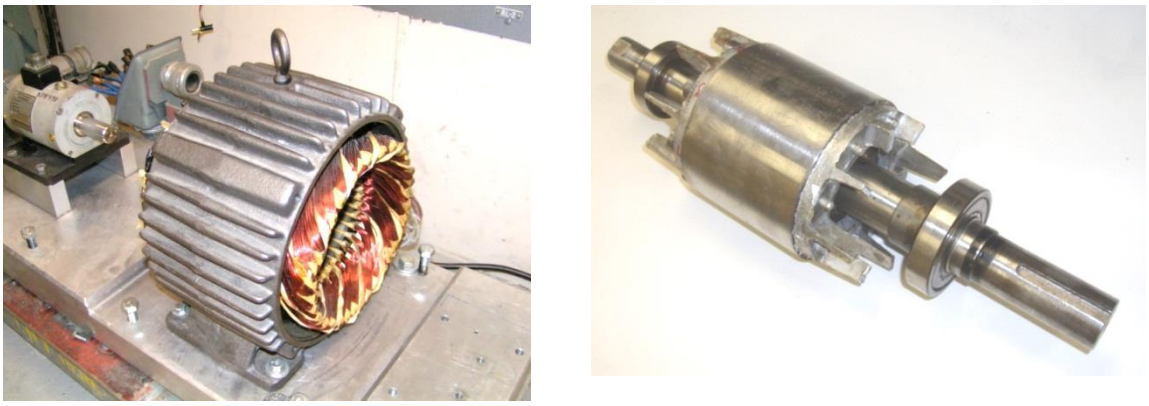

(a) (b)

Fig 2-1: Stator and rotor of the reference induction machines, (a) Stator of the reference induction machine, (b) Squirrel cage rotor

IIC. MMF Study of the NEMA Stator

Fig. 2-2 shows the distribution of the stator windings it the induction machine. This particular stator has dual layer winding with pitch factor of 8. To obtain the winding function of the machine, an arbitrary reference point has been selected according to the Fig. 2-3. The turn function of phase-A (n_A) is obtained according to the Fig. 2-4 assuming a linear distribution of 30 conductors of each layer in the slots.

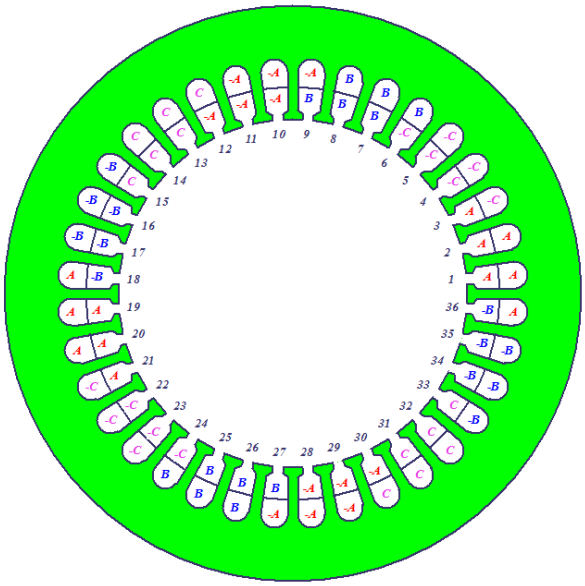

Fig 2-2: Winding configuration in the slots.

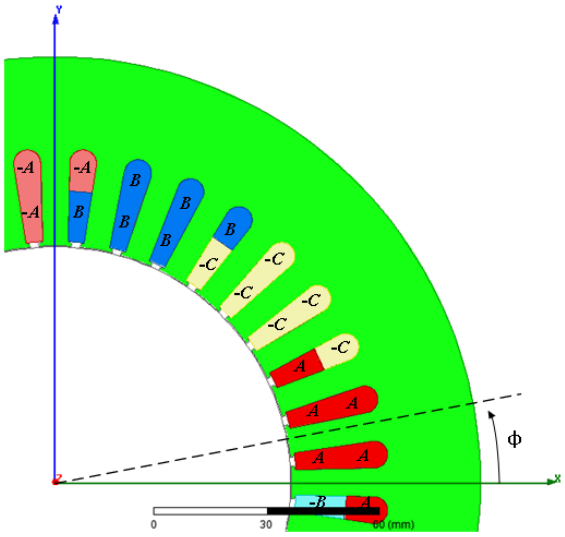

Fig 2-3: Arbitrary reference selection to obtain the turn function of phase A.

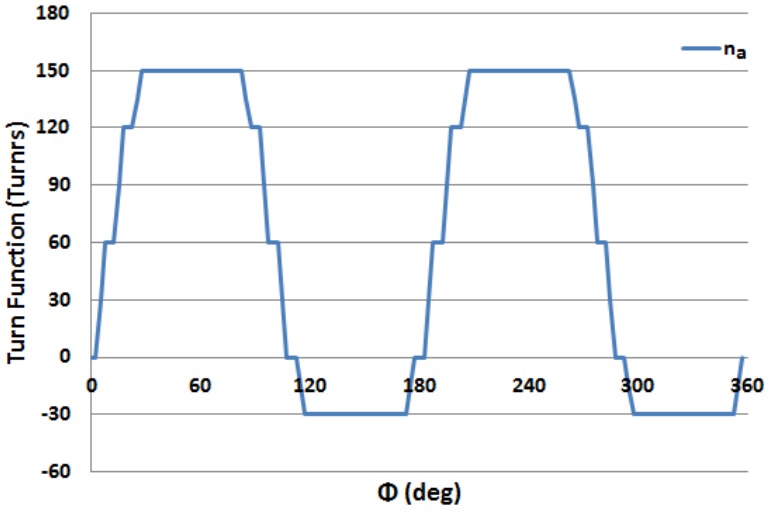

Fig 2-4: Turn function of phase A.

In order to find the phase winding function N(ϕ), the average of the turn function should be calculated and subtracted from the turn function according to (2-1) and (2-2). The average of the phase A is 60 ($< n_a(\Phi) > = 60$). Fig. 2-4 shows the winding function of the phase A. Also, using the same approach the winding function of phase B and C are obtained and shown in Fig. 2-5.

$$< n(\Phi) > = \frac{1}{2\pi}\int_0^{2\pi} n(\Phi)d\Phi \tag{2-1}$$

$$N(\Phi) = \mathrm{n}(\Phi) - < n(\Phi) > \tag{2-2}$$

The expression of the total MMF generated by the stator excitation at a certain point in the air gap is according to (2-3). Considering a balanced three phase excitation current applied to the windings, the MMF generated by the stator windings at time zero is shown in Fig. 2-6a (the rated current of 21 A is considered in this calculation). It is obvious that the MMF has a sinusoidal shape and a high fundamental is expected due to the

distributed winding in the stator. The FFT of the total MMF is shown in the Fig. 2-6b. It can be seen that the harmonic component are low but the 5^{th}, 17^{th} and 19^{th} are the most dominant harmonics in the MMF.

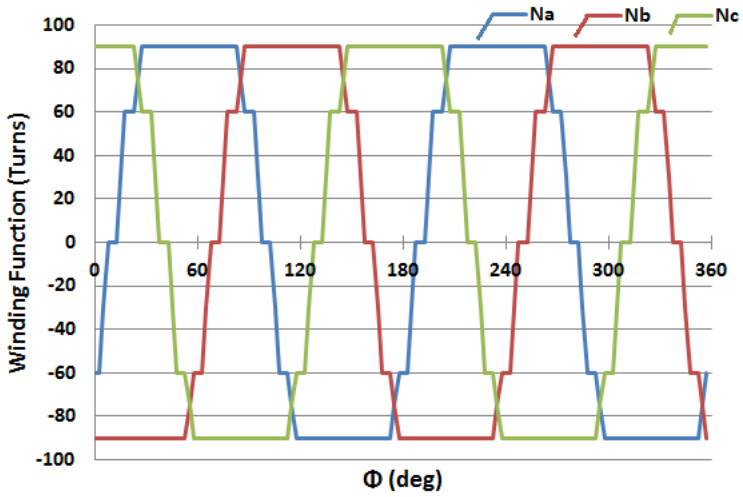

Fig 2-5: Winding function of all three phases.

$$F(\Phi) = N_a(\Phi)i_a + N_b(\Phi)i_b + N_c(\Phi)i_c \tag{2-3}$$

$$\begin{cases} i_a = \sqrt{2}I\cos(\omega_e t) \\ i_b = \sqrt{2}I\cos(\omega_e t - 2\pi/3) \\ i_c = \sqrt{2}I\cos(\omega_e t + 2\pi/3)_a \end{cases} \tag{2-4}$$

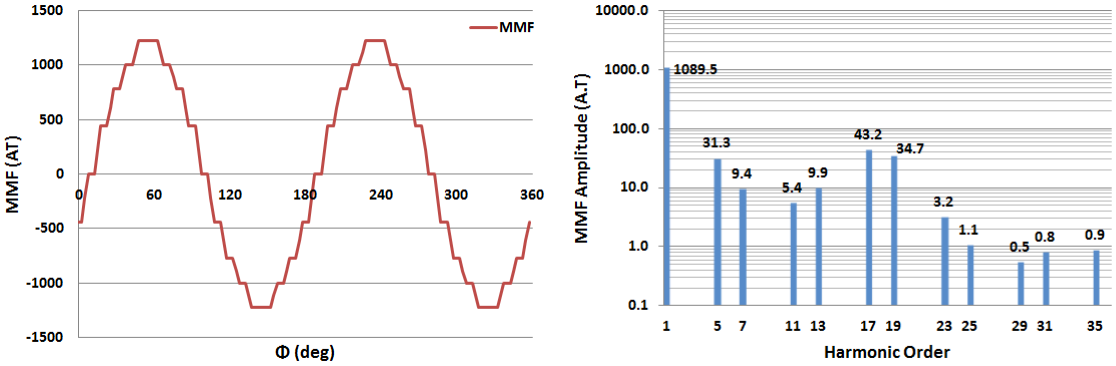

(a) (b)

Fig 2-6: MMF generated in the stator with rated current: (a) MMF waveform (b): Harmonic spectrum of the MMF.

Assuming the rotor as a circular shaped core, the Flux line distribution of such excitation is shown in Fig. 2-7. The flux density is measured in the middle of the air gap for demonstration purposes, which is shown in the Fig. 2-8. The sinusoidal flux density distribution can be observed in the air gap, which is the main objective of using distributed winding in the induction machine.

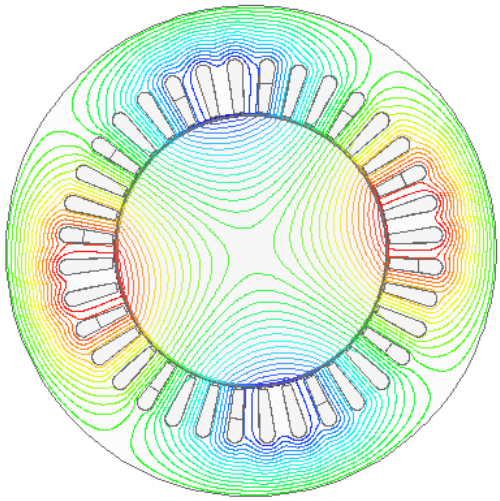

Fig 2-7: Flux line distribution due to the stator excitation.

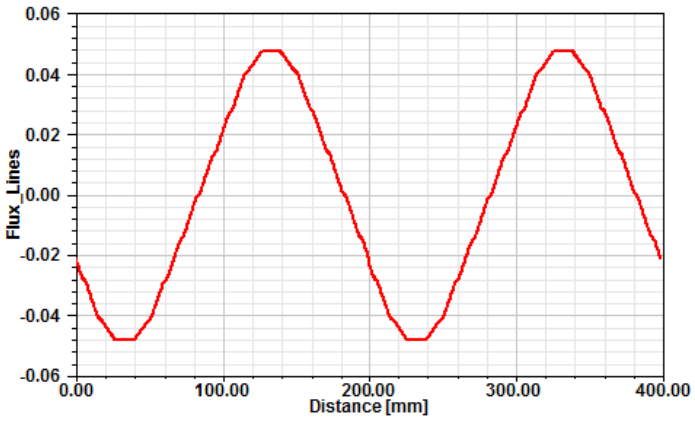

Fig 2-8: Flux distribution in the air gap due to the stator excitation.

IID. Simulation Results of the Induction Machine

As mentioned before, the stator of the reference induction machine is considered for the PMa-SynRM design. Therefore to compare the PMa-SynRM with the induction machine itself, the performance of the induction machine should be obtained.

In this case the FEA tool is used to simulate the reference induction machine. To observe the flux density in the air gap, stator teeth, and the stator yoke, the induction machine is modeled using FEA 2D. Fig. 2-9 shows the mesh applied to the geometry of the machine. A voltage excitation is considered (line start mode) in the model.

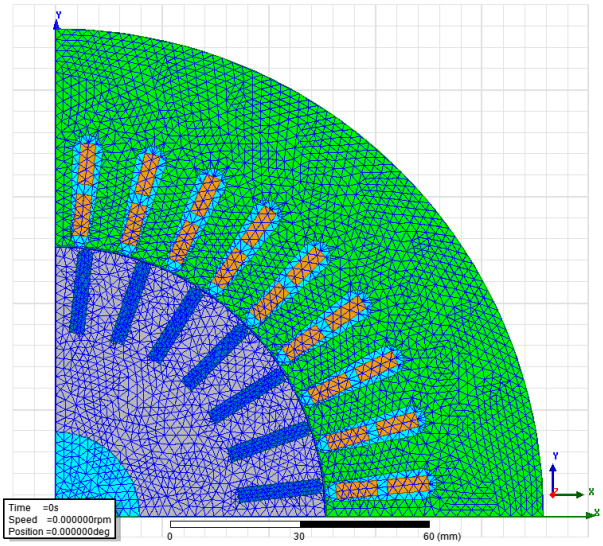

Fig 2-9: Applied mesh on 2D geometry of the induction machine for FEA analysis.

Fig. 2-10 shows the flux line distribution and the flux density in the machine during the steady state condition at rated load (30 N.m). It can be observed that the magnetic flux density in machine remains below the saturation point (1.5 T).

To measure the flux density of the stator in the stator yoke a contour is defined from point A to B inside the stator back iron as shown in the Fig. 2-11a. The flux density measure in the back iron across the contour AB is shown in the Fig. 2-11(b). The average flux density is about 1.18 T in the middle of the contour.

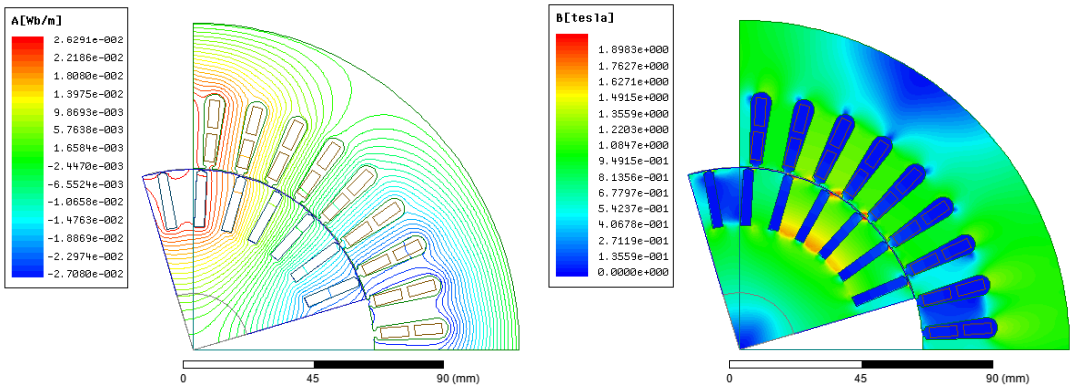

(a) (b)

Fig 2-10: FEA analysis field output on the induction machine: (a) Flux line, (b) Flux density.

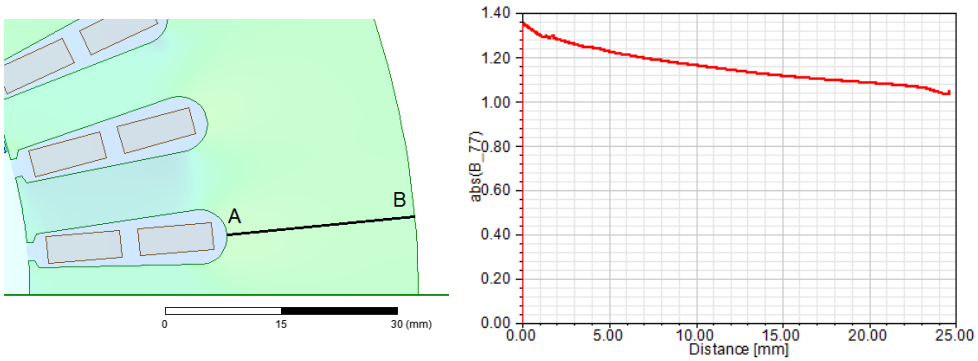

(a) (b)

Fig 2-11: Stator yoke flux density measurement: (a) Defined contour AB in the stator back iron, (b) Flux density measurement over the contour AB.

Also, the flux density in the middle of the stator teeth is measured over a pole pitch and is shown in Fig. 2-12(a). It can be seen that the maximum flux density in teeth is below 1.4(T), which is below the saturation point for the stator core steel (M45).

In addition, the flux density in the middle of the air gap at the rated load condition is measured and shown in the Fig. 2-12(b). It can be seen that the distribution of the flux

density has a sinusoidal shape with amplitude of 0.8 T and the maximum flux density in the air gap reaches to 1.25 T.

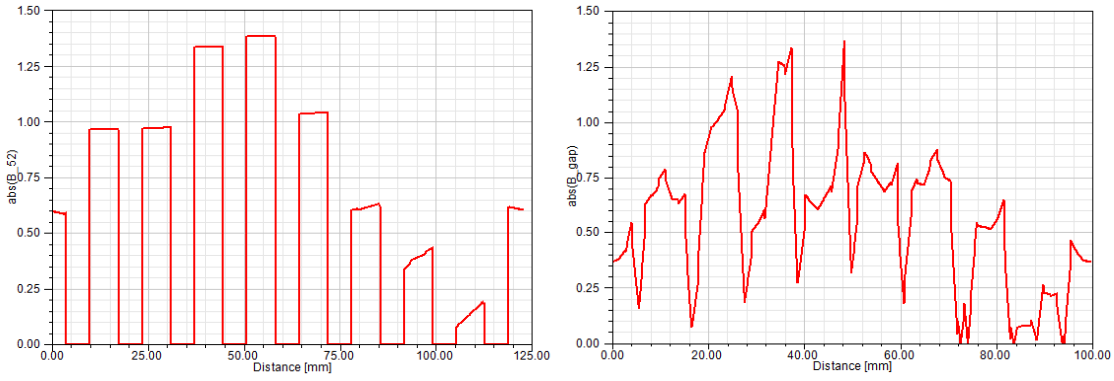

(a) (b)

Fig 2-12: Flux density of the induction machine operating at the rated condition in: (a) The middle of the stator teeth over a pole pitch and (b) Middle of the air gap.

IID1. Startup of the Induction Machine

Startup transient waveforms of the induction machine operating under rated load are shown in Fig. 2-13 and 2-14. Since a voltage source is used for the excitation, the current has a significant overshoot due to the startup under the rated torque. Fig. 2-13(a) shows the line current during the startup transient and steady state condition. The current reaches to the rated current at about 21(A) after 0.3 second. Fig. 2-13(b) shows the current in the rotor bars, which reaches to about 500 ampere in amplitude in steady state condition. The copper loss generated by this current will not exist in the PMa-SynRM. Therefore, higher efficiency is expected from the PMa-SynRM machine driving the same rated load. Fig. 2-14(a) shows the developed electromechanical torque, which reaches to 30 N.m (the same as the applied load). Acceleration of the machine can be

seen in the Fig. 2-14(b). In this case the machine reaches to a steady state speed of 1760 RPM, which is below the synchronous speed due to the rotor slip.

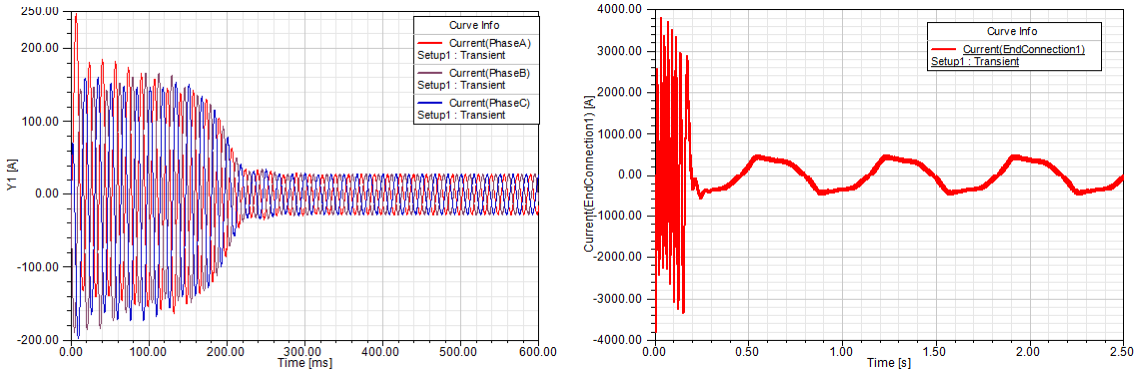

(a) (b)

Fig 2-13: Startup transient current waveforms of the induction machine under rated load: (a) Stator currents, (b) Rotor bar current.

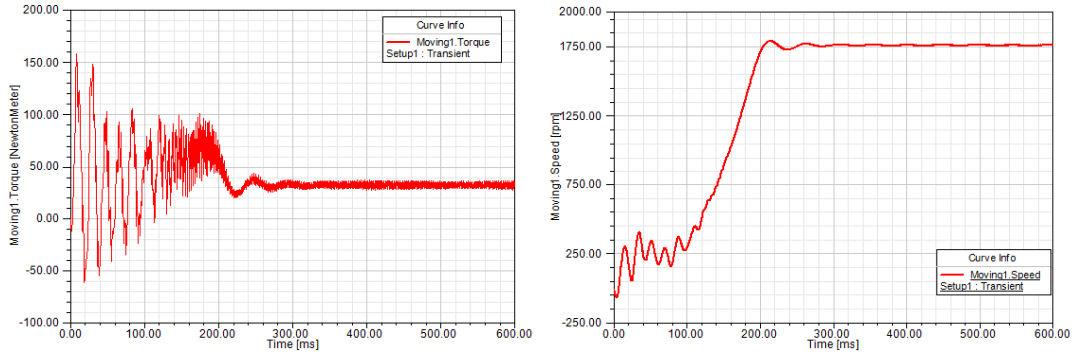

(a) (b)

Fig 2-14: Startup transient waveforms of the induction machine under rated load: (a) Torque output, (b) Speed.

IIE. Conclusion

In this chapter the performance of a general purpose NEMA induction machine is studied. Using analytical analysis and FEA tool, it is shown that the distributed winding

of the machine generates a sinusoidal MMF in the air gap and a high torque density can be achieved using this stator and winding and an optimized PMa-SynRM rotor. Also some other information such as flux density at the rated condition is obtained for comparison with PMa-SynRM in the next chapter.

CHAPTER III

PMA-SYNRM DESIGN AND OPTIMIZATION[*]

IIIA. Introduction

The PMa-SynRM machine is constructed as a synchronous reluctance machine with permanent magnets embedded inside the rotor core; therefore the machine can be considered as a PM machine with high saliency ratio and low flux linkage (compared to IPM). It is shown that the power factor of the machine is related to the flux linkage and the saliency ratio, therefore increasing these parameters will result in a machine with high torque and power factor.

A typical torque-speed characteristic of a PM machine is shown machine is shown in Fig. 3-1. The PM machine is able to generate the maximum torque in the stand still condition up to the base speed. After reaching the base speed, the machine has to operate in the field weakening region (constant power region), due to the limited bus voltage. In this operating region the generated torque drops due to the reduction in the torque

---

[*] © 2009 IEEE. Reprinted in part with permission from "Design and comparison of an optimized permanent magnet-assisted synchronous reluctance motor (PMa-SynRM) with an induction motor with identical NEMA Frame stators," by R. Vartanian and H. A. Toliyat, in Electric Ship Technologies Symposium, 2009. ESTS 2009. IEEE, 2009, pp. 107-112. 2977-2984.
© 2013 IEEE. Reprinted in part with permission from "Performance analysis of a rare earth magnet based NEMA frame Permanent Magnet assisted Synchronous Reluctance Machine with different magnet type and quantity," by R. Vartanian, Y. Deshpande, and H. A. Toliyat, in *Electric Machines & Drives Conference (IEMDC), 2013 IEEE International*, 2013, pp. 476-483.

component of the current and increment of the demagnetizing current. Neglecting the losses, the generated power remains constant at the base power region.

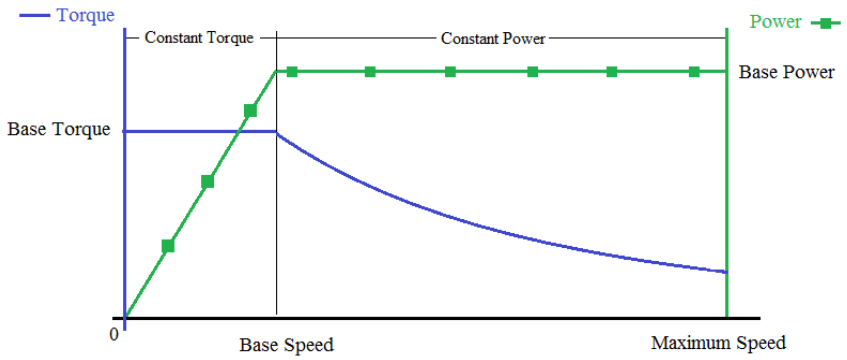

Fig 3-1: General torque and power characteristic of a PM machine.

According to the Affinity law, the load of fan or pump increases by increasing the speed. Therefore, in the electric machine design the nominal or base torque of the machine has to match with the maximum load torque. On the other word, the optimum design is to consider the maximum torque demand of the load as the torque base in the machine design, which happens at the rated speed of the load.

For the initial designs of PM machines, analytical models are presented in various works, which include the design of the stator and winding configuration. In most of the designs it is recommended to approve the analytical design by FEA tools since the finite element tool considers the non-linear characteristic of the material with high precision and the output results are very close to the prototype test results.

Because the stator and the housing of the induction machine will be used in this work, the parameters of the machine geometry such as stator outer diameter (OD), stator inner diameter (ID), winding configuration (number of layers and conductor turns), and the rotor inner diameter (shaft size) will be kept the same as the reference induction machine. The FEA analysis is selected for the optimization with the same excitation as that of the induction machine. Also the air gap (rotor outer diameter) used is the same as the induction machine and for the initial geometry. In this chapter the design procedure is presented.

IIIB. Design Criteria

The main objective is to design a rotor geometry, which satisfies the design criteria. To optimize the geometry of the PMa-SynRM rotor, some of the main performances of the machine are considered as the design criteria. These include the developed torque and back-EMF performance.

IIIB1. Torque Performance

The electromagnetic torque developed in the electric machine can be described as the following:

$$T_{out}(i_s, \theta_r, \lambda_{pm}) = T_{reluctnace}(i_s, \theta_r) + T_{magnet}(i_s, \theta_r, \lambda_{pm}) + T_{cogging}(\theta_r, \lambda_{pm}) \qquad (3\text{-}1)$$

The reluctance torque is due to the tendency of the rotor saliency to align with the stator field generated by the excitation of the stator winding. The magnet torque is due to the tendency of the rotor magnets to align with the stator field. Cogging torque is

interaction between the stator teeth and rotor magnet and can be expressed as the following:

$$T_{cogging}(\theta_r, \lambda_{pm}) = -\frac{1}{2}\lambda_{pm}^2 \frac{dR}{d\theta_r} \quad (3\text{-}2)$$

Therefore, torque performance improvement of a machine can be itemized as following [11, 58-60]:

- Maximizing the peak torque per ampere current. Usually this design criterion is not sufficient to provide the maximum average toque because of the existence of the ripple torque, which can reduce the average torque of the machine due to the variation in the air gap permeance.
- Minimizing the cogging torque
- Minimizing the ripple torque
- Maximizing the average torque

In this work, improving the torque performance will be done by analyzing different rotor core geometry in FEA and comparing the results since the stator geometry and winding configurations are pre-determined.

IIIB2. Back-EMF Performance

The back-EMF is the voltage induced in the stator winding due to the flux linkage generated by the permanent magnets in the rotor and is expressed as the following:

$$E_{pm} = \frac{d\lambda_{pm}}{dt} \quad (3\text{-}3)$$

It has been shown that the higher flux linkage results in better power factor of the PMa-SynRM. Therefore, the design approach will be to achieve a rotor geometry, which

generates the highest fundamental back-EMF component with lower harmonic content, while the magnet mass is kept constant.

IIIC. Computer Aid Design

To perform the design, FEA is an appropriate tool to obtain the performance of any electro-mechanical device. In this work, Ansys\Maxwell 2D software is used. The design using any FEA tool has the following steps:

- Pre-processing
- Processing
- Post-processing

In pre-processing, the geometry of the machine is defined. Then, the materials, excitations, and boundaries are specified. Fig. 3-2 shows the geometry of a PMa-SynRM and its components.

In the processing stage, the Maxwell equations (3-4 to 3-7), which describe the relationship of non-linear magnetic field to their sources are solved [55, 61]. In the numerical calculation method this is done by applying a mesh to the geometry and solving the equations for unknown variables.

$$\nabla \cdot \mathrm{B} = 0 \tag{3-4}$$

$$\nabla \cdot \mathrm{D} = \rho \tag{3-5}$$

$$\nabla \times \mathrm{H} = \mathrm{J} + \frac{\partial \mathrm{D}}{\partial \mathrm{t}} \tag{3-6}$$

$$\nabla \times \mathrm{E} = -\frac{\partial \mathrm{B}}{\partial \mathrm{t}} \tag{3-7}$$

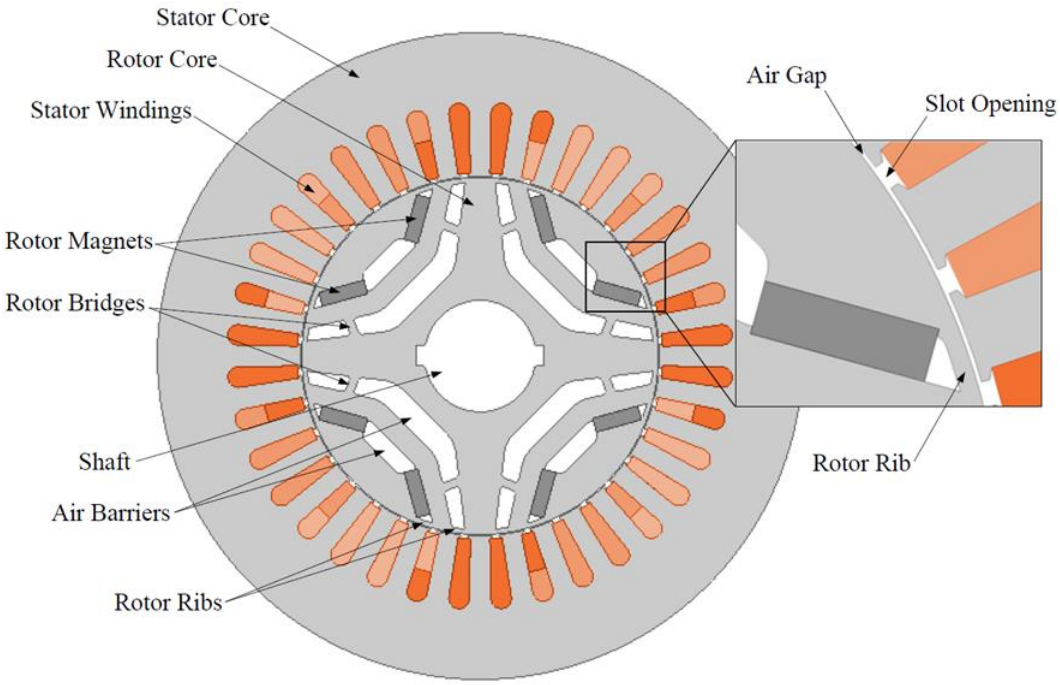

Fig 3-2: PMa-SynRM geometry structure.

Maxwell equations are related to the materials by the material laws:

$$B = \mu H \tag{3-8}$$

$$J = \sigma E \tag{3-9}$$

$$D = \varepsilon E \tag{3-10}$$

The precision of the calculation is related to the number of mesh elements in the geometry and large number of meshes will increase the solution time. Therefore, a fine mesh should be used for precise solution. Defining a fine mesh size in the air gap is necessary due to the fact that the developed torque in the air gap has to be calculated with high accuracy. Fig. 3-3 shows the mesh applied to a PMa-SynRM machine.

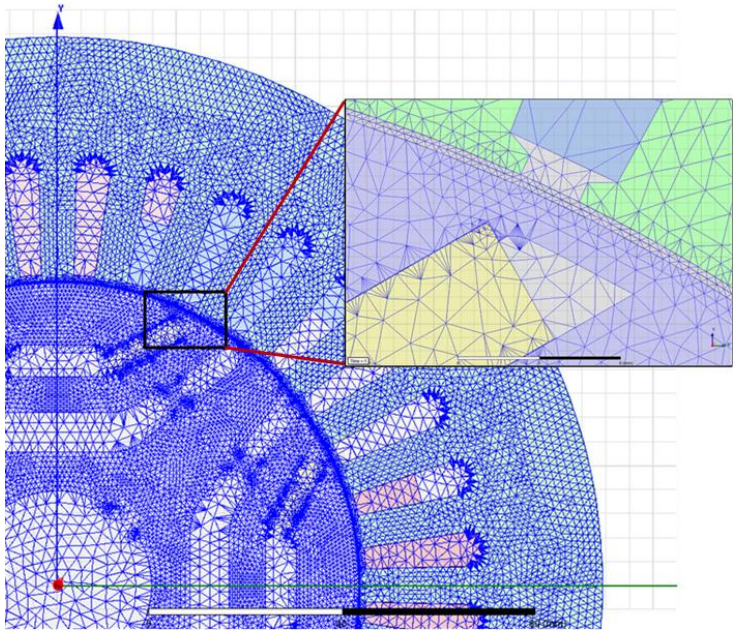

Fig 3-3: Mesh operator applied to the geometry of the PMa-SynRM.

To obtain the performance of the electric machine different electromagnetic excitation can be used:

- Free rotation with no excitation can be used to obtain the back-EMF and cogging torque of the machine.
- DC stator excitation (time invariant) can be used to obtain the maximum torque and maximum torque angle (or current angle).
- AC stator excitation (time variant) can be used to obtain the average torque and the torque ripple at the maximum torque angle operation obtained from previous step.

Finally, the obtained results are analyzed to match with the design criteria in Post-Processing stage.

IIID. Material Selection

Due to the fact that for the PMa-SynRM design the stator of the induction machine is considered, only rotor material should be selected.

IIID1. Core Material Selection

The steel used in the induction machine is M45-Guage26 and the same is considered for the rotor design. Fig. 3-4 shows the B-H curve of this steel, which has knee point around 1.4T.

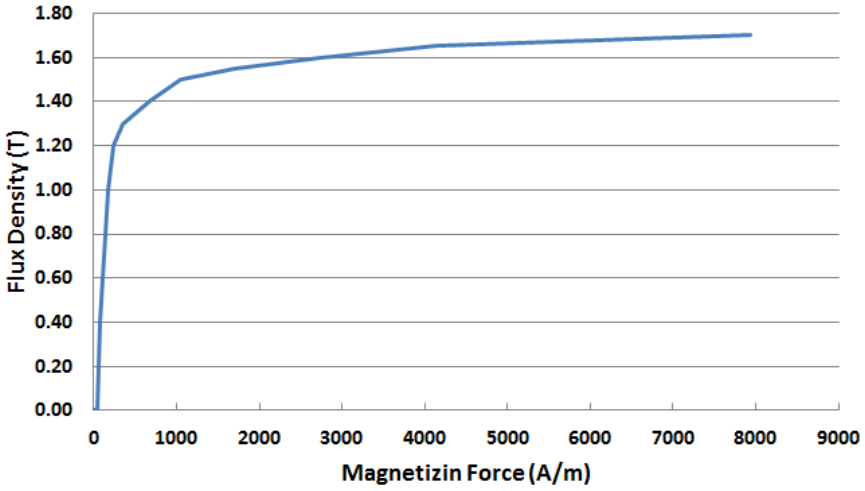

Fig 3-4: B-H curve of M45-G26.

IIID1a. Core Loss Parameters

The core loss in the steel is proportional to the flux density and the frequency. It consists of two major components, hysteresis and eddy current losses, expressed in classical form in (3-11)[55]:

$$P_v = P_h + P_c = k_h f(B_m)^2 + k_c(fB_m)^2 \quad (3\text{-}11)$$

To estimate the core loss when the flux density and frequency are excessively high, the advanced expression of the core loss is used as (3-12)[61]:

$$P_v = P_h + P_c + P_e = k_h f(B_m)^2 + k_c(fB_m)^2 + k_e(fB_m)^{1.5} \quad (3\text{-}12)$$

For the selected core material, in this work, the loss parameters are according to the Table 3-1.

Table 3-1: Stator core loss parameters.

Grade	Thickness[mm]	k_h	k_c	k_e
M45	0.47	164.2	0.712	0.82

IIID2. Permanent Magnet Selection

There are several permanent magnet types to consider in a machine design. Some magnets have high remanent flux density and higher cost but limited in operating temperature. On the other hand, some magnets are capable to operate in a higher temperature but the low energy product and flux density increases the mass of the magnet in the design[59]. Therefore the tradeoffs in the design have to be considered carefully. Some of the common type materials for the permanent magnet are: Samarium-Cobalt (SmCo), Neodymium-Iron-Boron (NdFeB), Alnico, and Ferrite. Some of the advantages and disadvantages of the above mentioned magnets are listed in Table 3-2.

Table 3-2: Different permanent magnet comparison.

Magnet Material	Advantages	Disadvantages
NdFeB	High operating temperature Very high flux density (1.4T)	High temperature coefficient Sensitive to corrosion Expensive
SmCo	High operating temperature High flux density (up to 1.2 T) Low temperature coefficient High resistance to demagnetization and corrosion	Most expensive magnet
Alnico	High operating temperature Low temperature coefficient	Easy to demagnetize
Ferrite	Least expensive magnet High operating temperature	Lowest remanent flux density (0.4T)

The operating temperature of the induction machine is limited below 110 (C) (Class F isolation), therefore NdFeB and ferrite type magnets are selected for the design. If the torque density is higher than the induction machine, the current needed to drive the same load will be less and more temperature drop will be expected. Because the maximum operating temperature is limited by the winding isolation class, the operating temperature can be used to simplify the magnet selection. Because NdFeB has higher flux density, the main design will be based on this magnet. Later, the ferrite magnets will be replaced with NdFeB magnets to compare the performances between them. Table 3-3 includes the permanent magnet information used in this study.

IIIE. Design Procedure

As it is mentioned before, the stator geometry and the excitation is considered to be the same as that of the NEMA frame reference induction machine. Due to the specification of the inner and outer diameter of the rotor, a PMa-SynRM with two barriers is selected with permanent magnet located on the sides.

The shape of barriers is designed to match with the stator flux path shown in Fig.2-8. Also, the second barrier has a bridge located under the permanent magnet position, which provides a better path for the magnet flux and increases the flux linkage. A simple strategy shown in Fig.3-5 is considered to optimize the rotor for the specified stator. Some of the important parameters such as ribs width, barrier distances and widths, and place of the magnets are changed in the case studies.

Table 3-3: Characteristics of the selected NdFeB and Ceramic permanent magnet.

Magnet Type	**NdFeB**	**Ferrite**
Grade	42SH	C8
Residual Induction Br	1.28-1.32 (T)	0.385 (T)
Relative Recoil Permeability	1.05	1.04
Coercive Force Hcb	987 (kA/m)	235 (kA/m)
Intrinsic Coercive Force Hci	1592 (kA/m)	242(kA/m)
Energy Product BH_{max}	318-342 (kJ/m3)	27.8(kJ/m3)
Max. Operating Temp.	150 °C	120 °C

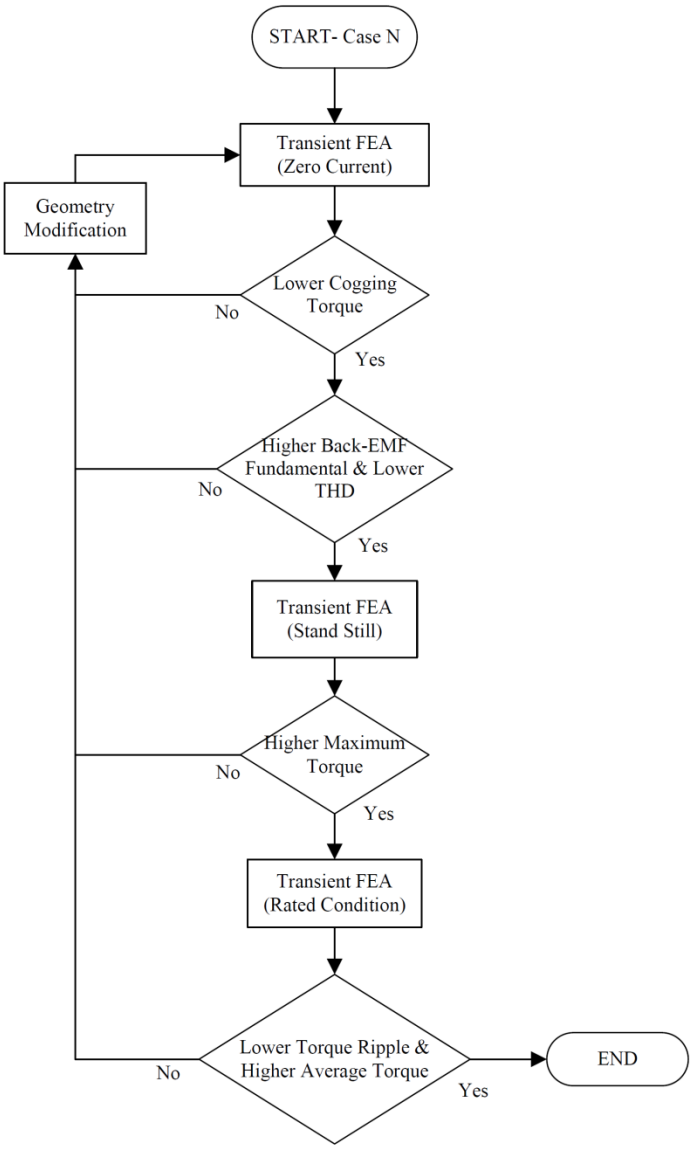

Fig 3-5: Optimization procedure with FEA.

The initial geometry has the configuration shown in Fig. 3-6(a) introduced in [29]. Fig. 3-7 shows the torque profile at different rotor position by each rotor at the rated current condition. Most of the rotors generate about 50Nm torque around 68deg; but the rotors with higher torque oscillation in the profile will generate higher torque ripple in the

output torque (i.e. rotor 4 and 6). In contrast, the rotors with smooth profile especially around the maximum torque generate output torque with less ripple (i.e. rotor 1, 7, and, 8).

Fig. 3-8 shows the cogging torque generated by each rotor. Comparing these outputs, the rotor, which generates less cogging torque, will be better candidate since the cogging torque also will be added to the output torque of the machine and it contributes in the vibration and noise. Among the compared cases, the rotor 1, 2 and 8 have low cogging torque. Also it can be observed that placing the magnet in the second barrier and small width on the d-axes has significant effect on the cogging torque. The main reason is that if the bridges are eliminated then the flux has to pass to the stator with higher intensity and that creates higher cogging torque. With the presence of the bridges and the proper width of the ribs, the cogging toque can be reduced significantly.

Fig. 3-9 shows the back-EMF of the machine at the rated speed (1800 RPM). It can be seen that the rotors, which creates more cogging torque also generates higher distortion in the back-EMF waveform (i.e. rotor 3 and 4). Also the effect of the ribs width can be observed by comparing rotor 7 and 8. Although the fundamental of the back-EMFs are close but narrow rib has generated high distortion in the back-EMF. Moreover, the rotors with magnet in the second barrier show high distortion in the back-EMF (rotor 3 and 4) or lower fundamental component (rotor5). Fig. 3-10 shows the harmonic spectrum of the back-EMFs. In this case the rotor with higher fundamental and less THD will be selected, which is rotor 8.

Fig. 3-11 shows the output torque of the compared rotors. Here, it is obvious that the rotors with higher distortion in the maximum torque profile and higher cogging torque have higher torque ripple. Although the maximum output torque of the rotors are close but the average output torque drops because of the different torque ripple amplitude. In this case, rotor 8 shows a high average torque and less torque ripple.

Fig. 3-12 shows the torque generated by the machine is obtained for each SynRM rotor (magnet-less rotor). In this case it is possible to study the average torque and the current ripple generated by each rotor without the magnet contribution. Comparing these cases with the PMa-SynRM cases shows the magnet utilization in the design. In the comparison of the rotors, it can be seen that the rotor 8 has less torque ripple with applicable average torque.

Table 3-4 compares the performance obtained for each rotor shown in Fig. 3-6. It can be seen that the rotor 8 has better performance of cogging torque, fundamental of the back-EMF, back-EMF distortion, average output torque and torque ripple compared to the other rotor geometries. Therefore, this rotor is considered as the optimized option for further studies.

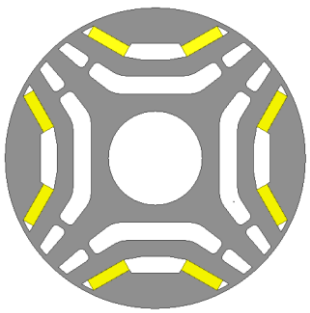

(a) Rotor1

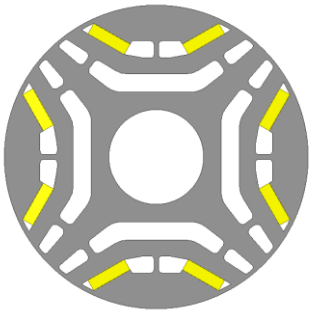

(b) Rotor2

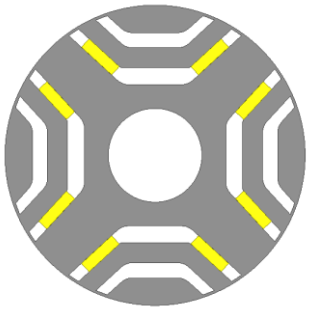

(c) Rotor3

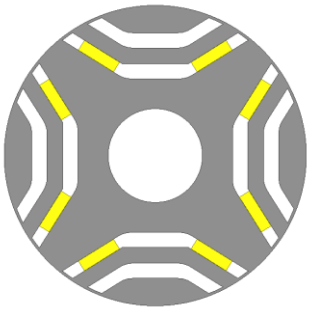

(d) Rotor4

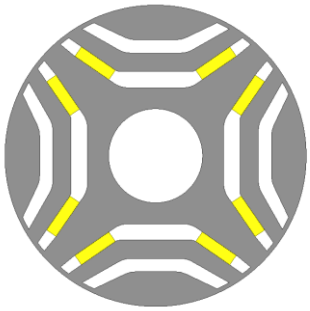

(e) Rotor5

(f) Rotor6

(g) Rotor7

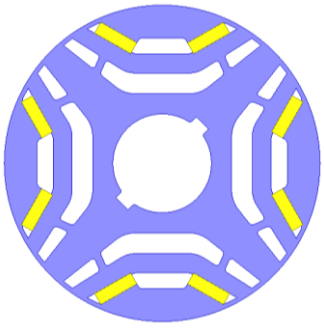

(h) Rotor8-Final Design

Fig 3-6: Rotor geometry variations in the case study.

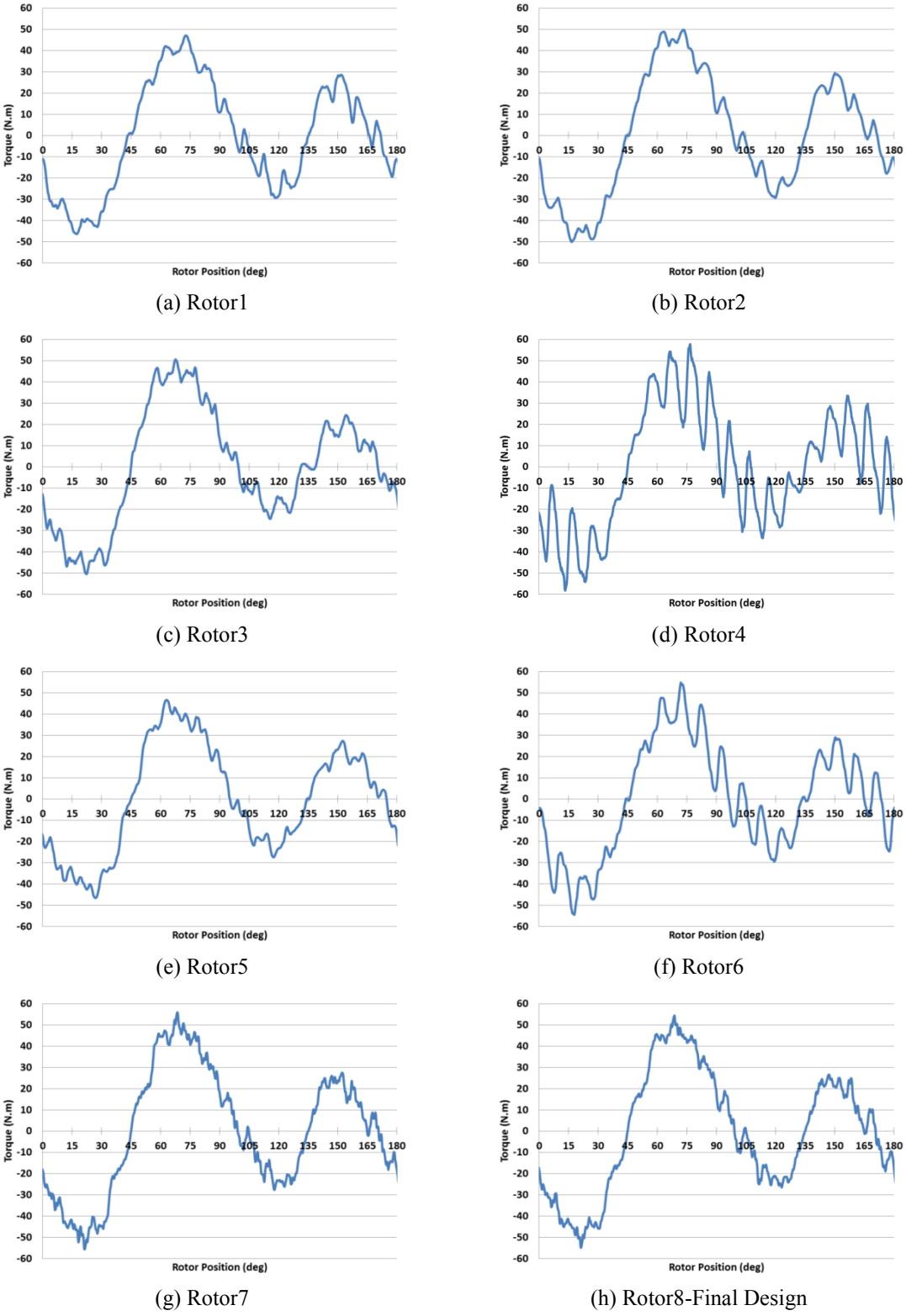

(a) Rotor1 (b) Rotor2

(c) Rotor3 (d) Rotor4

(e) Rotor5 (f) Rotor6

(g) Rotor7 (h) Rotor8-Final Design

Fig 3-7: Maximum torque profile of each rotor design variation.

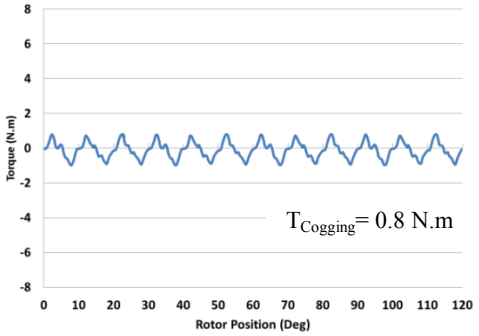

(a) Rotor1

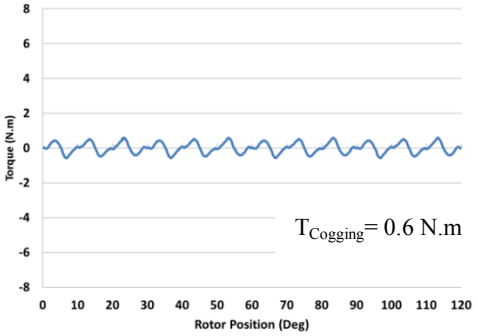

(b) Rotor2

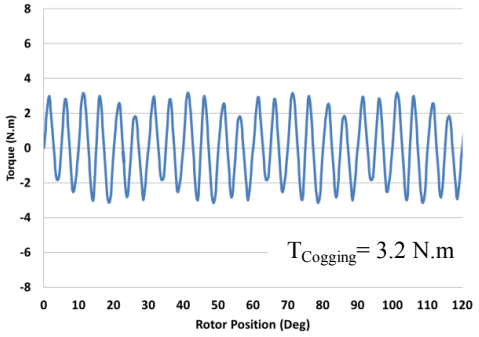

(c) Rotor3

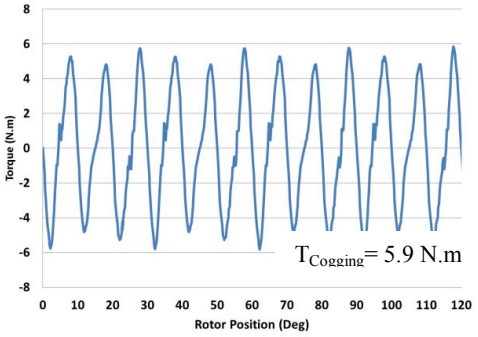

(d) Rotor4

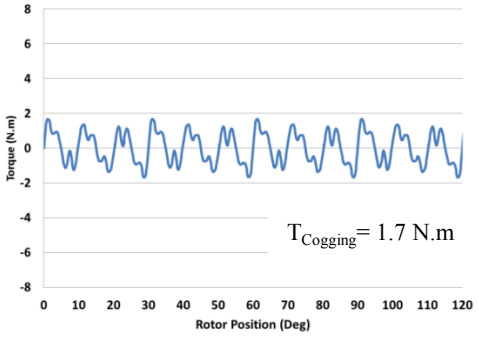

(e) Rotor5

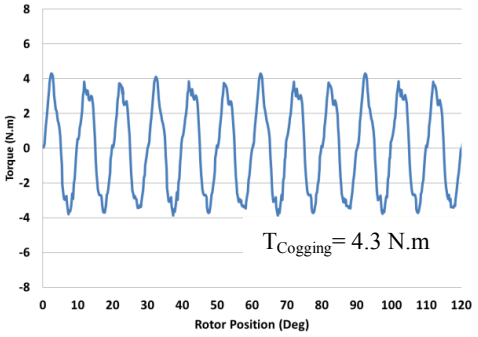

(f) Rotor6

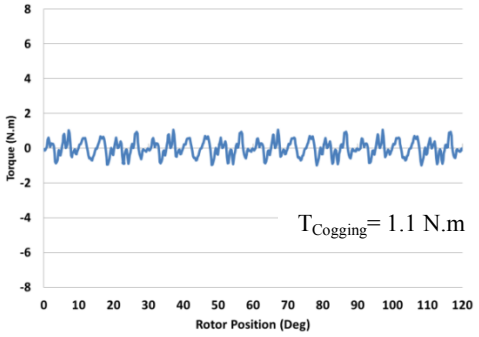

(g) Rotor7

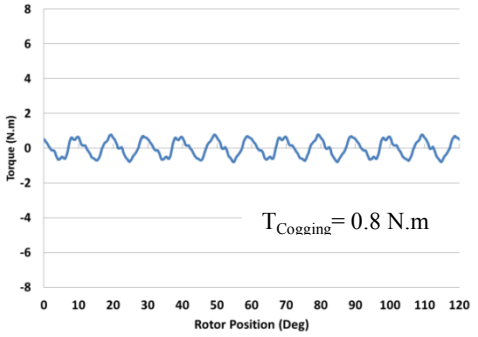

(h) Rotor8-Final Design

Fig 3-8: Cogging torque waveform generated by each rotor with zero excitation.

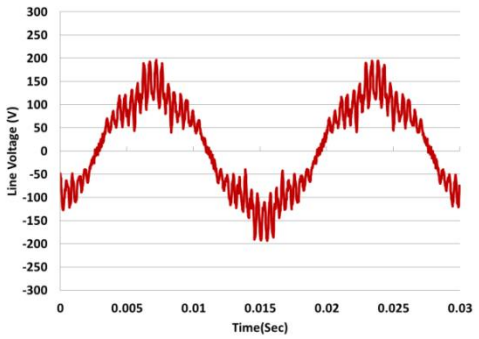

(a) Rotor1

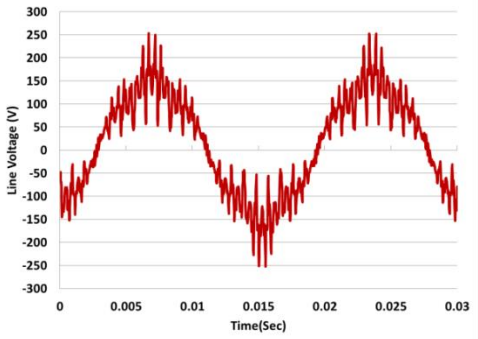

(b) Rotor2

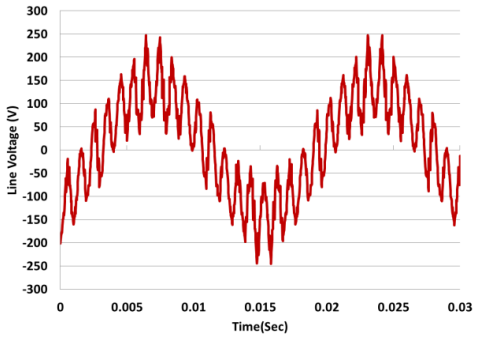

(c) Rotor3

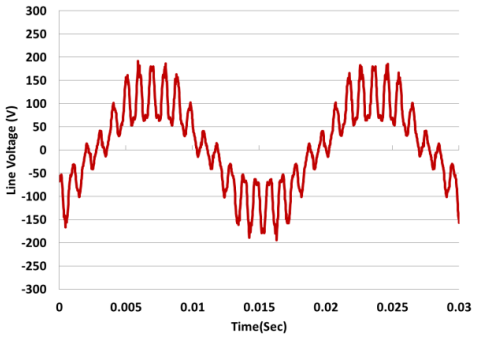

(d) Rotor4

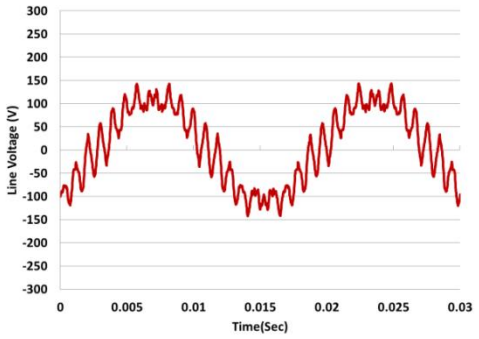

(e) Rotor5

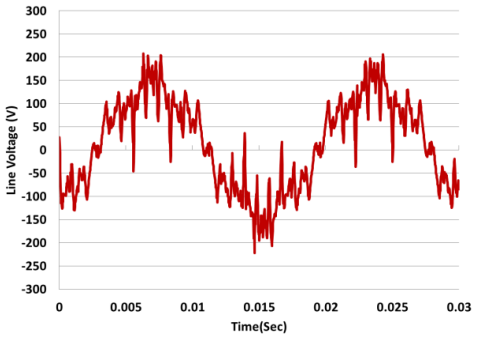

(f) Rotor6

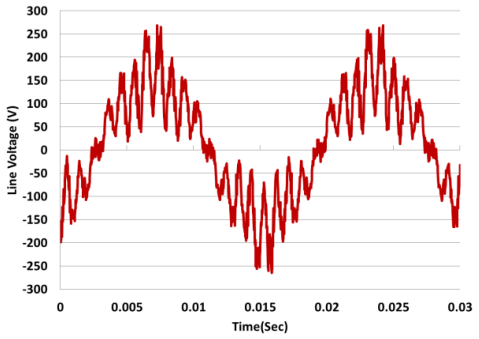

(g) Rotor7

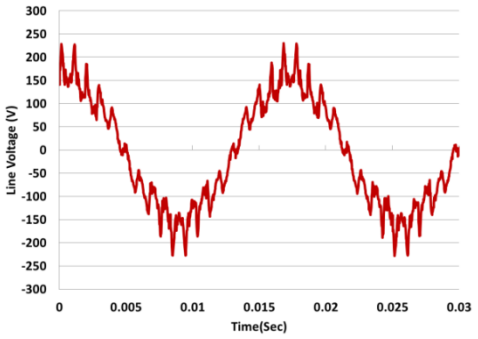

(h) Rotor8-Final Design

Fig 3-9: Back-EMF waveform generated by each rotor at rated speed.

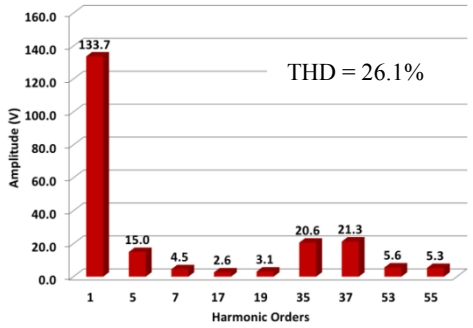

(a) Rotor1

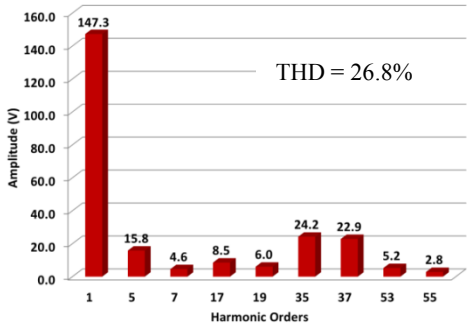

(b) Rotor2

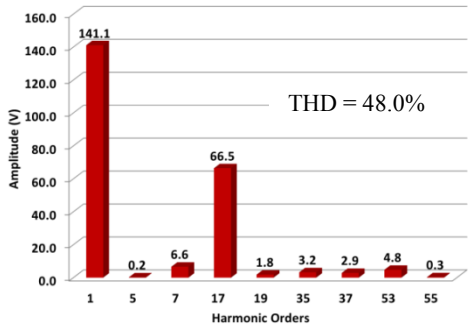

(c) Rotor3

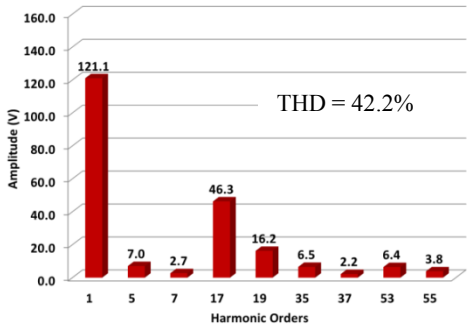

(d) Rotor4

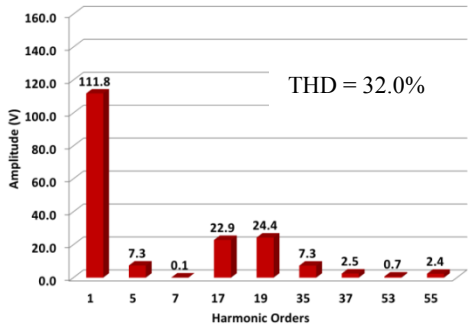

(e) Rotor5

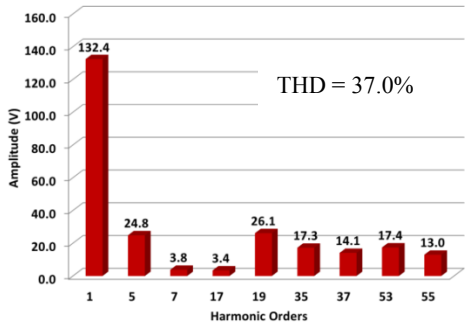

(f) Rotor6

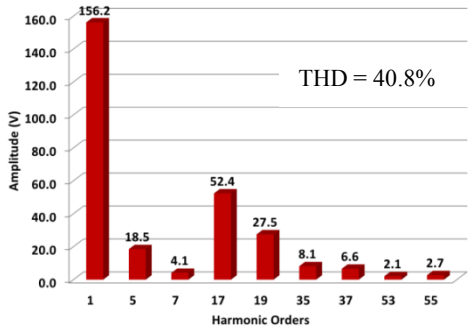

(g) Rotor7

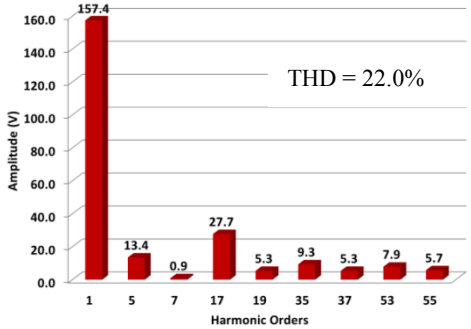

(h) Rotor8-Final Design

Fig 3-10: Back-EMF harmonic spectrum of each rotor at rated speed.

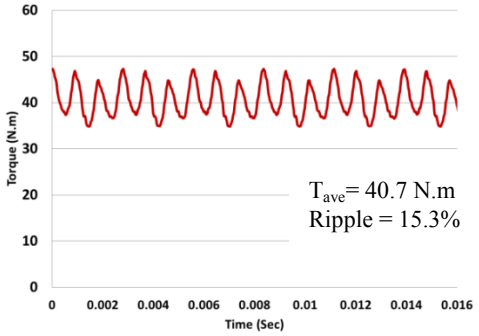

(a) Rotor1

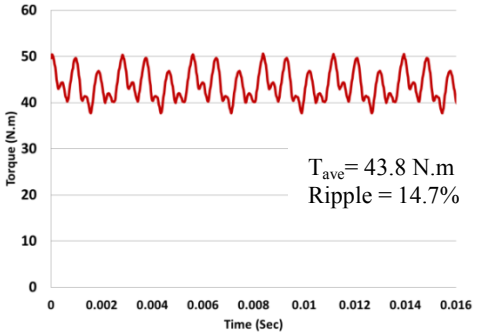

(b) Rotor2

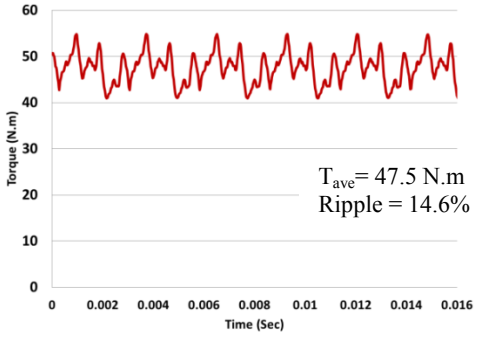

(c) Rotor3

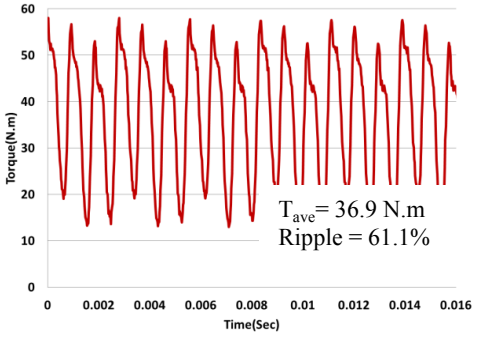

(d) Rotor4

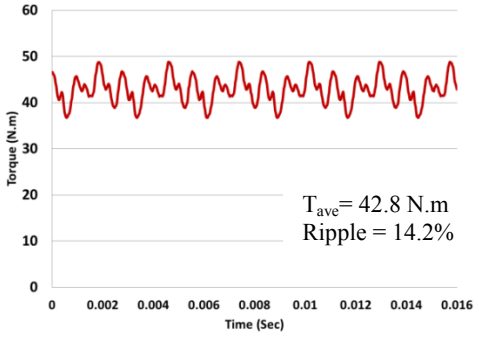

(e) Rotor5

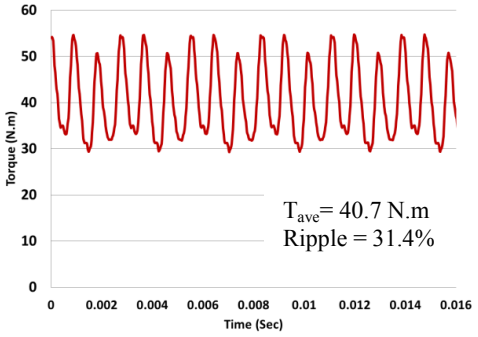

(f) Rotor6

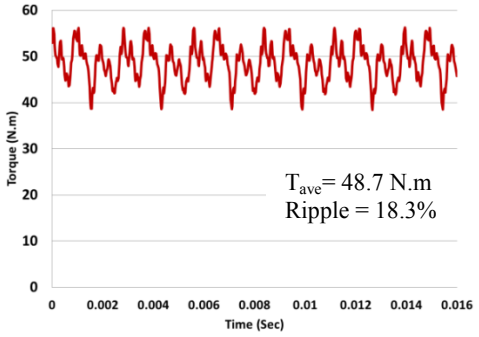

(g) Rotor7

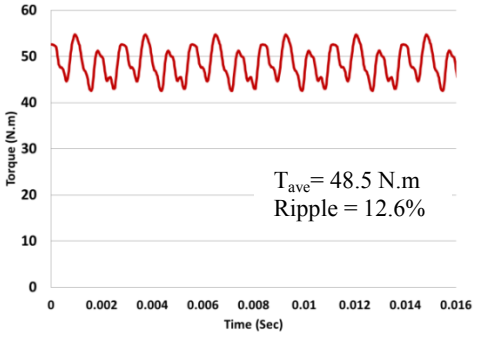

(h) Rotor8-Final Design

Fig 3-11: Output torque generated by each rotor at rated current and maximum torque angle.

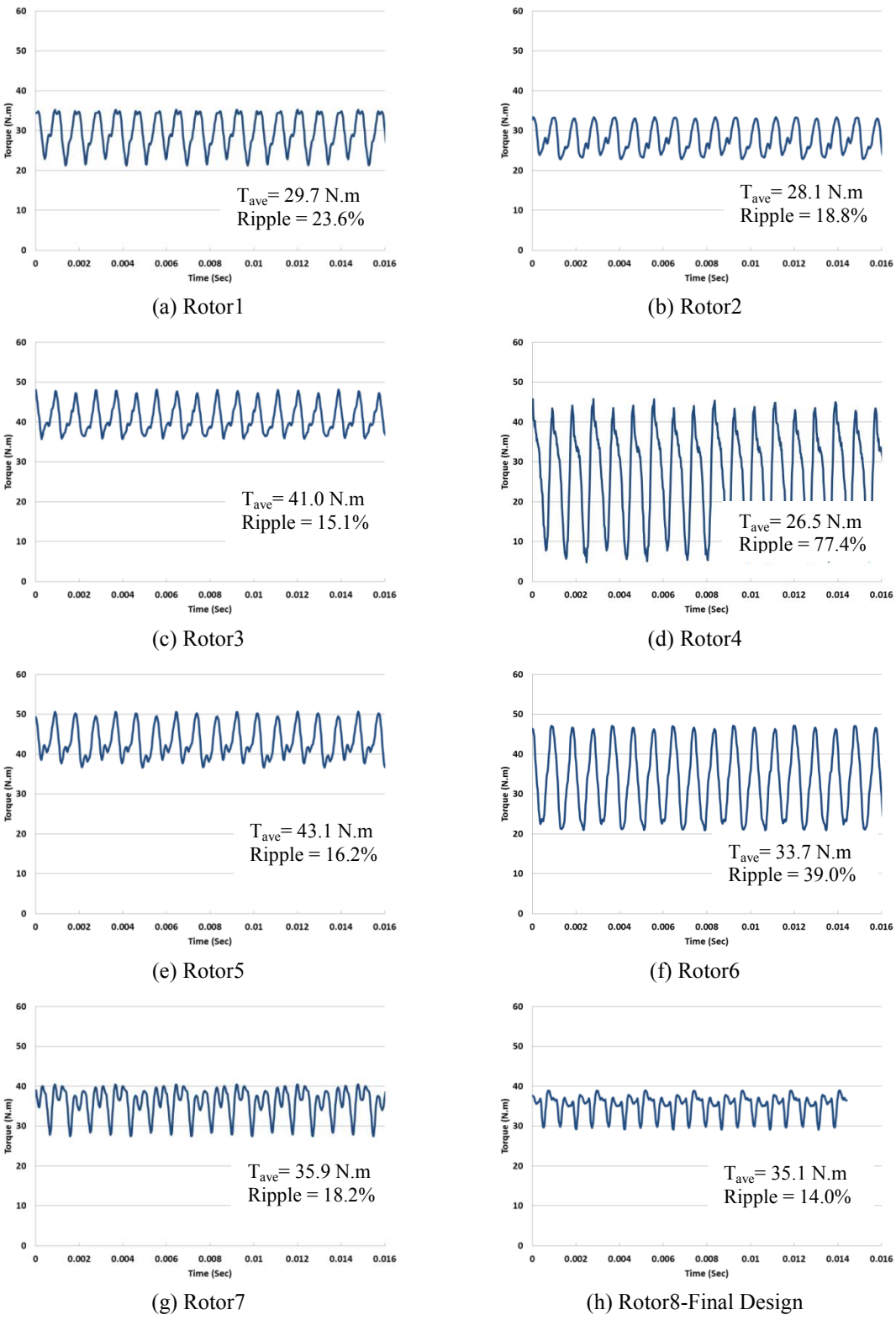

Fig 3-12: Reluctance torque generated by each rotor at rated current and maximum torque angle.

Table 3-4: Performance comparison of the studied rotors.

Rotor type	**Rotor1**	**Rotor2**	**Rotor3**	**Rotor4**	**Rotor5**	**Rotor6**	**Rotor7**	**Rotor8-Final**
PMa-SynRM Max Torque	47.10	49.91	50.55	**57.74**	46.72	54.91	55.92	54.46
PMa-SynRM Cogging Torque	**0.8**	**0.6**	3.2	5.9	1.7	4.3	1.1	**0.8**
Back-EMF Fundamental (pk)	133.7	147.3	141.1	121.1	111.8	132.4	**156.2**	**157.4**
PMa-SynRM Back-EMF THD (%)	26.1	26.8	48.0	42.2	32.0	37.0	40.8	**22.0**
PMa-SynRM Torque (AVE)	40.7	43.8	47.5	36.9	42.8	40.7	**48.7**	**48.5**
PMa-SynRM Torque Ripple (%)	15.3	14.7	14.6	61.1	14.2	34.8	18.3	**12.6**
SynRM Torque (AVE)	29.7	28.1	**41.0**	26.5	**43.1**	**31.4**	**35.9**	**35.1**
SynRM Torque Ripple (%)	23.6	18.8	15.1	77.4	16.2	39.0	18.2	**14.0**
Magnet Utilization (PMa-SynRM to SynRM Torque Ratio)	1.37	**1.56**	1.16	1.39	0.99	1.21	1.36	1.38

IIIF. FEA Analysis of PMa-SynRM and Comparison with Induction Machine

Based on the performance comparison between different rotor geometries, geometry of rotor 8 has been selected for more analysis. After finding the maximum torque angle of the rotor in the magnetostatic analysis using Maxwell 2-D, the transient analysis has been executed to obtain the transient torque and back- EMF of the machine. Because the stator is the same as the induction motor, the current used for excitation is 21A. The speed of the PMa-SynRM is considered to be the synchronous speed, which is 1800 RPM for 4-pole machine supplied at 60Hz.

The stator current is the same in order to keep the copper losses the same as the reference induction motor and to load the windings properly. In addition, comparing the

flux density of the PMa-SynRM and the induction machine at the rated current will be more meaningful.

IIIF1. Flux Density Investigation in Induction Machine and PMa-SynRM

After finding the average torque for the new design, to identify heavy saturation in the cores, the flux density in the rotor and stator core should be studied. In this study, the material used for both SynRM and PMa-SynRM is M-45 steel with the knee point approximately at 1.4 Tesla (the same as the material used in the induction motor).

Fig. 3-13 and Fig.3-14 show the flux line and flux density distribution of the PMa-SynRM-NdFeB and SynRM (magnet-less) at the maximum torque angle. In SynRM, the flux lines are more and the density is higher in some teeth whereas in PMa-SynRM, those are reduced. As a result, less core loss is expected in comparison with the SynRM with the same stator current.

To measure the flux density in the stator yoke, a linear geometry path has been selected in such a way to cross the maximum flux lines in the stator yoke. Fig. 3-15 shows that the flux density in the middle of the stator teeth for SynRM and PMa-SynRM with peak of 1.85 T. For both SynRM and PMa-SynRM the flux density in the stator yoke is studied. Fig. 3-16 shows the flux density variation in the stator yoke in the same geometry path used in induction machine. In this case, PMa-SynRM has an average of 1.65 T and SynRM has 1.75 T in the back iron.

Results show that the flux density in the stator teeth of the PMa-SynRM is high because of the use of magnet in the rotor core but it is not local saturation. The flux density in the PMa-SynRM is higher than the induction machine and hence, the PMa-

SynRM has more torque density. So it is possible to reduce this flux density by decreasing the stator current and maintaining the load torque. Also, in the air gap, the SynRM and PMa-SynRM have higher flux densities compared with the induction motor.

As the rotor of PMa-SynRM has a low core loss and no copper loss, the increased power loss in the stator might be ignored.

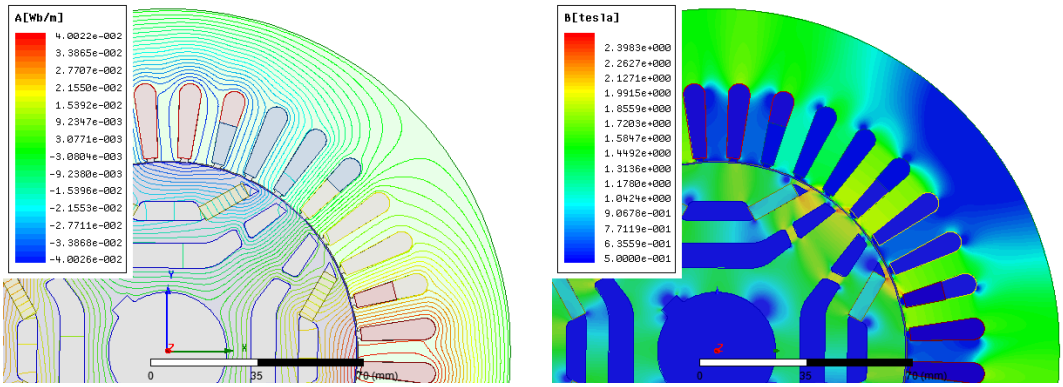

(a) (b)

Fig 3-13: FEA analysis field output on the PMa-SynRM-NdFeB: (a) Flux line, (b) Flux density.

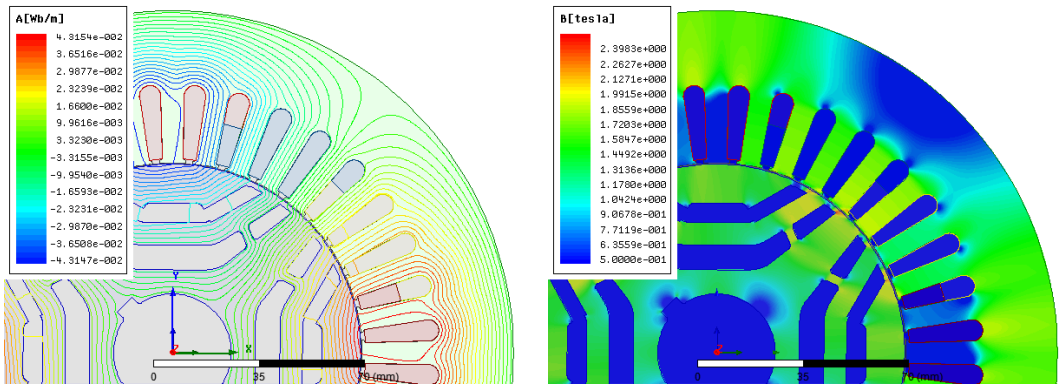

(a) (b)

Fig 3-14: FEA analysis field output on the SynRM: (a) Flux line, (b) Flux density.

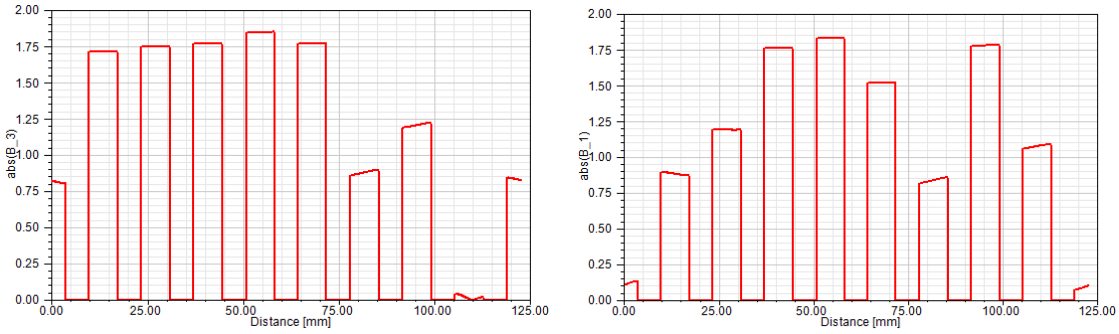

(a) (b)

Fig 3-15: Flux density in the middle of the stator teeth over a pole pitch in: (a) SynRM, (b) PMa-SynRM-NdFeB.

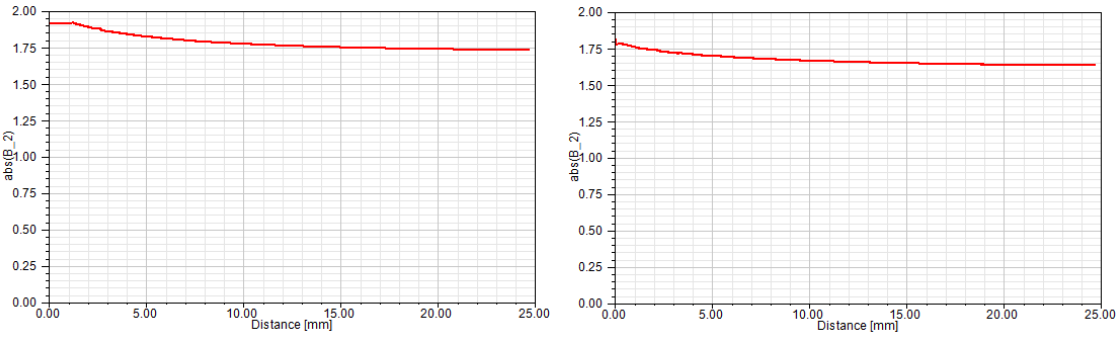

(a) (b)

Fig 3-16: Flux density in the stator yoke in: (a) SynRM, (b) PMa-SynRM-NdFeB.

Table 3-5: Comparison of flux densities of all motors.

Maximum Flux Density	Induction	PMa-SynRM	SynRM
Stator Teeth (T)	1.40	1.85	1.85
Stator Yoke (T)	1.18	1.65	1.75
Air Gap (T)	1.25	1.58	1.49

IIIF2. Output Torque Comparison of the Induction Machine and PMa-SynRM

The output torque generated by optimized PMa-SynRM and the reference induction machine are compared in Fig. 3-17 using the same excitation current (rated condition). It can be seen that the SynRM itself generates more torque than the induction machine and using the permanent magnets has significantly increased the output torque. Based on the results of these studies, the geometry of this PMa-SynRM is selected for fabrication.

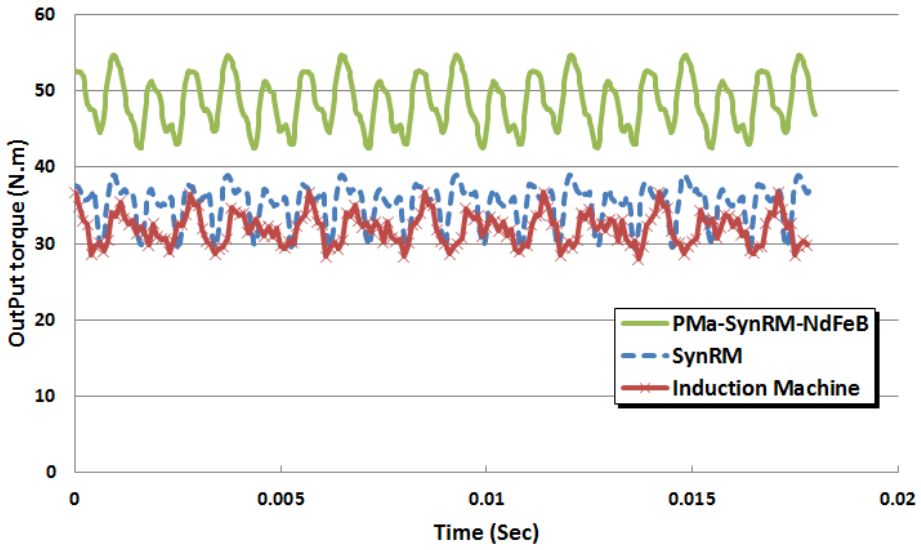

Fig 3-17: Output torque of the compared machines.

IIIG. Optimized PMa-SynRM Rotor Structure

Based on the final optimization results obtained from finite element analysis, the rotor core is fabricated. Fig. 3-18 shows the optimized rotor core geometry and the fabricated one.

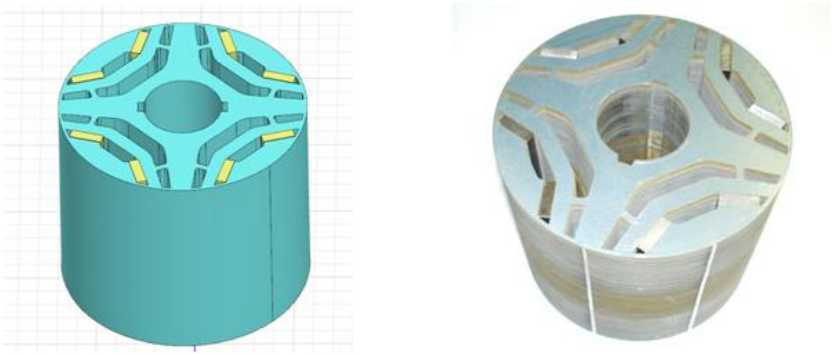

(a) (b)

Fig 3-18: Optimized PMa-SynRM-NdFe: (a) Designed rotor core, (b) Fabricated rotor core.

The magnets for this rotor are 4 inches long (the same as the rotor stack length). In order to place the magnets conveniently, they are fabricated in half-length so that two pieces are inserted in each slot from both sides. Also, using splinted magnets instead of the full size magnet has the benefit of decreasing the magnet loss (due to eddy currents) and due to this; the machine efficiency will increase slightly.

Fig. 3-19 shows the permanent magnets used in the rotor core and the fabricated prototype rotor. The rotor includes the shaft and bearings (the same size of the reference induction machine) and the magnets inside the rotor are secured by aluminum end disks. This rotor is replaced in the NEMA-frame induction machine to complete the PMa-SynRM fabrication.

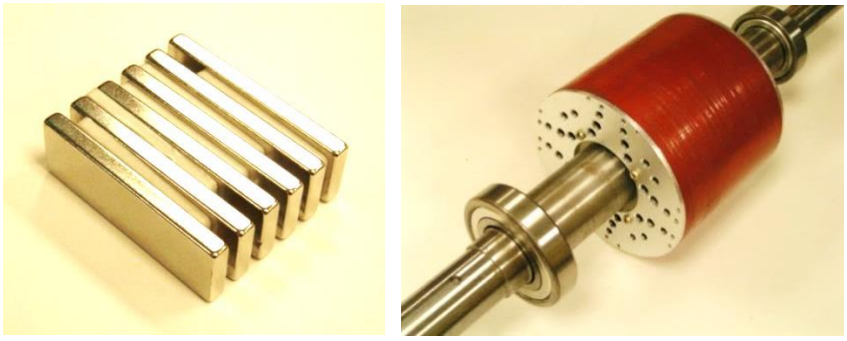

(a) (b)

Fig 3-19: PMa-SynRM rotor: (a) NdFeB magnet blocks installed in the rotor steel core, (b) Fabricated PMa-SynRM rotor with shaft and bearings.

IIIG1. Back-EMF Measurement

The permanent magnets in the rotor generate magnetic flux, which links the stator coils. Fig. 3-20 shows the FEA calculated flux density in the middle of the air gap due to the permanent magnets.

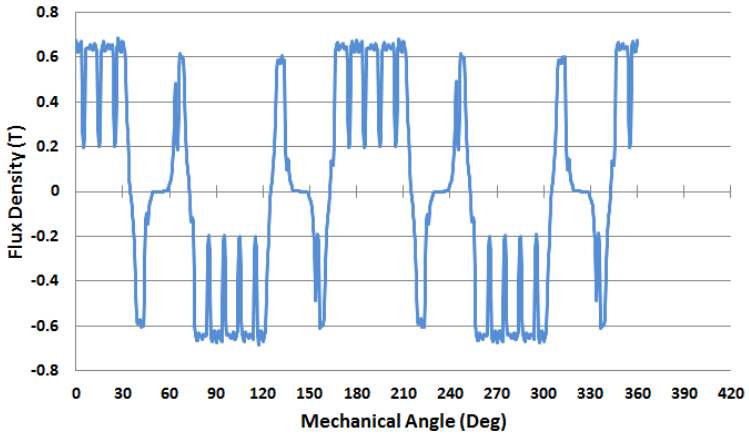

Fig 3-20: Flux density in the middle of the air gap due to the NdFeB magnets.

The flux linkage has significant effect on the current angle calculation mentioned before. Obtaining this parameter can simply be done by measuring the back-EMF of the machine and using (3-3).

A DC machine is used in the test bed to rotate the PMa-SynRM-NdFeB and the terminal voltage of the machine is measured. Fig. 3-21 shows the waveform of the induced line to line voltage in the stator of the PMa-SynRM at 1800 RPM. It can be seen that the voltage has a sinusoidal waveform due to the distributed winding of the stator. Because of the distribution form of the stator winding, it was expected to have a low total harmonic distortion and a high fundamental component in back-EMF. Fig. 3-22 shows the harmonic spectrum of the back-EMF (the voltages are scaled down by the differential probe used in the test).

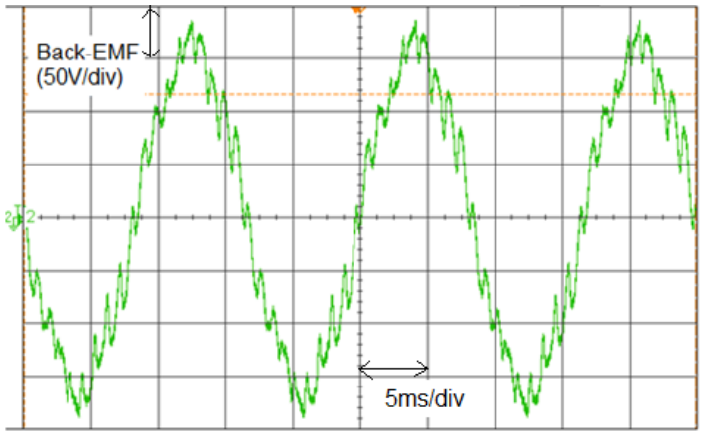

Fig 3-21: Measured back-EMF waveform of PMa-SynRM-NdFeB at 1800 RPM.

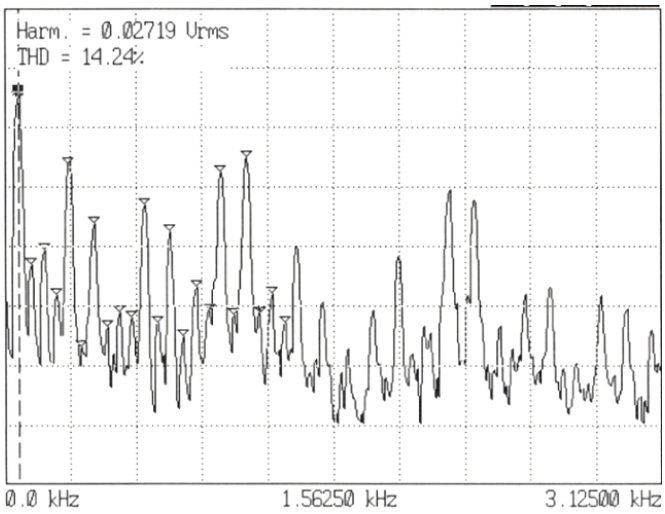

Fig 3-22: Harmonic spectrum of the back-EMF voltage at 1800 rpm (20dB/div).

The spectrum analyzer shows that the THD of the back-EMF is 14.2%, which is significantly low compared to the motors with concentric winding. The FFT spectrum obtained from the FFT measurement of the oscilloscope shows 16% of THD. Table 3-6 shows that the major harmonics of the back-EMF are 5^{th}, 17^{th}, and 19^{th}. The harmonic spectrum shown in Fig. 3-23 exhibits that the major harmonics in the back-EMF are $18n\pm1$ ($n=1, 2, \ldots$), which are the results of the existence of the harmonics in the winding function and air-gap function.

The back-EMF obtained from the FEA is compared with the experimental measurement in Fig. 3-24. It is obvious that the back-EMF calculated by FEA is very close to actual back-EMF and the slight difference is because of the calculation method used in FEA. The FEA measures the flux linkage of the coil and calculates the flux variation in time to obtain the back-EMF; therefore the geometry selected by the

software to find flux passing the coil can affect the measurement. Also the harmonic content could be affected by the FEA flux measuring method in the software.

Table 3-6: Harmonic components of the back-EMF.

Harmonics	Amplitude Experiment	
	RMS (V)	Per unit (%)
Fundamental (1st)	162.0	100
5	11.7	7.23
7	1.1	0.67
11	2.0	1.21
13	1.1	0.69
17	6.9	4.27
19	20.9	12.9
35	4.7	2.9
37	2.6	1.62
53	2.3	1.4
55	0.3	0.16

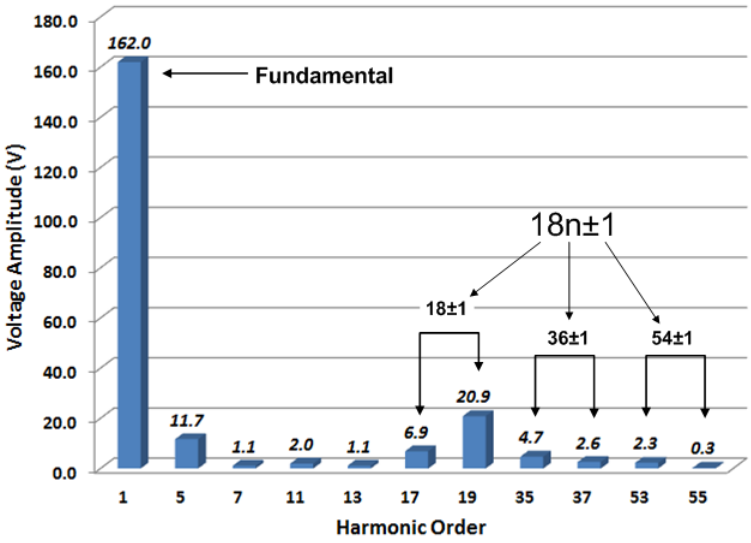

Fig 3-23: Harmonic spectrum of the measured back-EMF.

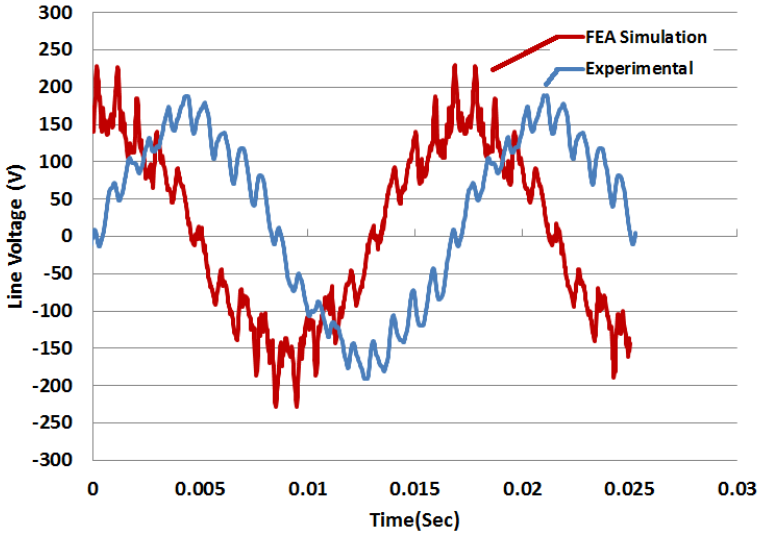

Fig 3-24: Comparison of FEA and measured back-EMF of PMa-SynRM-NdFeB at 1800 RPM.

IIIH. Skew Effect on PMa-SynRM NdFeB

Skewing the rotor is a conventional way to reduce the torque ripple in each electric machine. In addition, with a proper skew angle, the cogging torque can be completely eliminated.

In order to skew a PM machine in manufacturing process, the permanent magnet pieces have to be skewed. This process will increase the cost of manufacturing and for low cost machine driving a fan or a pump it may not be justified. Achieving a low ripple torque is possible by step skewing. In this section by using FEA tool and sliced machine model, the effect of rotor skewing on the torque ripple, cogging torque, and the back-EMF is studied.

To obtain the torque and the back-EMF performance of the machine with skewed rotor, a discrete skew form is used. Fig. 3-25 shows a visualization of the skew study.

Considering Θ=0° as the reference, the rotor can be initially displaced around the reference by resolution of -γ- in positive and negative direction. By obtaining the performance of the machine in each step and averaging the results in skew range the final torque and back-EMF will be calculated over the desired skew angle (eq. 3-15 and 3-16). Assuming a resolution of 0.5° and skew angle of 10°, the skew step (k_γ) is 20 steps, which will be applied 10 steps positive and 10 steps negative. In practice, the machine then can be made of 21 slices.

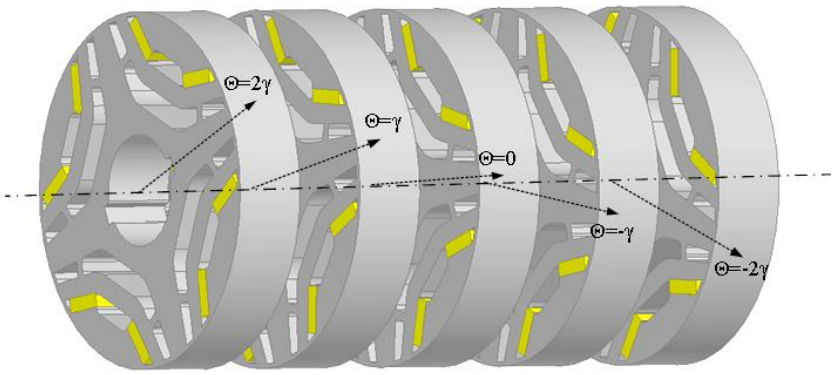

Fig 3-25: Model used for analysis of the skew effect on torque and back-EMF.

$$k_\gamma(Skew\ Step) = \frac{Skew\ Angle}{\gamma} \tag{3-13}$$

$$N_{slice} = k_\gamma + 1 \tag{3-14}$$

$$EMF_{average} = \frac{1}{N_{slice}} \sum_{n=-int(k_\gamma/2)}^{int(k_\gamma/2)} EMF(initial\ \theta = n * \gamma) \tag{3-15}$$

$$T_{average} = \frac{1}{N_{slice}} \sum_{n=-int(k_\gamma/2)}^{int(k_\gamma/2)} T(initial\ \theta = n * \gamma) \tag{3-16}$$

IIIH1. Effect of Skewing on Cogging Torque

By applying this method, the cogging torque of the PMa-SynRM-NdFeB is calculated and shown in Fig. 3-26. As it is expected, skewing the rotor reduces the cogging torque of the machine. Since the stator has 36 slots (10° slot openings) skewing the rotor with 10° results in the minimum cogging torque (close to zero).

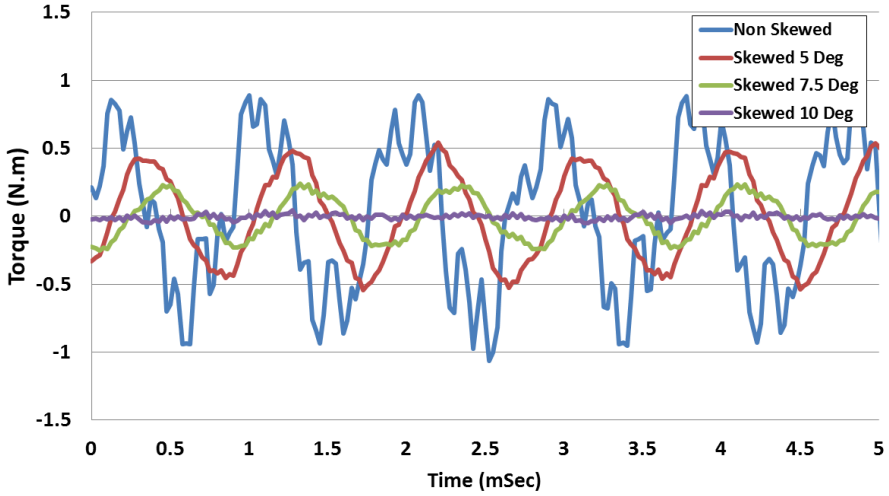

Fig 3-26: Skew effect on cogging torque of the PMa-SynRM.

IIIH2. Effect of Skewing on Back-EMF

Using (3-15), the back-EMF of the skewed rotor is calculated for 10° skew angle (in this study the actual measurement is used). Fig. 3-27 compares both skewed and non-skewed rotor back-EMF waveforms (for clear comparison the waveforms are shifted intentionally). It can be seen that even the discrete skew reduces the harmonics of the back-EMF without significant effect on the fundamental component. The harmonic spectrums of the back-EMFs are shown in Fig. 3-28. The harmonics such as 17^{th}, 19^{th},

35th, and 37th are reduced significantly but the fundamental is reduced slightly. The back-EMF THD is reduced from 15.9% to 6.2%.

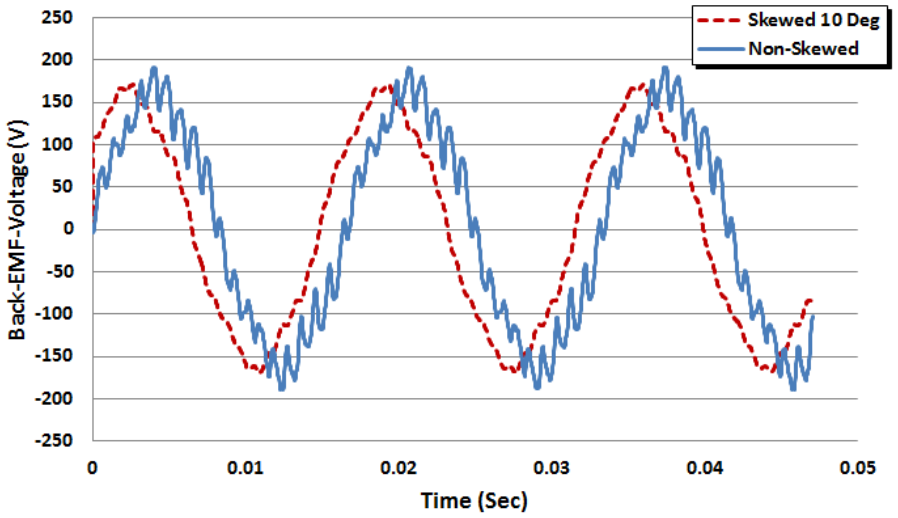

Fig 3-27: Skew effect on the back-EMF (waveforms shifted intentionally).

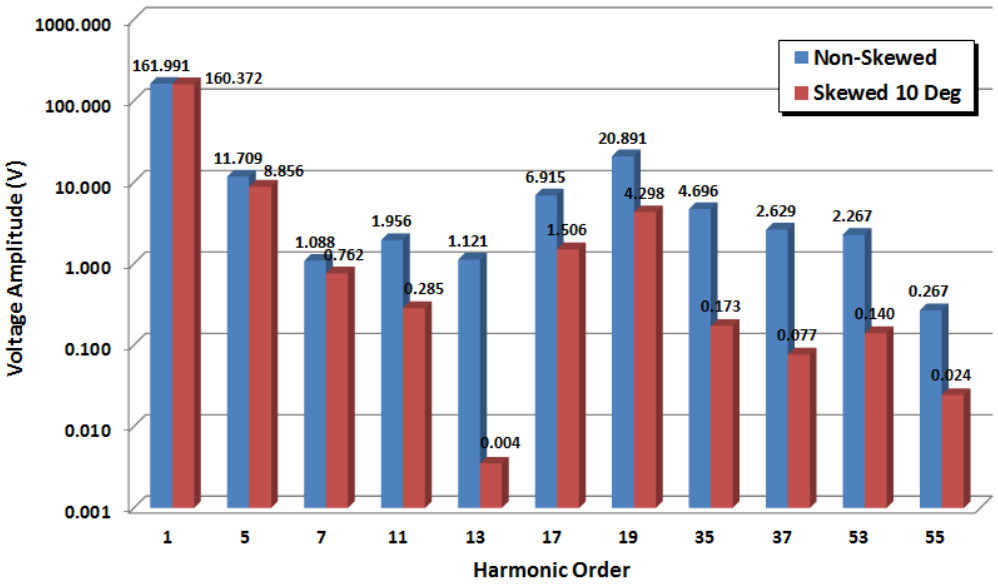

Fig 3-28: Effect of the skew on the harmonic spectrum of the back-EMF.

IIIH3. Effect of Skewing on Steady State Torque

Again, the same method is used to measure the ripple torque of the machine under the maximum load condition. Table 3-7 includes the average torque calculated for the PMa-SynRM-NdFeB with different rotor skew angles. It can be seen that skewing the rotor by 10 degree reduces the ripple significantly and skewing more than 10 degree does not improve it. Also, it can be seen that the skewed rotor has slightly lower average torque but the torque ripple is reduced from 17% to 4%. Fig. 3-29 shows the comparison of the output torque in non-skew and skewed rotor. As it was mentioned before, this method uses discrete form of calculation and a fully skewed rotor with skewed magnets will have less ripple torque.

Table 3-7: Skew angle effect on PMa-SynRM-NdFeB and SynRM torque output.

Skew angle (Deg)	**PMa-SynRM-NdFeB**		**SynRM**	
	Average (Nm)	**Ripple (%)**	**Average (Nm)**	**Ripple (%)**
Non-Skewed	48.5	12.8	35.1	10.8
5	48.05	8.3	34.7	6.7
7.5	47.8	5.8	34.5	5.1
10	**47.46**	**4.1**	**34.1**	**3.6**
12.5	47.01	5.2	33.6	4.9
15	46.56	5.2	33.0	4.4

Fabrication of a skewed SynRM core can be easy and cheap since there is no magnet inside the rotor. Therefore, the same study is done on the SynRM core to observe the effect of skewing on the SynRM rotor with the specified NEMA frame stator. Table 3-7 includes the average torque and the torque ripple of the SynRM with different skew angles. The comparison shows that skewing the SynRM rotor by 10 degree reduced the

ripple torque up to 80% while the average torque has a slight drop. Fig. 3-29 also shows the transient torque of the SynRM with non-skewed rotor and 10 degree skew.

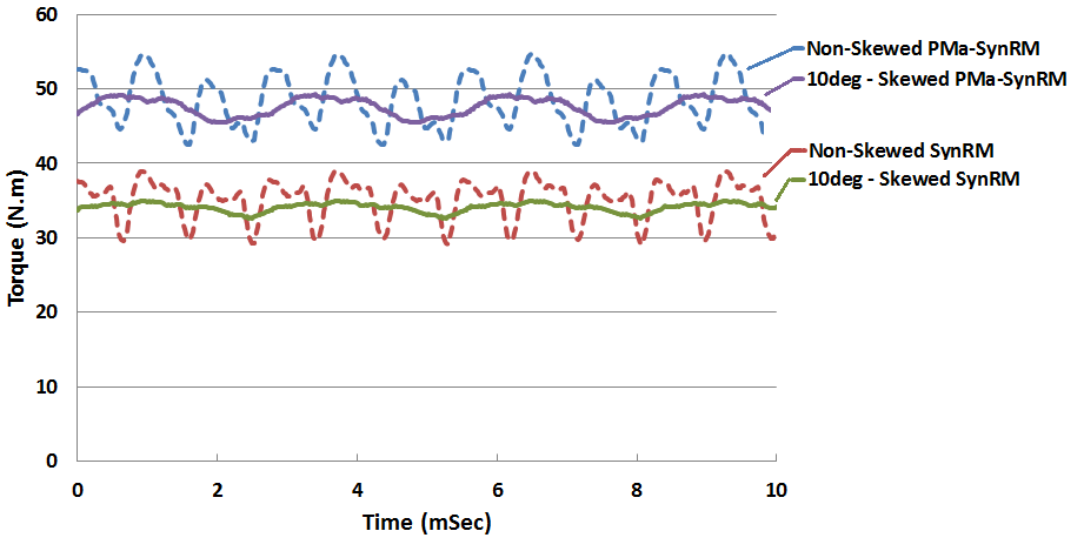

Fig 3-29: Skew effect on the output torque of the machines.

IIII. Effect of the Magnet Variation on the Flux Linkage

The permanent magnet type has a significant effect on the performance of the PMa-SynRM. Therefore, the NdFeB magnets are removed from the rotor to form a SynRM core shown in Fig. 3-30(b). The SynRM core is not optimized for the stator but its performance will be compared with the original PMa-SynRM machine. Another PMa-SynRM rotor core is constructed by replacing the NdFeB magnets with ferrite magnets. This rotor, named as C8-R1, is shown in Fig. 3-30(c). Also, extra ferrite magnets are added to the C8-R1 rotor on the q-axis and a rotor with higher ferrite quantity is formed. This rotor, named as C8-R2, is shown in Fig. 3-30(d). Another option is to add one magnet piece on the q-axes in the second air barrier (forming C8-R3 rotor); however, the

FEA analysis has illustrated that the flux density in the air gap stays the same and the flux linkage of the machine stays the same as C8-R2. The FEA comparison of C8-R2 and C8-R3 rotors are included in this section.

(a) (b) (c) (d)

Fig 3-30: Studied rotors: (a) Original rotor with NdFeB magnets, (b) Magnet-less rotor core, (c) PMa-SynRM-C8-R1, (d) PMa-SynRM-C8-R2.

IIII1. Air Gap Flux Density and Back-EMF Variation in Different PMa-SynRM Rotors

Permanent magnet with higher remanent flux density will generate higher flux density in the air gap resulting significant flux linkage in the machine. Fig. 3-31 shows the flux density of the air gap for the different rotor formations (for better waveform illustration different initial rotor positions are applied). The NdFeB rotor generates high flux density in the air gap with fundamental of 0.46 T, and C8-R1, C8-R2 generate 0.21 T and 0.11 T, respectively. In this machine, replacing NdFeB with ferrite has reduced the air gap flux density by 76%, whereas the remanent flux density of the ferrite is 64% less. The reason of this significant difference is the leakage of a significant portion of the flux generated by the permanent magnet through the ribs in the C8-R1 rotor. The back-EMF measurement is shown in Fig. 3-32.

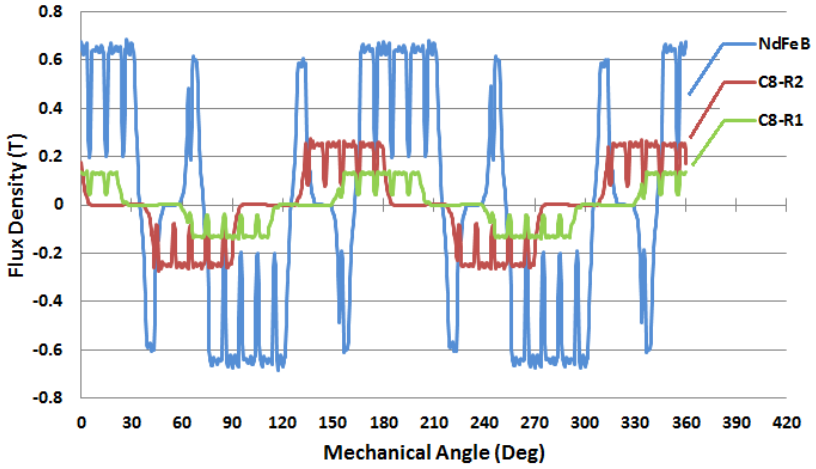

Fig 3-31: Flux density distribution in the air-gap of the PMa-SynRMs in no load condition.

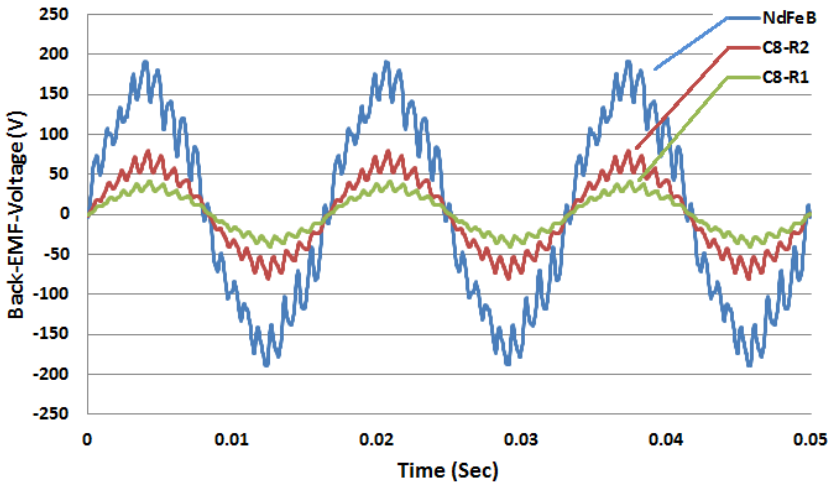

Fig 3-32: Back-EMF waveforms of the PMa-SynRMs at 1800 RPM.

Fig. 3-33 shows the flux line distribution in different rotors and the flux leakage through the ribs in each case. Fig. 3-33(a) shows the rotor with NdFeB magnet and illustrates less than 20% flux leakage; whereas using ferrite magnets, more than 45% of the generated flux bypasses through the ribs (C8-R1 case shown in Fig. 3-33b) and

hence, those flux lines will not link the stator coils. This is because the width of the ribs is optimized for the NdFeB magnet and it is wide for ferrite, allowing a significant portion of the flux generated by ferrite magnets to bypass through it. By comparing the back-EMF of the NdFeB version with C8-R1 it is obvious that although the magnet quantity is the same in both machines the flux linkage in the NdFeB machine is 2.5 times higher; therefore it is expected that the PMa-SynRM with ferrite magnets will have less toque density and power factor.

Comparing the C8-R1 and C8-R2 version shows that although the extra magnet is only 50%, the flux linkage is doubled. Since the ribs are already saturated by the flux generated by the first set of ferrites, the flux generated by the second set of magnet passes to the stator and the extra magnet is fully utilized, which is shown in Fig. 3-33(c). This effect causes the flux linkage to increase up to 100% with only 50% increase in the magnet mass.

Placing magnets on the second barrier on q-axis (shown as B in Fig. 3-33d) has been studied. The flux distribution shows that the extra magnet on the second barrier will not improve the flux linkage therefore it is not useful to add this set of magnets to the rotor and this case is not practiced.

The back-EMF induced in the stator winding is measured by rotating the rotor with a certain speed using a primary mover. Then, with the obtained back-EMF, the flux linkage of the inserted permanent magnets can be calculated using (3-3). Table 3-8 includes the fundamental of the measured back-EMF and the flux linkage of the machines.

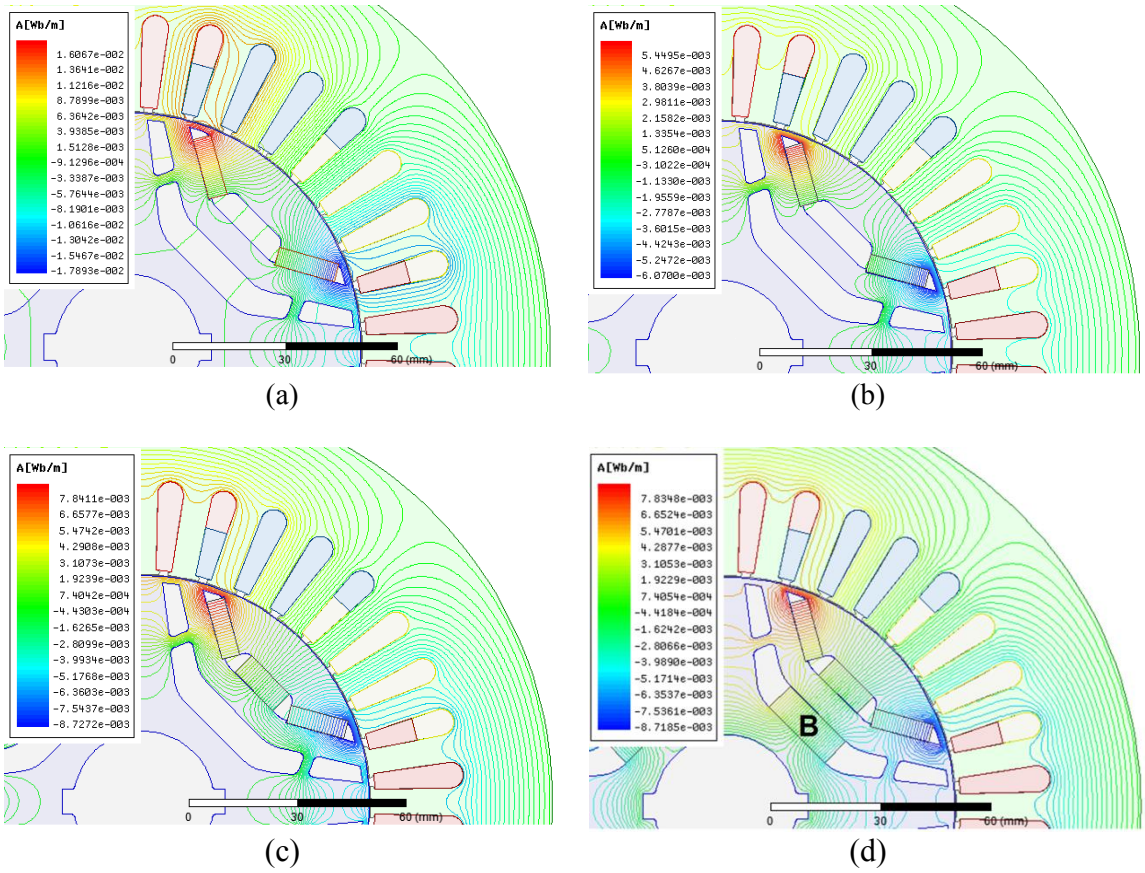

Fig 3-33: Magnetic flux line distribution in PMa-SynRMs generated by the permanent magnets in the rotor: (a) NdFeB42, (b) C8-R1 rotor, (c) C8-R2 rotor, (d) C8-R3 rotor (not fabricated).

Table 3-8: Back-EMF measurement and the flux linkage of each machine.

Machine type	**Magnet Type**	**Line Back-Emf (V) at 1800 rpm**	**λ_{PM} (wb)**
SynRM	0	0	0
PMa-SynRM-C8-R1	Ferrite-C8	23.1	0.05
PMa-SynRM-C8-R2	Ferrite-C8	46.0	0.1
PMa-SynRM-NdFeB	NdFeB42H	115.9	0.25

The back-EMF of the PMa-SynRM with NdFeB magnet is higher than the one with ferrites. This is due to the higher flux density of the NdFeB magnets. Comparing the flux linkage of the NdFeB rotor with C8-R2, it can be seen that the magnet quantity is the same in both machines; but the flux linkage in the NdFeB machine is 2.5 times higher; therefore it is expected to have less toque density and power factor for the PMa-SynRM with ferrites. Also comparing the C8-R1 and C8-R2 version shows that although the addition magnet is only 50%, the flux linkage is doubled. The reason is that a significant amount of the flux generated by the permanent magnet is leaking through the ribs in the rotor and is not linking any coil in the stator.

Also, comparing the flux density in the stator back iron shows the above explained effects. The magnetic flux densities of the PMa-SynRM with different rotors are shown in Fig. 3-34 and the saturation in the ribs can be seen in all cases. Also it shows that the C8-R3 rotor does not generate more flux in the stator than the C8-R2 rotor (less magnets).

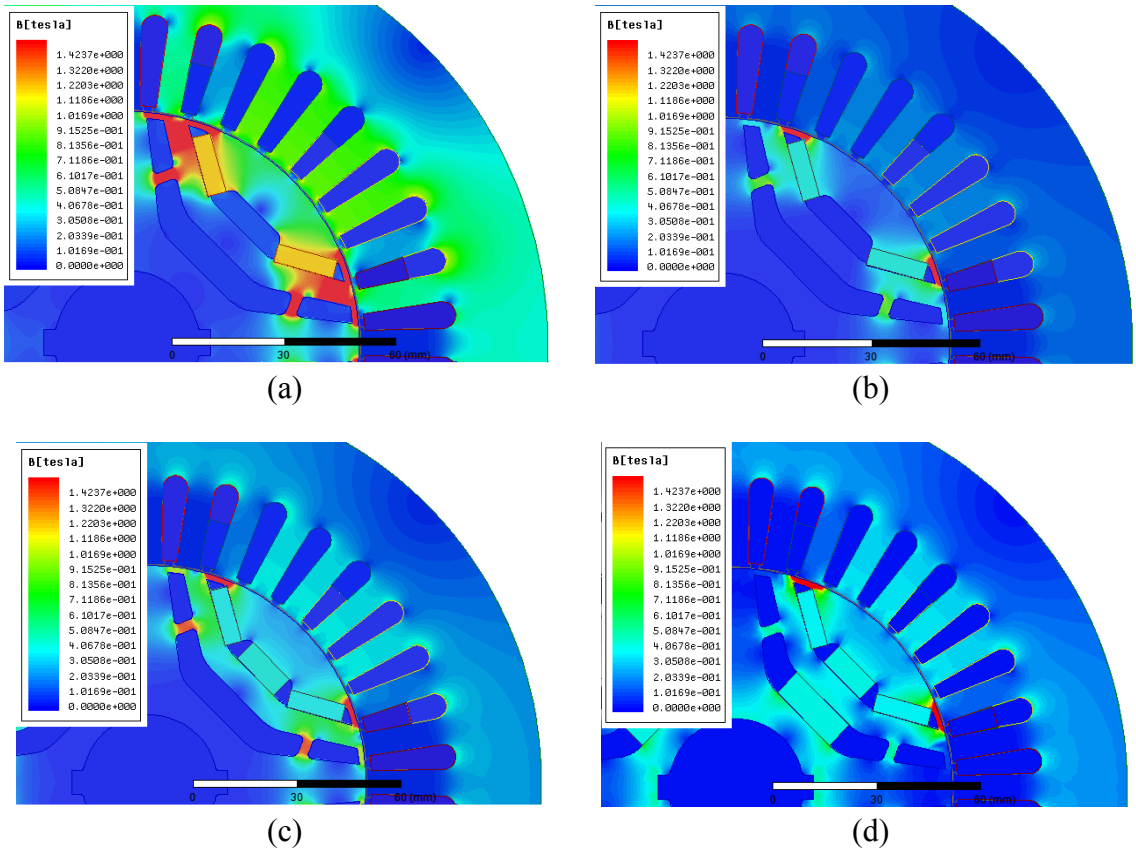

Fig 3-34: Magnetic flux density in PMa-SynRMs: (a) NdFeB rotor, (b) C8-R1 rotor, (c) C8-R2 rotor, (d) C8-R3 rotor.

IIII2. FEA of the PMa-SynRM with Different Magnet Type and Quantity under the Rated Load Condition

The FEA analysis of each machine is performed to obtain the current needed to generate the rated torque matching the induction machine, which is about 30N.m. Fig. 3-35 and Fig. 3-36 show the flux density and flux line distribution in each machine at the rated torque condition. In each case, the excitation current is adjusted to generate 30 N.m torque. Table 3-9 includes the excitation current level of each machine. It can be seen that the PMa-SynRM-NdFeB needs the least current since it has highest torque density and the SynRM needs the most. Also, the flux density in the stator yoke of the PMa-

SynRM-NdFeB is lower according to Fig. 3-35 and this will result in less core loss in the stator. Therefore, higher efficiency is expected in NdFeB case when operated under the rated torque condition.

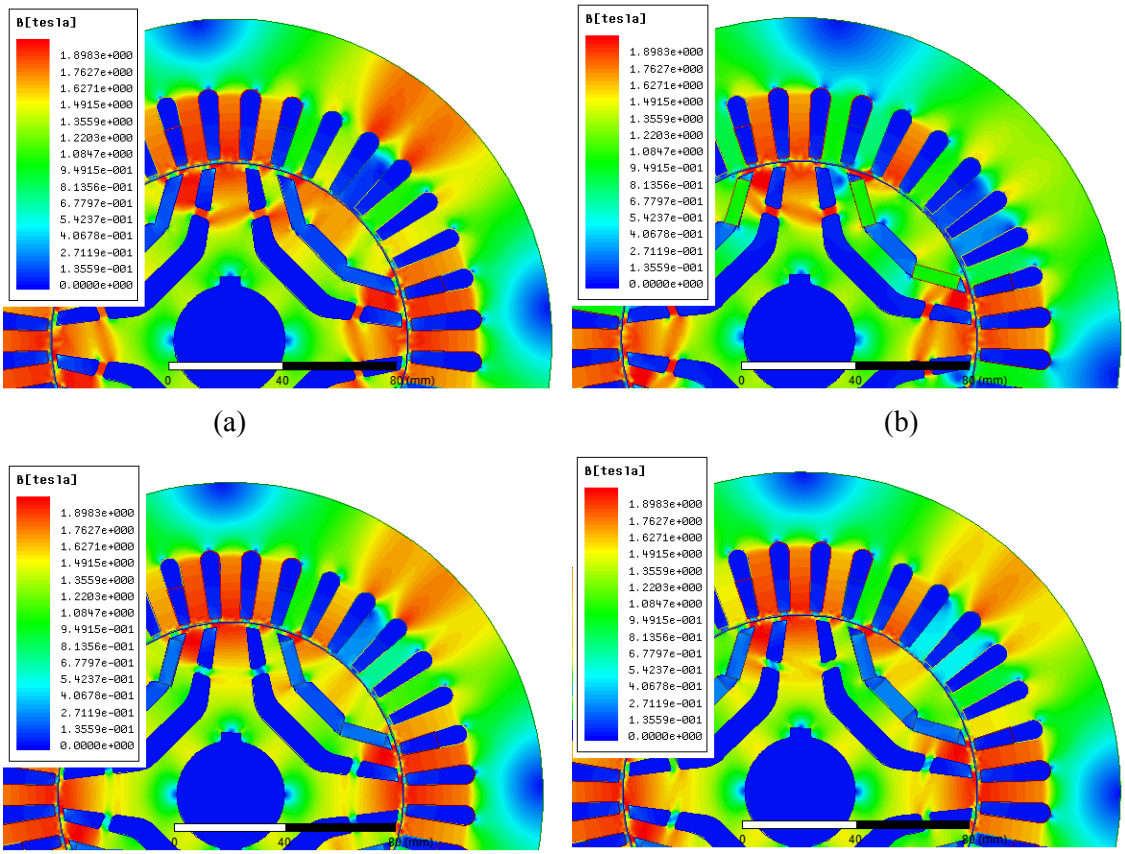

Fig 3-35: Flux density of the machines in rated torque condition: (a) SynRM, (b) PMa-SynRM-NdFeB42, (c) PMa-SynRM-C8-R1, (d) PMa-SynRM-C8-R2.

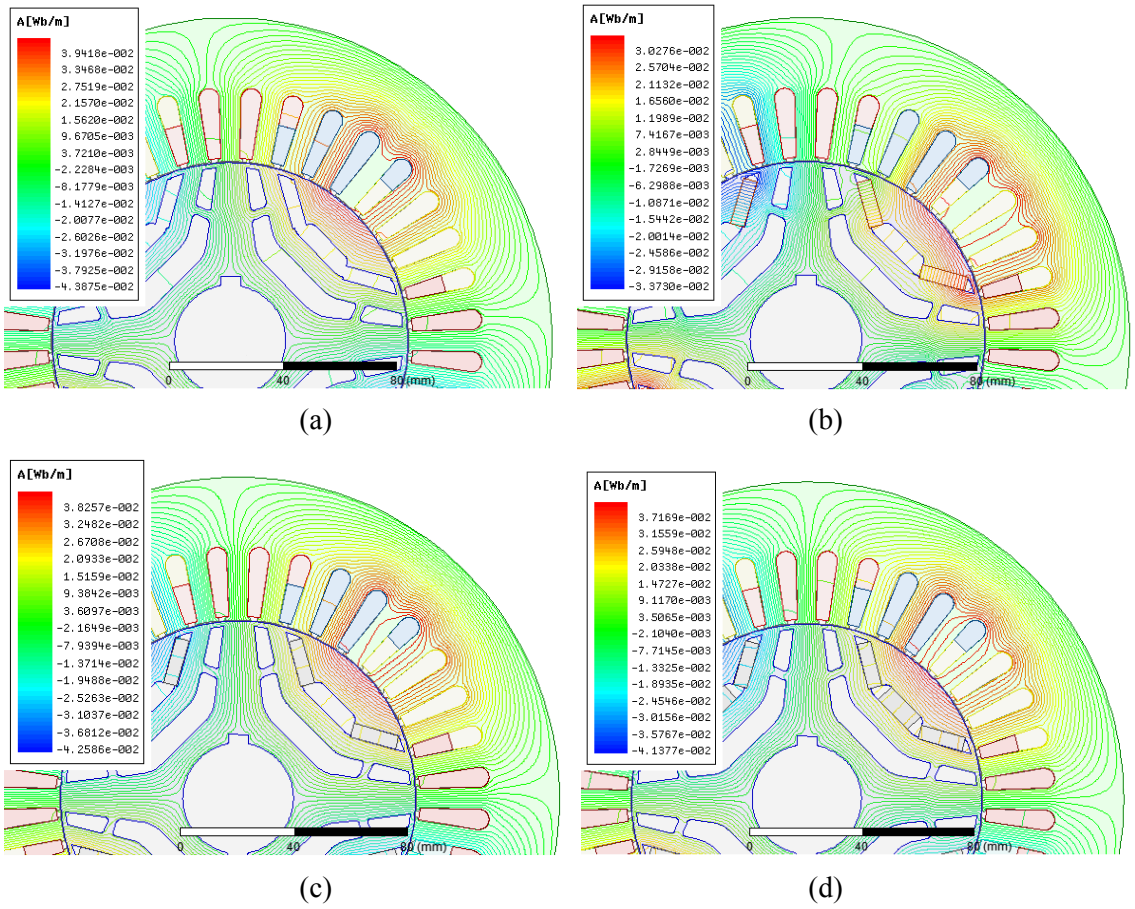

Fig 3-36: Flux line distribution of the machines in rated torque condition: (a) SynRM, (b) PMa-SynRM-NdFeB42, (c) PMa-SynRM-C8-R1, (d) PMa-SynRM-C8-R2.

Table 3-9: Excitation current in rated torque condition of each machine.

Machine Type	**Line current (A)**
PMa-SynRM-NdFeB	16.5
PMa-SynRM-C8-R1	20
PMa-SynRM-C8-R2	18.8
SynRM	21.5
Induction Machine	21

The above results show that the PMa-SynRM-NdFeB needs 15% less current to drive 30N.m load, compared to the original induction machine. Therefore, the temperature of

the windings in PMa-SynRM will be less and longer winding isolation life will be expected for this machine.

IIII2a. Demagnetization Effect

One of the major problems in the permanent magnet machine is the demagnetization of the magnets due to the high flux opposing the permanent magnets flux orientation, which generally happens in the field weakening operation region (constant power region). In this study the PMa-SynRM machine operates in the constant torque region but the q-axes flux opposes the magnets flux and it can demagnetize the magnets. Therefore, the flux density inside the permanent magnets is studied in PMa-SynRM using the FEA analysis. For each machine with different permanent magnet type (NdFeB and ferrite) the flux density is shown in Fig. 3-37. The flux density inside the NdFeB magnet remains above 0.9 T. The B-H curve of the NdFe42SH indicates that operating at 0.4 T is above the irreversible demagnetization; therefore in this design a lower temperature NdFe42 such as grade M (operating at 100 °C) can be used without any demagnetization risk. For the ferrite-C8 magnets the knee point is around 0.1 T at 20 °C and the FEA shows that the flux density inside the magnets are above 0.1 T (knee point of C8). Hence, the magnets are operating in a safe region and above the irreversible demagnetization. Moreover, the temperature inside the machine is above the room temperature therefore the stator current cannot demagnetize the ferrites.

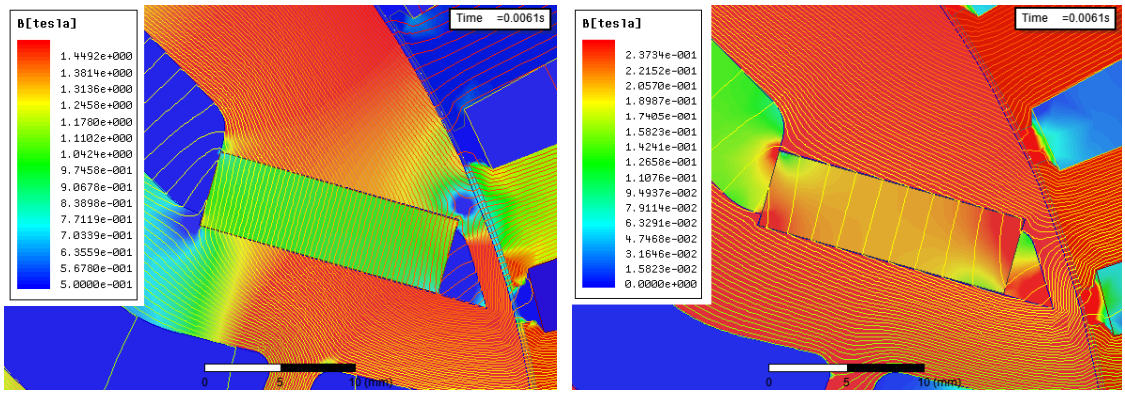

(a) (b)

Fig 3-37: Flux density distribution in the permanent magnets in PMa-SynRM under the rated load condition: (a) NdFeB magnets, (b) Ferrite magnets.

IIII2b. Temperature Effect on the Magnet Flux Density

In the permanent magnet machines, the temperature has significant effect on the flux density and the remanent flux density drops at higher temperature. In this study to investigate the effect of the temperature on the magnets and observe the performance of the designed PMa-SynRMs, temperature is monitored using sensors installed inside the machine. For each PMa-SynRM, the back-EMF of the machine is compared before and after operating under full current. Fig. 3-38 shows the effect of the temperature on the back-EMF with NdFeB and ferrite magnets.

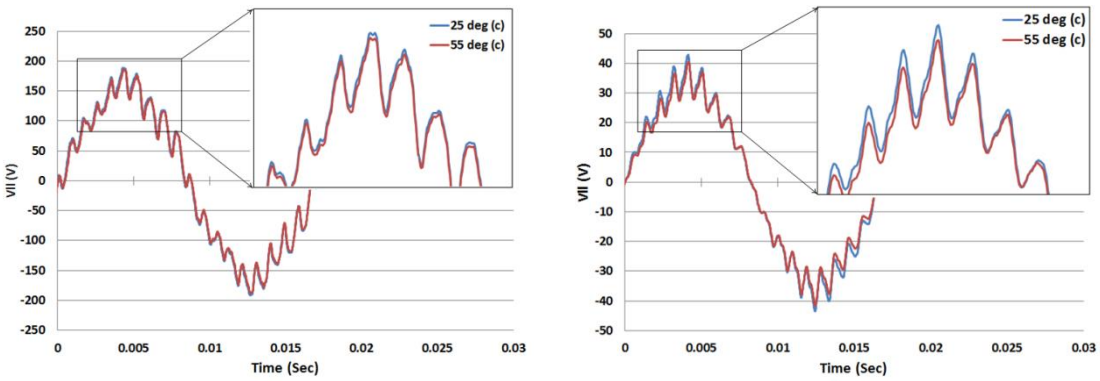

(a) (b)

Fig 3-38: Effect of the temperature on the back-EMF of the machines: (a) PMa-SynRM-NdFeB and (b) PMa-SynRM-C8R1.

For NdFeB magnets the back-EMF is reduced about 1% and for ferrite the back-EMF drop is about 4%. According to the measured parameters, it can be concluded that both NdFeB and ferrite are suitable permanent magnet options for PMa-SynRM in this application due to a very low effect of the temperature on the magnets in this application.

IIIJ. Material Consumption

One of the major items in comparison between electric motors is comparing the material consumption in the motors. As mentioned before, the PM-SynRM uses the same stator frame and stator winding used in the induction motor and other mechanical dimensions are the same. Since the stator lamination and winding configuration are the same in both motors, we just need to compare the rotor material used in both machines.

Table 3-10 includes the material consumption of the machines obtained from RM-expert and Maxwel-2D. Appendix C includes the model and the information used in material consumption estimation.

Table 3-10: Material consumption and weight of main components.

Item	IM	PM-SynRM		
		NdFeB	C8-R1	C8-R2
Stator Copper Weight (kg)	7.2	7.2	7.2	7.2
Stator Core Steel Weight (kg)	17.1	17.1	17.1	17.1
Rotor Core Steel Weight (kg)	7.0	5.8	5.8	5.8
Rotor Aluminum Weight (kg)	1.24	N/A	-	-
NdFeB (kg)	-	0.48	-	-
Ferrite (kg)	-	-	0.31	0.47
Shaft and Bearings (kg)	4.2	4.2	4.2	4.2
Total Rotor Weight (kg)	12.4	10.5	10.3	10.5

By comparing the material consumption, it can be seen that the weight of the PMa-SynRM rotor with NdFeB magnets is 15% less than the rotor of the induction machine. Therefore, longer bearing life and less maintenance cost are expected for the PMa-SynRM. Also, the mass of the NdFeB magnet is only about 8% of the total PMa-SynRM rotor weight, which indicates that the permanent magnet quantity used in the machine is significantly low.

IIIK. Conclusion

In this chapter, the procedure to optimize a two-barrier PMa-SynRM was presented. According to the FEA results, it is shown that it will be possible to use the stator of the induction machine and its rated excitation current to achieve a PMa-SynRM design with acceptable performance. The torque generated by the PMa-SynRM-NdFeB is higher, which means in the same operating load, the PMa-SynRM will need less current and will operate with higher efficiency due to the less stator loss and zero rotor copper loss. The fact that the PMa-SynRM needs less current to drive the same load as the induction

machine shows that the temperature of the winding will be less; therefore the life of the winding will be longer in PMa-SynRM. Also, it is shown that skewing the PMa-SynRM rotor will reduce the cogging torque and torque ripple significantly, with slight drop in the average torque. In addition, the back-EMF has lower THD compared to the non-skewed rotor.

Using ferrite magnet is also investigated and the FEA shows that it is possible to use this type of magnet in the same geometry and the PMa-SynRM with ferrite magnets generates higher torque than the reference induction machine without any demagnetization.

Finally, the mass comparison shows that the PMa-SynRM machine with both NdFeB and ferrite magnet has less weight compared to the induction machine and that will result in less bearing maintenance cost in the machines life time.

CHAPTER IV

DESIGN EVALUATION*

IVA. Introduction

To verify the prototype design and run the machine a test setup including necessary hardware and control software has to be setup. The hardware includes the motor, test bed and the drive circuit. The control software is the developed on a DSP platform based on TI-TMS28F335. In this chapter PMa-SynRM model and the developed control scheme is presented along with the measurement methods used to obtain the machine parameters used in the control scheme.

IVB. Drive Circuit

To drive the PMa-SynRM an IGBT based voltage source inverter is used according to the schematic shown in Fig. 4-1. The gate commands are generated by DSP and a signal conditioning circuit is used to pull up the DSP level signal to higher level for controlling the switches. The same as the most PM synchronous machines, to drive the PMa-SynRM a field oriented vector control has been considered.

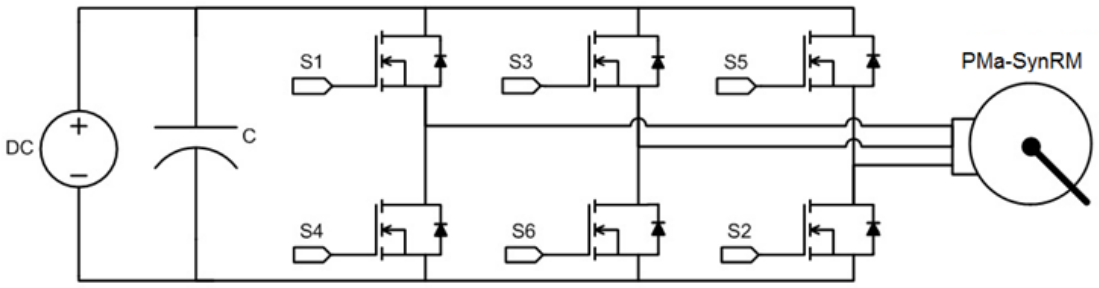

Fig 4-1: IGBT based voltage source inverter.

To drive the designed PMa-SynRM, the embedded Maximum Torque per Ampere (MTPA) control strategy in Field Oriented Vector Control (FOC) is considered. In this method of control, it is possible to control the field and torque component of the current, therefore the direct torque control will be achieved. Since the rated current of the machine is already determined, MTPA can be used to develop the maximum torque without exceeding the rated current. To develop this control method, the mathematical model of the machine has to be studied to identify the necessary parameters needed for control purposes.

IVC. PMa-SynRM Mathematical Model

To develop a control program and explain the effect of each parameter on the performance of the PMa-SynRM, it is necessary to study the model of the machine. For the vector control purposes, the equivalent circuit of the machine is usually modeled in two axes reference frame (direct and quadrature axes).

Because a PMa-SynRM is constructed by embedding permanent magnets in a SynRM rotor core, the d-q model of a SynRM machine could be used to model the PMa-

SynRM by considering the effect of the embedded permanent magnets in the rotor. Fig. 4-2(a) shows the d-q axes alignment of the SynRM. Usually the d-axis is defined on the axis with higher tendency to align with the stator magnetic field. In SynRM the d-axis is the axis with the less magnetic reluctance and q-axis is the path with high magnetic reluctance (passing the air barriers). By placing the magnets in the rotor, the PMa-SynRM structure with axis defined in Fig. 4-2(b) will be obtained[28, 62, 63].

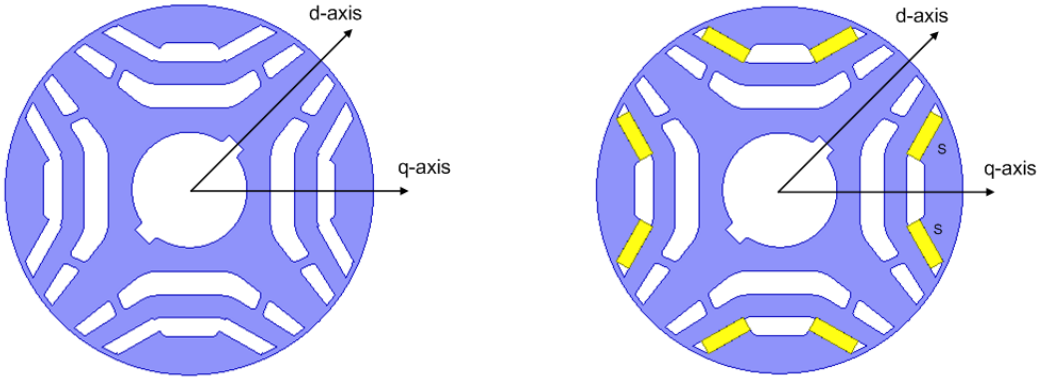

(a) (b)

Fig 4-2: d-q axes definition in machines (a) SynRM, (b) PMa-SynRM.

A general form of a d-q axes model for a SynRM is represented in (4-1). The current angle, γ determines the magnetizing and torque component of the current (i_d and i_q accordingly).

$$\begin{bmatrix} v_d \\ v_q \end{bmatrix} = \begin{bmatrix} R_s + pL_d & -\omega_e L_q \\ \omega_e L_d & R_s + pL_q \end{bmatrix} \begin{bmatrix} i_d \\ i_q \end{bmatrix} \tag{4-1}$$

$$\begin{cases} i_d = i_s \cos\gamma \\ i_q = i_s \sin\gamma \end{cases} \tag{4-2}$$

Based on the defined d–q axis in Fig. 4-3 and the orientation of embedded permanent magnets, the dynamic voltage equation of a SynRM can be modified and the model of a PMa-SynRM will be described according to (4-3). Note that since the flux linkage of the embedded permanent magnet opposes the generated flux by the q-axes component of the current (i_q), the generated back-EMF will appear on the d-axes:

$$\begin{bmatrix} v_d \\ v_q \end{bmatrix} = \begin{bmatrix} R_s + pL_d & -\omega_e L_q \\ \omega_e L_d & R_s + pL_q \end{bmatrix} \begin{bmatrix} i_d \\ i_q \end{bmatrix} + \begin{bmatrix} \omega_e \lambda_{pm} \\ 0 \end{bmatrix} \tag{4-3}$$

By defining the d-q axes flux linkages according to (4) the equivalent circuit of the PMa-SynRM can be expressed as the Fig. 4-3:

$$\begin{cases} \lambda_d = L_d I_d \\ \lambda_q = L_q I_q - \lambda_{pm} \end{cases} \tag{4-4}$$

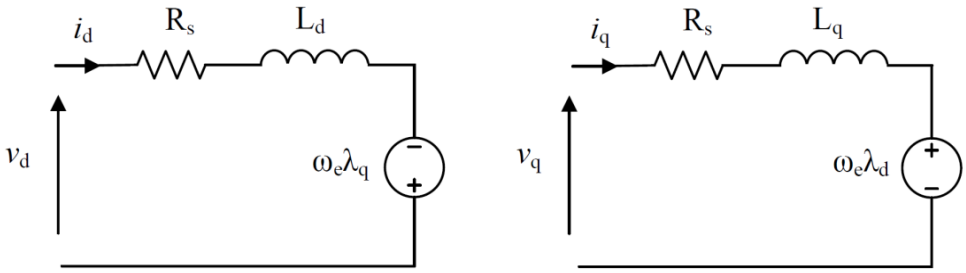

Fig 4-3: Equivalent circuit of the PMa-SynRM.

In the steady state operation when the machine current and voltage has reached the steady state values, the relation between voltage and current of the machine can be simplified according to (4-5):

$$\begin{bmatrix} V_d \\ V_q \end{bmatrix} = \begin{bmatrix} R_s & -\omega_e L_q \\ \omega_e L_d & R_s \end{bmatrix} \begin{bmatrix} I_d \\ I_q \end{bmatrix} + \begin{bmatrix} \omega_e \lambda_{pm} \\ 0 \end{bmatrix} \tag{4-5}$$

This model can be re-written to separate the speed variant from the speed invariant elements as follows:

$$\begin{bmatrix} V_d \\ V_q \end{bmatrix} = \begin{bmatrix} R_s & 0 \\ 0 & R_s \end{bmatrix} \begin{bmatrix} I_d \\ I_q \end{bmatrix} + \begin{bmatrix} -\omega_e L_q I_q + \omega_e \lambda_{pm} \\ \omega_e L_d I_d \end{bmatrix} \tag{4-6}$$

In all of the above equations, by eliminating the flux linkage due to the permanent magnets ($\lambda_{pm} = 0$) the SynRM model will be obtained again.

The back-EMF induced in the stator winding can be measured by rotating the rotor in a certain speed with a primary mover. Then by obtained back-EMF, the flux linkage of the inserted permanent magnets can be calculated using (4-7):

$$E_{pm} = P\omega_r \lambda_{pm} \tag{4-7}$$

Finally, the terminal voltage of the machine can be described as (8):

$$\vec{V}_a = R_s \vec{I}_a + jX_d \vec{I}_d + jX_q \vec{I}_q + \vec{E}_{pm} \tag{4-8}$$

Fig. 4-4 shows the phasor diagram of the PMa-SynRM. The current angle γ, leading the d-axis, is the main control variable when the maximum torque per ampere is considered.

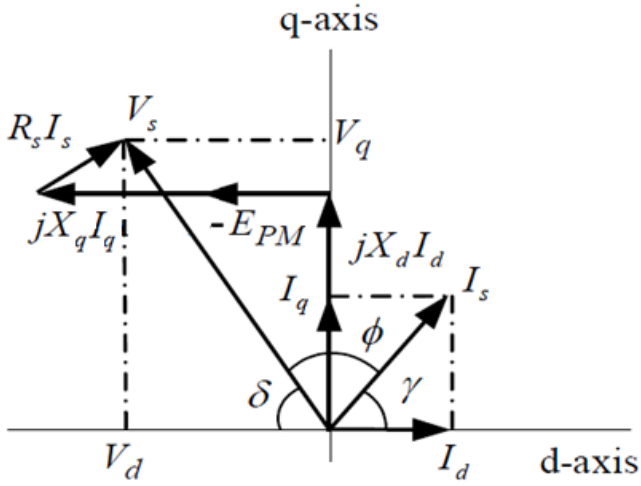

Fig 4-4: Phasor diagram for PMa-SynRM (motoring operation).

Since the current angle is adjusted by the control system, for a certain current level, the voltage of the machine will be available by (4-6); therefore, the voltage angle δ can be calculated according to (4-9):

$$\delta = \tan^{-1}\left(\frac{V_d}{V_q}\right) \tag{4-9}$$

By obtaining the voltage angle, the power factor of the machine can be calculated by (4-10):

$$\begin{cases} \phi = 180° - \delta - \gamma & if\ V_d < 0 \\ \phi = \delta - \gamma & if\ V_d \geq 0 \end{cases} \tag{4-10}$$

Neglecting the losses for a synchronous machine, the general form of the electromagnetic torque in the d q-frame is given by (4-11). The first component of the torque represents the reluctance torque developed by the saliency of the machine and the second component is the magnet torque developed by the permanent magnets.

$$T_e = \frac{3}{2}\frac{P}{2}\left(\lambda_d\, I_q - \lambda_q\, I_d\right) = \frac{3}{2}\frac{P}{2}\left\{\left(L_d - L_q\right) I_d\, I_q + \lambda_{pm}\, I_d\right\} \tag{4-11}$$

IVC1. Maximum Torque Generation

As it was mentioned before, the main objective of the control system should be controlling the machine in a steady state condition while developing the maximum torque in the machine. The magnetizing and torque component of the current can be control by FOC method assuming the stator current and the rotor position are being measured continuously. Equation (4-11) can be written in terms of motor line current (i_s) and the current angle γ using (4-2):

$$\begin{aligned} T_e &= \frac{3}{2}\frac{P}{2}\left\{\left(L_d - L_q\right) I_s^2 \cos\gamma \sin\gamma + \lambda_{pm} I_s \cos\gamma\right\} \\ &= \frac{3}{2}\frac{P}{2}\left\{\frac{1}{2}\left(L_d - L_q\right) I_s^2 \sin 2\gamma + \lambda_{pm} I_s \cos\gamma\right\} \end{aligned} \tag{4-12}$$

The current angle has to be calculated in order to control the machine under the certain load torque. Differentiation of the equation (4-12) has to be zero In order to maximize the torque under a certain current:

$$\frac{dT_e}{dI_s} = 0 \tag{4-13}$$

By solving (4-13), the current angle, which maximizes the torque in a certain current, will be obtained:

$$\gamma = \sin^{-1}\left(\frac{-\lambda_{pm} + \sqrt{\lambda_{pm}^2 + 8\left(L_d - L_q\right)^2 I_s^2}}{4\left(L_d - L_q\right) I_s}\right) \tag{4-14}$$

This equation can be further simplified by defining a new time invariant variable I_{FC}:

$$I_{FC} \stackrel{\text{def}}{=} \frac{\lambda_{pm}}{\left(L_d - L_q\right)} \tag{4-15}$$

Hence:

$$\gamma = \sin^{-1}\left(\frac{-I_{FC}+\sqrt{I_{FC}^2+8I_S^2}}{4I_S}\right) = \sin^{-1}\left\{\frac{1}{4}\left(\sqrt{\left(\frac{I_{FC}}{I_S}\right)^2+8}-\frac{I_{FC}}{I_S}\right)\right\} \quad (4\text{-}16)$$

For SynRM the flux linkage is zero, therefore IFC is zero and results in $\gamma = 45°$, which was expected for this type of machine at maximum torque operating point (considering a constant d-q axis inductances).

Since by knowing the three major parameters of the machine (Ld, Lq, and λpm), IFC will simply be calculated by (4-15). This new expression of the current angle makes the calculation simpler in the digital signal processing by using less calculation steps and to develop maximum output torque in each current level, the proper current angle can be simply calculated by (4-16).

To consider the regenerative torque of torque control in field weakening region, the electric torque definition can be re-written using I_{FC} as the following:

$$T_e = \frac{3}{2}\frac{P}{2}\left(\left(L_d - L_q\right)I_d\, I_q + \lambda_{pm}\, I_d\right) = \frac{3}{2}\frac{P}{2}\left(L_d - L_q\right)\left(I_d\, I_q + I_{FC}\, I_d\right) = \frac{3}{2}\frac{P}{2}\left(L_d - L_q\right)\left(I_d\, I_q + I_{FC}\, I_d\right) \Rightarrow T_e = \frac{3}{2}\frac{P}{2}\left(L_d - L_q\right)\left(I_q + I_{FC}\right)I_d \quad (4\text{-}17)$$

This form of expression for developed torque in PMa-SynRM indicates that because of the positive offset generated by I_{FC} in the term $\left(I_q + I_{FC}\right)$, the possible way to regenerate power (negative torque) is to negate the I_d (whereas in SynRM the general form of regenerating power is negating the I_q). In this case the machine will operate in generative mode and can return the power to the source.

The toque equation can be also expressed in terms of line current and current angle:

$$\xrightarrow{(4-17,4-2)} T_e = \frac{3}{2}\frac{P}{2}\left(L_d - L_q\right)(I_s \sin\gamma + I_{FC})\, I_s \cos\gamma \qquad (4\text{-}18)$$

In the field weakening region (constant power-variable torque), γ will be advanced to higher value starting from the initial MTPA angle (this will simply reduce the I_q and the q-axis magnetic flux).

IVD. Control Scheme of the PMa-SynRM

The control method considered for PMa-SynRM is the same as the other PM machine controls based on the field oriented vector control. Because the PMa-SynRM machine has a d-q axes model, a field oriented vector control (FOC) can be used for control algorithm. Based on the obtained model and control strategy (MTPA), FOC can develop a fully controlled electromagnetic torque in the machine [51]. Also, this type of control enables the machine to have a fast dynamic response. The main control feedbacks needed for FOC are the line current and rotor position information (also DC bus voltage in shaft sensorless application). Fig.4-5 shows a general control block diagram of a field oriented control for a PM machine.

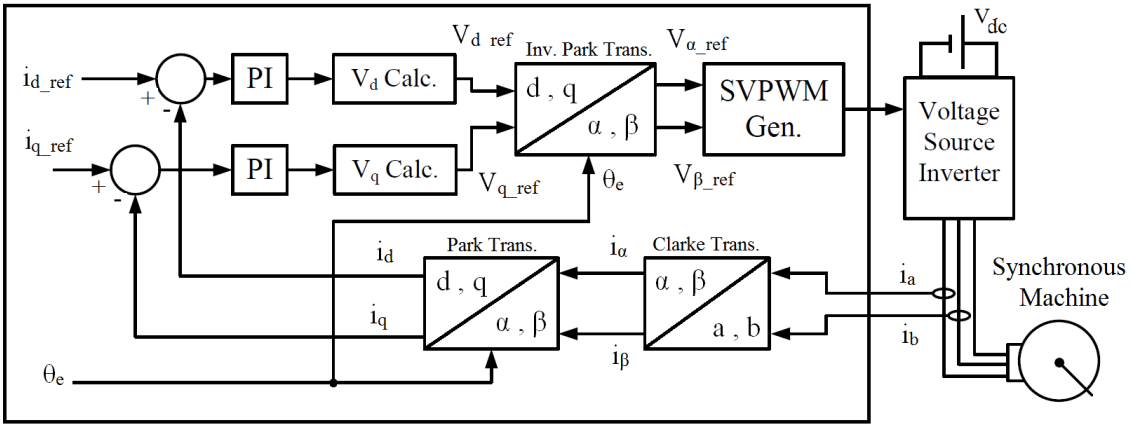

Fig 4-5: Overall block diagram of FOC.

This control scheme consists of the following main sections:

- Clarke Transformation
- Park Transformation
- Inverse Park Transformation PI Controller
- Space Vector PWM generator

One of the popular forms of machine analysis is to convert the three-phase time-variant machine parameters to a two phase time-invariant form through the mathematic conversion known as Park transformation using (4-19)[55, 57, 64]:

$$\begin{bmatrix} f_d \\ f_q \\ f_0 \end{bmatrix} = \frac{2}{3}\begin{bmatrix} \cos\omega t & \cos\left(\omega t - \frac{2\pi}{3}\right) & \cos\left(\omega t + \frac{2\pi}{3}\right) \\ \sin\omega t & \sin\left(\omega t - \frac{2\pi}{3}\right) & \sin\left(\omega t + \frac{2\pi}{3}\right) \\ \frac{1}{2} & \frac{1}{2} & \frac{1}{2} \end{bmatrix}\begin{bmatrix} f_a \\ f_b \\ f_c \end{bmatrix} \tag{4-19}$$

This conversion also can be split into two parts. In the first part, the balances three-phase quantities can be converted into a balanced two-phase quantity (known as Clarke

transformation). The quantities in three-phase stationary reference frame can be transformed into two-phase stationary reference frame by (4-20):

$$\begin{bmatrix} f_\alpha \\ f_\beta \\ f_0 \end{bmatrix} = \frac{2}{3}\begin{bmatrix} 1 & -\frac{1}{2} & -\frac{1}{2} \\ 0 & \frac{\sqrt{3}}{2} & -\frac{\sqrt{3}}{2} \\ \frac{1}{2} & \frac{1}{2} & \frac{1}{2} \end{bmatrix}\begin{bmatrix} f_a \\ f_b \\ f_c \end{bmatrix} \tag{4-20}$$

In an electric machine, this conversion can be realized as converting a there phase machine into a two phase machine. In this form, the three-phase machine supplied by three-phase current with 120° phase shift is converted to an equivalent two-phase machine supplied by two-phase current with 90° phase shift (shown in Fig. 4-6).

Second conversion, known as Park transformation, will transfer the vectors from two-phase stationary reference frame into two-phase rotational reference using (4-21) and (4-22). If the speed of the rotating reference frame is the same as the rotor, then this transformation will convert all time variant vectors in stationary reference frame into time-invariant parameters in the rotating reference frame. Fig. 4-7 shows all three coordinates in the phasor format.

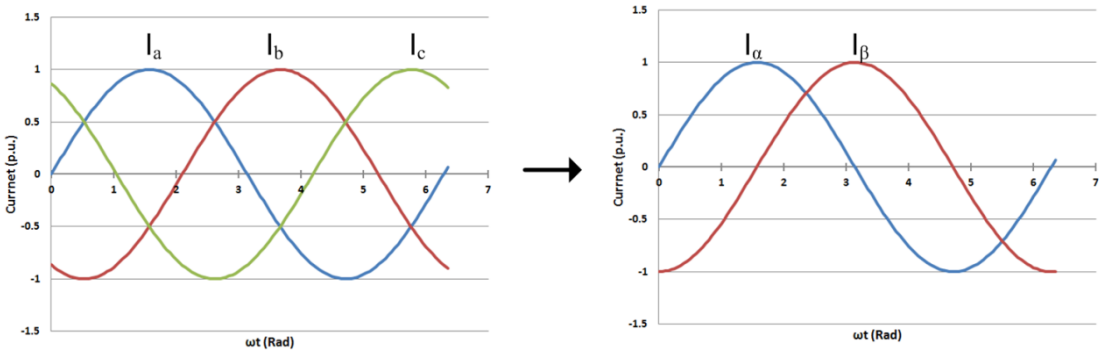

Fig 4-6: Conversion of three-phase balanced currents into equivalent two-phase currents.

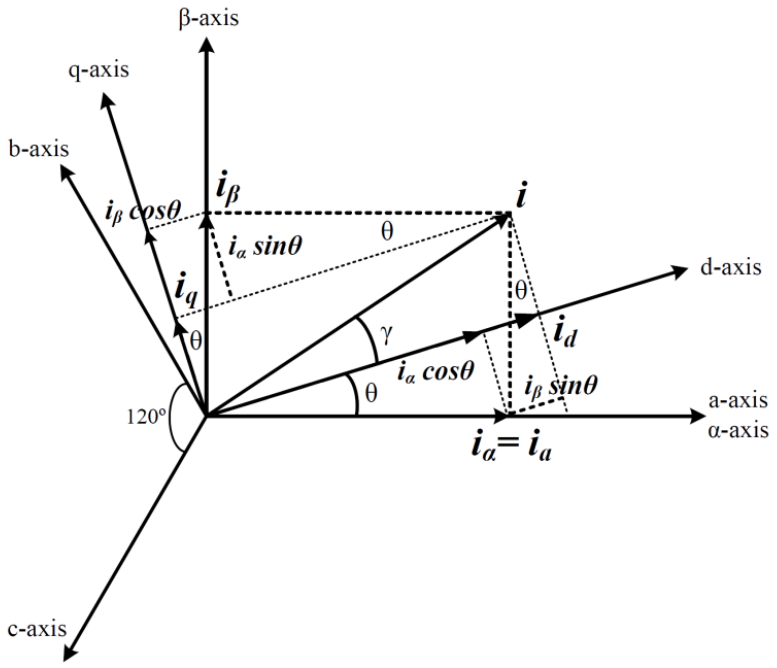

Fig 4-7: Conversion of three-phase balanced currents into equivalent two-phase currents in stationary and rotating reference frames.

$$\begin{cases} I_d = I_\alpha \cos\theta + I_\beta \sin\theta \\ I_q = -I_\alpha \sin\theta + I_\beta \cos\theta \end{cases} \tag{4-21}$$

$$\begin{cases} V_d = V_\alpha \cos\theta + V_\beta \sin\theta \\ V_q = -V_\alpha \sin\theta + V_\beta \cos\theta \end{cases} \tag{4-22}$$

Note that the a-axis on the three-phase system in aligned with the α-axis of the two phase stationary reference frame. Also, if the d-axis of the rotor is aligned with d-axis of the rotating reference frame, the current angle γ simply relates the phase current of the machine to d-q axes currents mentioned in (4-2). Therefore, the main control parameters in the vector control of the machines, which were I_d and I_q, become the current angle γ

obtained in (4-14). The speed obtained from the shaft encoder (position sensor) will be used as the speed feedback and the output of the speed controlled will generate the torque command. Since the machine utilized both magnet and reluctance torque, therefore the MTPA calculation block diagram (4-2) will be used to generate both I_d and I_q commands. Fig. 4-8 shows the final control block diagram of the PMa-SynRM.

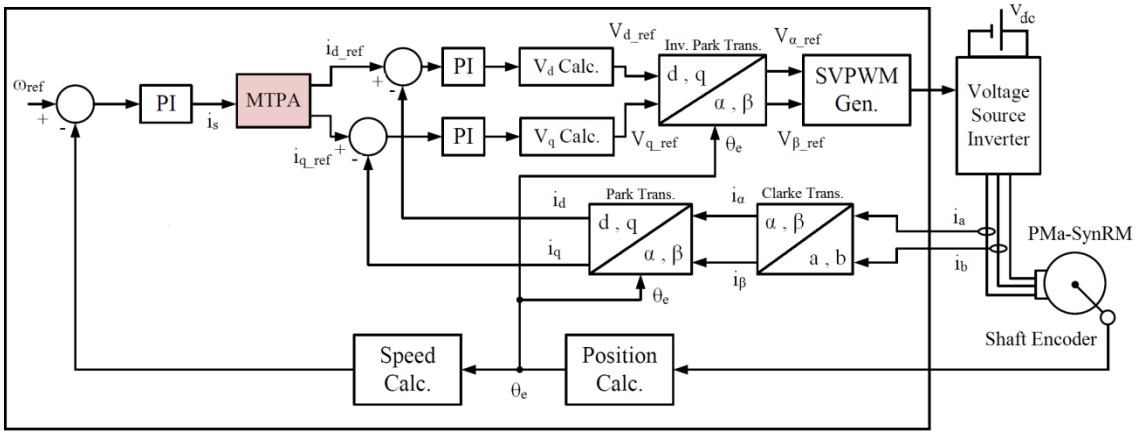

Fig 4-8: Overall block diagram of the field oriented control of PMa-SynRM.

Current commands will generate the voltage command through the PI controllers and d-q axes voltage calculation based on (4-3). After this stage, the d-q axes voltages will be transferred to the stationary reference frame using inverse Park transformation according to (4-23). The inverse Park transformation of the current is expressed in (4-24).

$$\begin{cases} V_\alpha = V_d \cos\theta - V_q \sin\theta \\ V_\beta = V_d \sin\theta + V_q cos\theta \end{cases} \quad (4\text{-}23)$$

$$\begin{cases} I_\alpha = I_d \cos\theta - I_q \sin\theta \\ I_\beta = I_d \sin\theta + I_q cos\theta \end{cases} \quad (4\text{-}24)$$

Finally, the space vector modulation unit uses the voltage references in the stationary reference frame to generate the proper PWM commands for the inverter.

The active and reactive powers entering to the machine can be calculated by (4-25):

$$\begin{cases} P = V_d I_d + V_q I_q \\ Q = V_q I_d - V_d I_q \end{cases} \tag{4-25}$$

Also in the stationary reference frame the active and reactive power can be calculated by (4-26). It is important to notice that calculating the power is independent from the rotor position in the stationary reference frame and a simple Clark transformation will be needed.

$$\begin{cases} P = V_\alpha I_\alpha + V_\beta I_\beta \\ Q = V_\beta I_\alpha - V_\alpha I_\beta \end{cases} \tag{4-26}$$

Generally, the machine terminal voltages can be obtained by measuring the inverter DC bus voltage and the status of the inverter switches[65]. Assuming the switch state vector S can be described as:

$$S = \begin{bmatrix} S_a \\ S_b \\ S_c \end{bmatrix} \quad \text{Where} \quad S_a, S_b, S_c = \begin{cases} 1 & \text{when the up switch is on} \\ 0 & \text{when the up switch is off} \end{cases} \tag{4-27}$$

Then the phase voltage vectors can be related to the switch start vector according to (4-28):

$$\begin{bmatrix} V_a \\ V_b \\ V_c \end{bmatrix} = \frac{1}{3} V_{dc} \begin{bmatrix} 2 & -1 & -1 \\ -1 & 2 & -1 \\ -1 & -1 & 2 \end{bmatrix} \begin{bmatrix} S_a \\ S_b \\ S_c \end{bmatrix} \tag{4-28}$$

After calculating the phase voltages, the stationary reference frame voltages can be obtained by Clarke transformation described in (4-20). In sensorless control, the knowledge of the machine voltage is crucial since the voltage and current of the machine can be used to identify the position of the rotor based on the model of the machine and the algorithm employed in position estimation. In this work, the terminal voltage is measured to evaluate the linearity of the machine. Also, the speed and position information are obtained from the shaft encoder on the shaft. Fig. 4-9 shows the quadrature encoder pulse (QEP) signals of the shaft encoder.

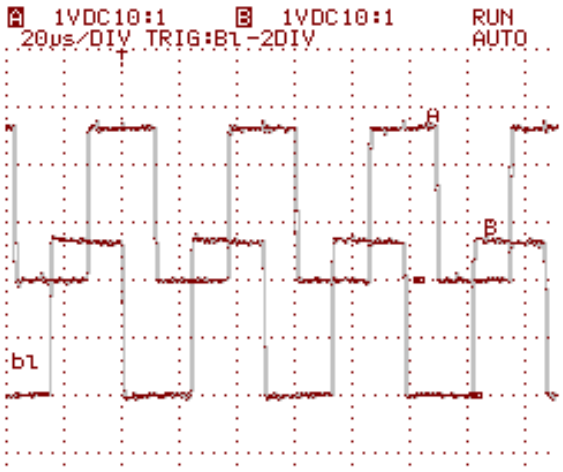

Fig 4-9: Shaft encoder signal waveforms.

Finally, by calculating the stationary reference frame voltages and current, the power factor can be calculated according to (4-29):

$$pf = \tan^{-1}\left(\frac{P}{Q}\right) \tag{4-29}$$

IVE. Parameter Measurement of the PMa-SynRM

According to the (4-6) and (4-14), the most important parameters in PMa-SynRM model are L_d, L_q, and λ_{PM}. The L_d and L_q will be measured based on the static measurement (and will be completed by FEA for higher current range) and the λ_{PM} will be obtained directly from the back-EMF measurement.

IVE1. Flux Linkage Calculation

Using the fundamental component of the back-EMF, the flux linkage of the machine can be calculated. The fundamental component for NdFeB rotor is 162.0V, (maximum amplitude of the line-to line voltage). Since the machine has 4 poles (2-pole pair), the λ_{PM} will be 0.25 (Wb) based on (4-7). By changing the magnets for other version of the rotors, the same experiment has been conducted and the back-EMF is measured for each case. Fig. 4-10 shows the back-EMF of each case, which indicates the significant increment of the back-EMF in C8-R2 version while the additional magnet is 50% more. Table 4-1 includes the measurement results for each rotor.

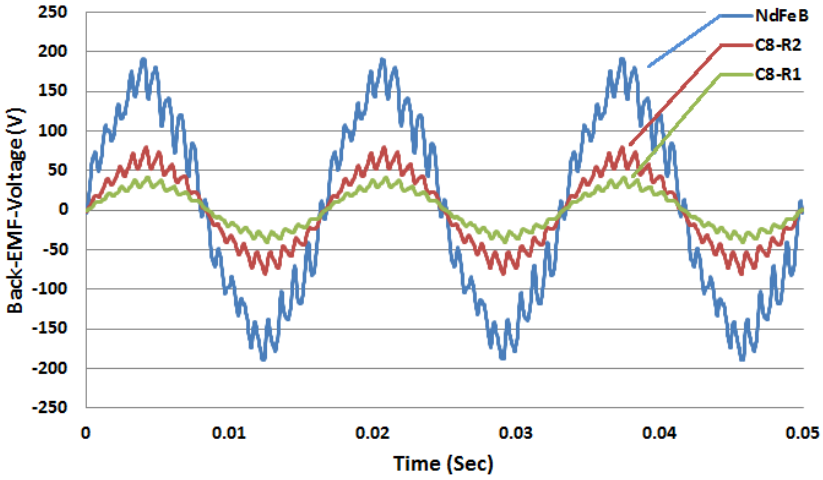

Fig 4-10: Back-EMF waveforms of the PMa-SynRMs with different magnet type and quantity at 1800 RPM.

Table 4-1: Magnetic property of each rotor.

Machine type	**Magnet Type**	**Magnet Br (T)**	**Magnet Mass (gr)**	**Line Back-Emf (V) at 1800 rpm**	**λ_{PM} (wb)**
SynRM	-	-	0	0	0
PMa-SynRM-C8-R1	Ferrite-C8	~0.39	330	23.1	0.05
PMa-SynRM-C8-R2	Ferrite-C8	~0.39	500	46.0	0.1
PMa-SynRM-NdFeB	NdFeB42H	~1.31	500	115.9	0.25

IVE2. L_d and L_q Static Measurement

For control purposes, the remaining parameter necessary to measure, are d-q axes inductances according to (4-14). In this work the main objective is to obtain the maximum torque per ampere and estimation of the current angle close to the optimum angle can be accepted, provided that during the operation of the machine an automatic or manual compensation applies to the current angle the optimize the operating point for MPTA[66]. To find the initial current angle, a static value of d-q axes inductances can be

used. It should be noticed that the direct axis inductance is highly dependent on the d-axis current (because of non-linear characteristic of its reluctance path) and the quadrature axis inductance has less dependency to the q-axes current (because of the air barriers located in its path). To obtain these inductances, a static measurement can be used besides the FEA measurements. In this method a single AC voltage source is connected to the terminals of the machine according to the Fig. 4-11.

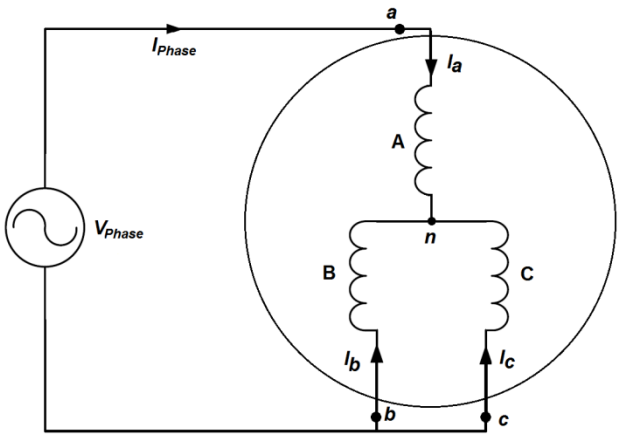

Fig 4-11: Motor terminal connections for the inductance measurement.

Fig. 4-12 shows the terminal inductance variation by changing the rotor position, which is because of the saliency of the rotor. The minimum inductance (maximum reluctance) is generated when the q-axis of the rotor is aligned with the a-axis (θ=0°). In this case the terminal inductance is proportional to L_q. In opposite, the maximum inductance (minimum reluctance) happens when the d-axis of the rotor is aligned with the a-axis (θ=90°). In this case the reluctance path of the flux is the minimum and it is

proportional to L_d. the variation of the terminal inductance will be a waveform according to Fig.4-12.

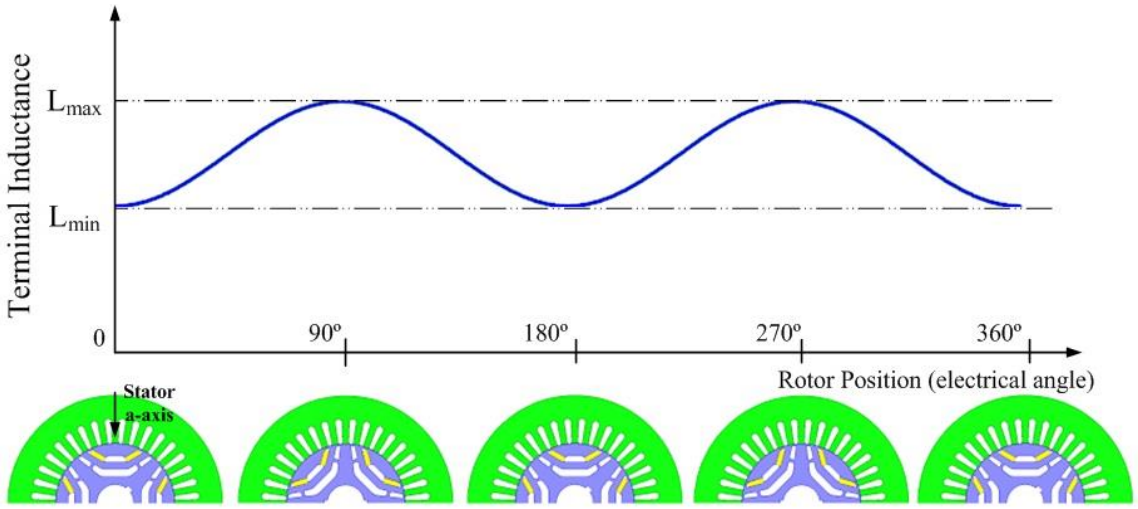

Fig 4-12: Motor terminal inductance variation versus position.

To find the relation between the terminal inductance and the d-q axes inductances based on the rotor position, it is possible to use the same Clarke and Park transformation to transfer the three-phase machine to the d-q axis. The same as the control methodology, a three phase model can be transferred to the two-phase model (stationary form) using the Clarke transformation. In this case $V_{bn}=V_{cn}$ and $I_a=-I_b/2=-I_c/2$ and the voltage and current of the machine in the two-phase stationary reference frame can be derived:

-Clarke transformation of the voltage:

$$\begin{bmatrix} V_\alpha \\ V_\beta \\ V_0 \end{bmatrix} = \frac{2}{3}\begin{bmatrix} 1 & -\frac{1}{2} & -\frac{1}{2} \\ 0 & \frac{\sqrt{3}}{2} & -\frac{\sqrt{3}}{2} \\ \frac{1}{2} & \frac{1}{2} & \frac{1}{2} \end{bmatrix}\begin{bmatrix} V_{an} \\ V_{bn} \\ V_{cn} \end{bmatrix} \tag{4-30}$$

$$\xrightarrow{(4-30)} \begin{cases} V_\alpha = \frac{2}{3}\left\{V_{an} - \frac{1}{2}(V_{bn} + V_{cn})\right\} \\ V_\beta = \frac{2}{3}\left\{\frac{\sqrt{3}}{2}(V_{bn} - V_{cn})\right\} \end{cases} \xrightarrow{V_{bn}=V_{cn}} \begin{cases} V_\alpha = \frac{2}{3}(V_{an} - V_{bn}) \\ V_\beta = 0 \end{cases} \Rightarrow \begin{cases} V_\alpha = \frac{2}{3}V_{Phase} \\ V_\beta = 0 \end{cases} \tag{4-31}$$

- Clarke transformation of the current:

$$\begin{bmatrix} I_\alpha \\ I_\beta \\ I_0 \end{bmatrix} = \frac{2}{3}\begin{bmatrix} 1 & -\frac{1}{2} & -\frac{1}{2} \\ 0 & \frac{\sqrt{3}}{2} & -\frac{\sqrt{3}}{2} \\ \frac{1}{2} & \frac{1}{2} & \frac{1}{2} \end{bmatrix}\begin{bmatrix} I_a \\ I_b \\ I_c \end{bmatrix} \tag{4-32}$$

$$\xrightarrow{(4-32)} \begin{cases} I_\alpha = \frac{2}{3}\left\{I_a - \frac{1}{2}(I_b + I_c)\right\} \\ I_\beta = \frac{2}{3}\left\{\frac{\sqrt{3}}{2}(I_b - I_c)\right\} \end{cases} \xrightarrow{I_b=I_c=-I_a} \begin{cases} I_\alpha = \frac{2}{3}\left\{\frac{3}{2}(I_a)\right\} \\ I_\beta = 0 \end{cases} \Rightarrow \begin{cases} I_\alpha = I_{Phase} \\ I_\beta = 0 \end{cases} \tag{4-33}$$

For L_d measuring, the d-axis is aligned and locked to a-axis of the stator therefore θ=0 and according to (4-21) and (4-22) the d-q axes voltage and current will be obtained per the following:

$$(4-21) \xrightarrow{\theta=0} \begin{cases} I_d = I_\alpha \\ I_q = I_\beta \end{cases} \xrightarrow{(4-33)} \begin{cases} I_d = I_{Phase} \\ I_q = 0 \end{cases} \tag{4-34}$$

$$(4-22) \xrightarrow{\theta=0} \begin{cases} V_d = V_\alpha \\ V_q = V_\beta \end{cases} \xrightarrow{(4-31)} \begin{cases} V_d = \frac{2}{3}V_{Phase} \\ V_q = 0 \end{cases} \tag{4-35}$$

Considering the locked rotor condition (ω_e=0) and neglecting the stator resistance, the relationship between terminal voltage and current in the steady state condition (p= jω) can be expressed according to (4-36):

$$V_d = (R_s + \mathrm{j}\omega L_d) I_d \xrightarrow{(R_s=0)} L_d = \left| \frac{1}{\mathrm{j}\omega} \left(\frac{V_d}{I_d} \right) \right|$$

$$\xrightarrow{(4-27,4-28)} L_q = \left| \left(\frac{1}{\mathrm{j}\omega} \right) \frac{\frac{2}{3} V_{Phase}}{I_{Phase}} \right| \Rightarrow L_d = \frac{2}{3} \left| \frac{Z_{Terminal}}{\omega} \right| \tag{4-36}$$

Likewise, for L_q measuring the q-axis is aligned and locked to a-axis of the stator therefore θ=90° and according to (4-21) and (4-22):

$$(4-21) \xrightarrow{\theta=90^\circ} \begin{cases} I_d = I_\beta \\ I_q = -I_\alpha \end{cases} \xrightarrow{(4-33)} \begin{cases} I_d = 0 \\ I_q = -I_{Phase} \end{cases} \tag{4-37}$$

$$(4-22) \xrightarrow{\theta=90^\circ} \begin{cases} V_d = V_\beta \\ V_q = -V_\alpha \end{cases} \xrightarrow{(4-31)} \begin{cases} V_d = 0 \\ V_q = -\frac{2}{3} V_{Phase} \end{cases} \tag{4-38}$$

Considering the same condition mentioned at the above, L_q can be obtained using (4-39):

$$V_q = \left(R_s + \mathrm{j}\omega L_q\right) I_q \xrightarrow{(R_s=0)} L_q = \left| \frac{1}{\mathrm{j}\omega} \left(\frac{V_q}{I_q} \right) \right|$$

$$\xrightarrow{(4-29,4-30)} L_q = \left| \left(\frac{1}{\mathrm{j}\omega} \right) \frac{-\frac{2}{3} V_{Phase}}{-I_{Phase}} \right| \Rightarrow L_q = \frac{2}{3} \left| \frac{Z_{Terminal}}{\omega} \right| \tag{4-39}$$

Based on the measurement method mentioned above, the terminal inductance of the PMa-SynRM with NdFeB magnets is measured. Fig. 4-13 shows the obtained results. Because of the air barrier and permanent magnet located on the q-axes, the current

variation has less effect on the reluctance of this axis and the q-axis inductance is almost constant. But the d-axis reluctance varies because it includes the rotor core steel, which has non-linear characteristics. Higher current saturates the d-axis and causes the decrement of the L_d. Table 4-2 includes the initial current for the machine operating to generate the maximum torque per ampere at rated current.

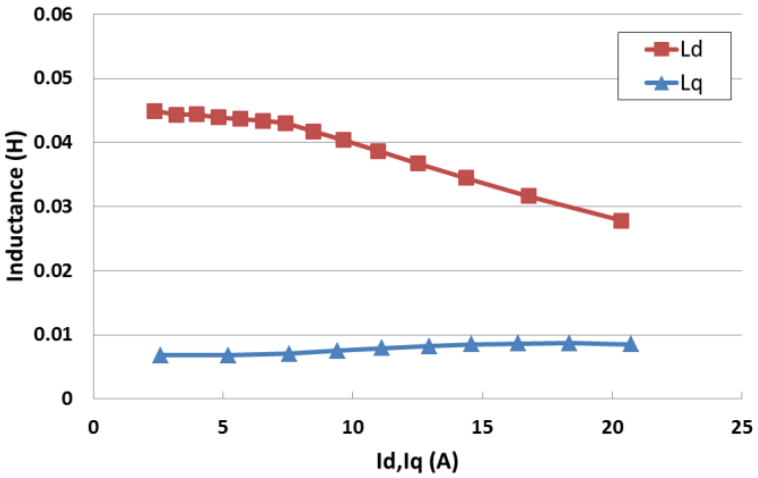

Fig 4-13: D-q axes inductance of the PMa-SynRM-NdFeB.

Table 4-2: Initial current angle at rated current.

Machine type	**Magnet Type**	**λ_{PM} (wb)**	**I_{FC} (A)**	**γ (°)**
SynRM	-	0	0	45
PMa-SynRM-C8-R1	Ferrite-C8	0.05	1.4	43.8
PMa-SynRM-C8-R2	Ferrite-C8	0.1	2.9	42.6
PMa-SynRM-NdFeB	NdFeB42H	0.25	7.14	39.3

IVF. Experimental Test Results under the Rated Current

After obtaining the necessary parameters for the machine control the test setup has been established to evaluate the machine performance. The setup includes the motor drive test bed and the control section, which consists of the inverter and the DSP based drive circuit monitored by computer in real time.

IVG. Motor Drive Test Bed

The simulation result of the PMa-SynRM-NdFeB shows that the maximum average torque of the machine operating at rated current will reach 46Nm. Therefore, the motor drive test bed has been built for 50Nm rated torque. Fig. 4-14 shows the NEMA machine coupled to the torque transducer and the dynamometer on the prepared test bed.

This dynamometer can apply 25Nm torque to the machine and to reach 50Nm. There is second dynamometer coupled to the first one. The same setup can be used to measure the back-EMF of the PMa-SynRM by running the DC machine on the dynamometer as the primary mover. For speed and position measurement of the PMa-SynRM the setup is equipped with a two-channel shaft encoder with 2048 (line/rev).

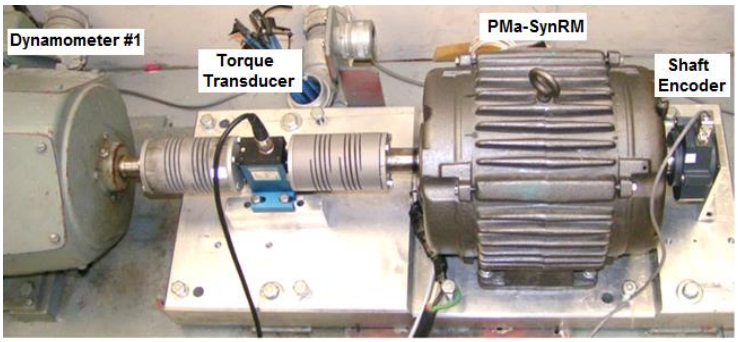

Fig 4-14: Experiment test-bed for induction machine and PMa-SynRMs.

The maximum torque of each machine is measured using the test bed shown in Fig. 4-1 assuming the maximum excitation current is applied to the stator. Field oriented control (FOC) using MTPA method is implemented with DSP to control the speed in closed loop form.

Fig. 4-15 shows the control board setup based on TI-TMS28F335 DSP used for the machine control. The setup also includes the current and voltage sensors and interface board for analog to digital signal conditioning and PWM signal pull up. Code Composer Studio and its motor control library provided by Texas Instrument are used for DSP programming. The on board emulator provides the real time parameter monitoring, which enables the user to change the desired parameter while the machine is operating.

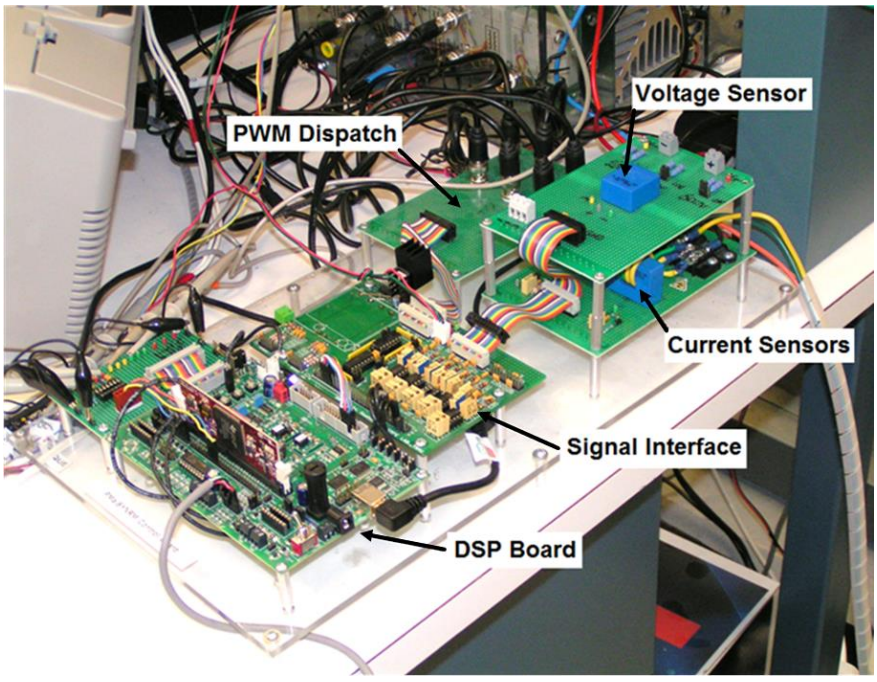

Fig 4-15: DSP based control hardware with current and voltage sensors.

IVH. Experimental Results

By exciting the machine at the rated current in the maximum torque angle, the PMa-SynRM-NdFeB generates 41.4 N.m with 21A excitation current whereas the induction machine generates 30 N.m with the same excitation. Fig. 4-16 shows the torque and the line current waveform of the machine at 450 RPM. The measured torque ripple is about 5% and it can be seen that the torque ripple is less than the simulation results because of the effect of the inertia of both PMa-SynRM and dynamometers rotors. Thermal imaging of the machine shown in Fig. 4-17 shows that the case temperature of the machine is higher than the steady state temperature of the induction machine (mentioned on the name plate), which is because of the absence of the cooling fan.

Fig 4-18 shows the speed response and phase current variation of the machine to the step change of the speed reference. In this case the dynamometers excitation and output terminal resistance is constant; therefore it applies a linear torque load to the machine proportional to its shaft speed. Fig. 4-19 the variation of the I_d and I_q currents during the acceleration and deceleration of the machine.

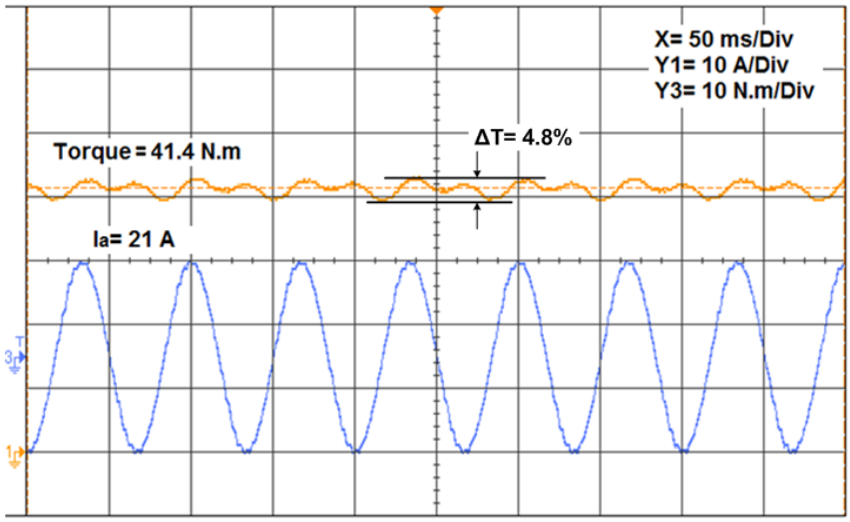

Fig 4-16: Torque and current of the PMa-SynRM-NdFeB machine.

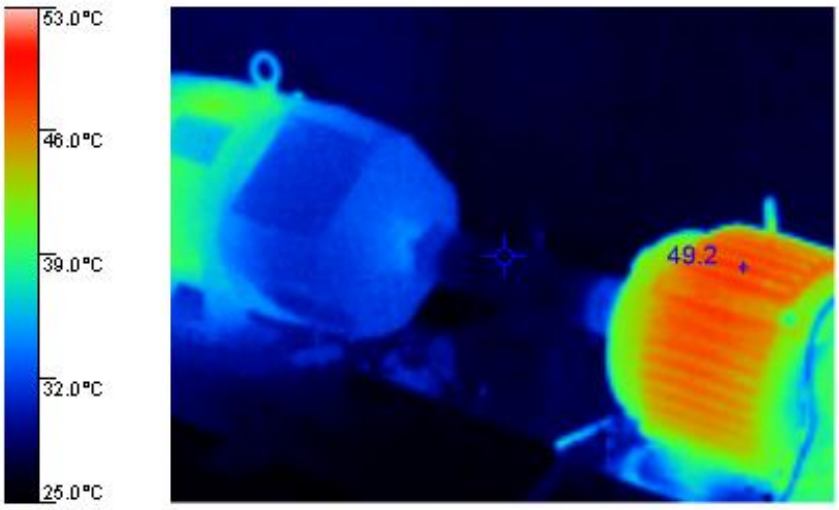

Fig 4-17: Thermal image of the PMa-SynRM-NdFeB machine running under rated excitation current.

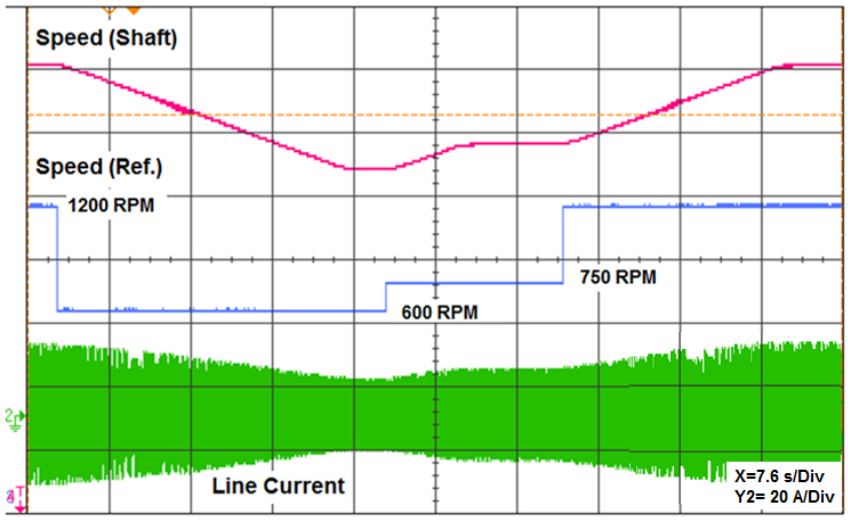

Fig 4-18: Speed response of PMa-SynRM-NdFeB machine.

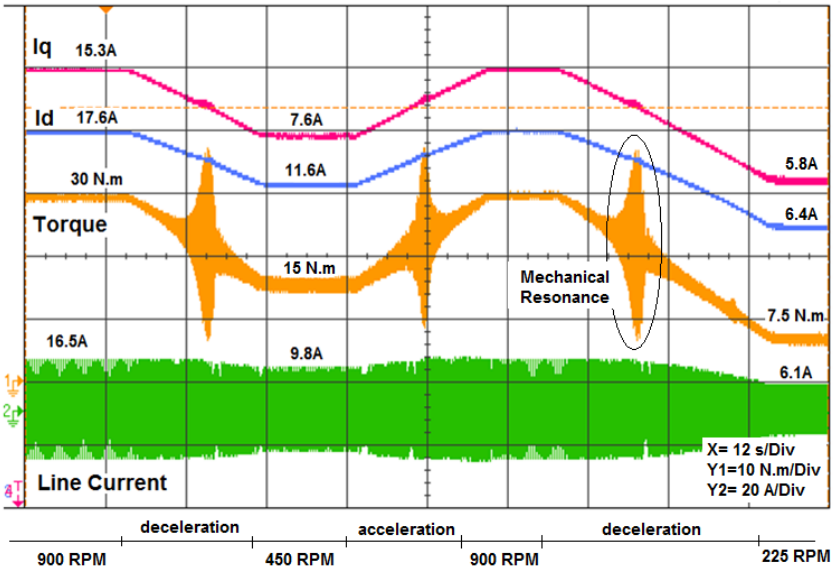

Fig 4-19: Torque and I_d,I_q current variation during the linear speed-load change of PMa-SynRM-NdFeB machine.

The MTPA control is applied to obtain the maximum torque at the rated current of each PMa-SynRM machines with different magnets. Fig. 4-20 shows the output torque

of the machines with rated current excitation and operating at 450 RPM. The torque is applied by the dynamometer the same as before, until the rated excitation current is reached. Table 4-3 includes the torque measurements for each machine and as expected the torque density of NdFeB is the highest compared to the other machines and it generates 38% more torque compared to the reference induction machine. This results show that using rare earth magnet has significant effect on the torque density of the PMa-SynRM compared to SynRM (about 40%) and using Ceramic magnet increases the SynRM output torque by 16% (C8R2 case). In all cases, the PMa-SynRM machines generate more torque than the induction machine at rated excitation current.

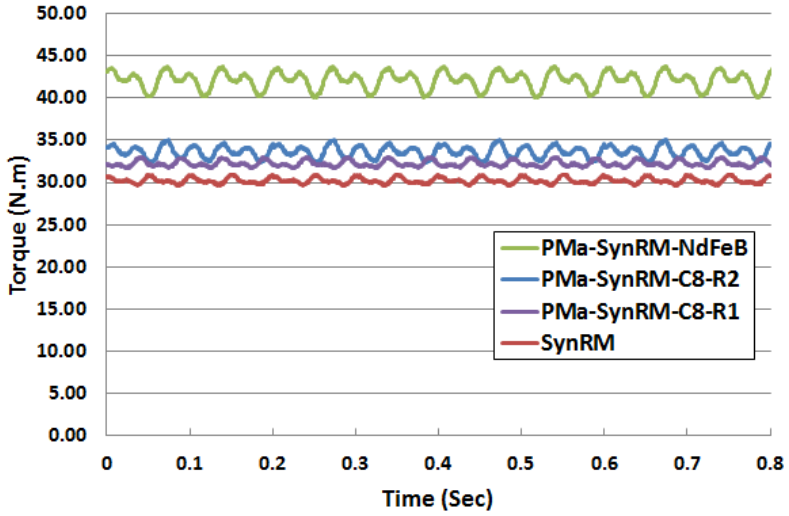

Fig 4-20: Torque output of the PMa-SynRMs and SynRM operating with 21A excitation current.

Table 4-3: Torque performance comparison of the machines operating under the rated current condition at 21 (A) excitation.

Machine Type	Average Torque (N.m)	Torque Density (N.m/A)	Normalized Torque Density
PMa-SynRM-NdFeB	41.4	1.97	1.38
PMa-SynRM-C8-R2	34.2	1.63	1.14
PMa-SynRM-C8-R1	32.1	1.53	1.07
SynRM	29.5	1.41	0.98
Induction Machine	30.0	1.43	1.00

IVI. Inductance Variation of the Machines

By applying a different torque load to the machines running at certain speeds, the voltage, current, and the power factor are measured. Using that information and the model of machine described in Chapter III, the d-q inductances are achievable (note that the current angle is available through the control program). Fig. 4-21 shows the obtained characteristic of L_d versus the magnetizing current (I_d). In all cases, the saturation effect can be seen at higher current level. Fig. 4-22 shows the variation of L_q. With less flux density in the rotor core, the flux passing through the ribs of the core causes a nonlinear L_q characteristic; but with high flux density the ribs are saturated and L_q becomes more linear.

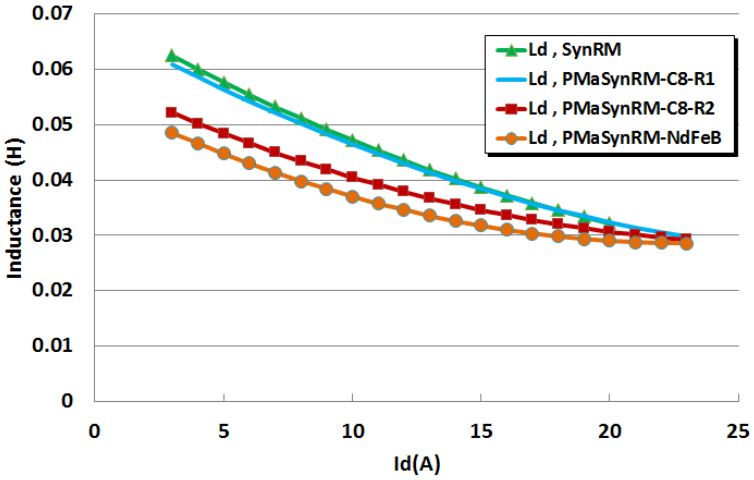

Fig 4-21: Direct axis inductance (L_d) comparison of the PMa-SynRM machines.

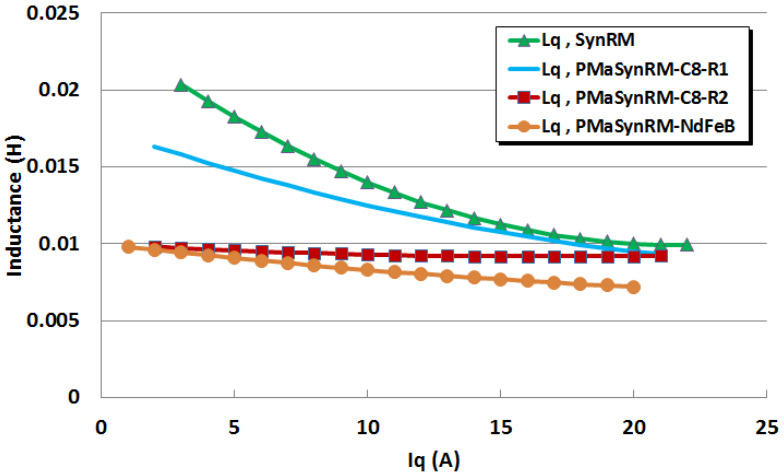

Fig 4-22: Quadrature axis inductance (L_q) comparison of the PMa-SynRM machines.

IVJ. PMa-SynRM Terminal Voltage

The rotor position information is a major control parameter in the control on the permanent magnet or synchronous machines. Since the cost of the shaft encoder or resolvers are effecting on the cost and reliability of the machine, the sensorless control

has become popular while the high speed DSPs are available with reasonable cost to execute complicated algorithm for rotor position estimation. There are several methods to estimate the rotor position based on the machine parameters and terminal voltages such as observer based control, MARS (model adaptive reference system) control, and flux based control. Since the only available parameters for the control are the terminal voltage and current of the machine the precision of the estimation relies on the quality of those parameters. Therefore, lower harmonics result accurate parameter estimation in d-q frame if the fundamental components are used for estimation [63, 65, 67-77].

To evaluate the PMa-SynRM machine for sensorless control capabilities, the terminal voltage and current of the machine is measured and transferred to the DSP. Fig. 4-23 shows the PMa-SynRM-C8-R1 current (from probes) and voltages (transferred to the stationary reference frame) at full excitation current condition. It can be seen that the sinusoidal shape of the current and voltage creates a high potential for sensorless control.

Table 4-4 includes the THD of the machine terminal voltage and currents. Since the voltage waveforms of the machine on the stationary reference frame contain low harmonic components. The low harmonic content of the current and voltage makes it possible to achieve a high accuracy in voltage/flux based sensorless control methods in of the NEMA frame PMa-SynRM.

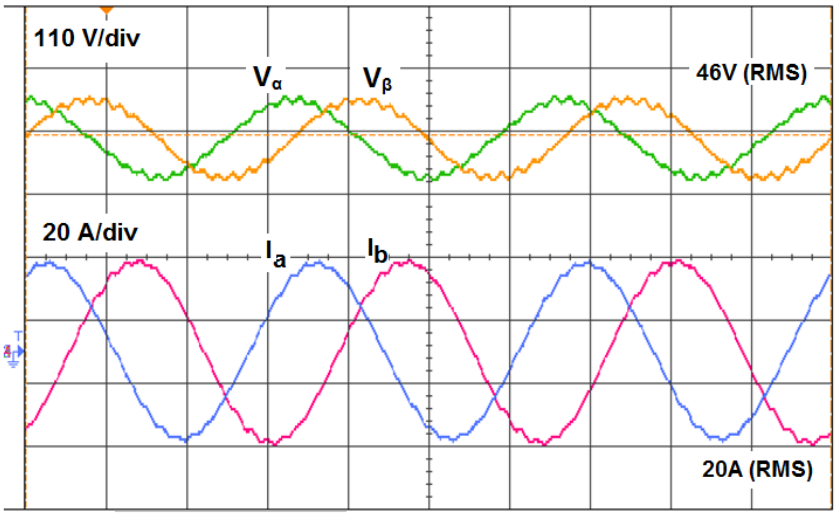

Fig 4-23: Voltage and current waveforms at full load- 450 RPM for PMa-SynRM-C8-R1

Table 4-4: Harmonic content of the voltages and currents.

Parameter	THD (%)
V_alpha	6.91
V_beta	6.8
Ia	2.3
Ib	2.5

IVK. Conclusion

In this chapter the d-q model of the PMa-SynRM has been studied and the necessary parameters to control the machine using FOC control method are identified and the measurement method used to obtain the machine parameters are studied. The obtained results show that the magnet type and quantity have a significant effect on the torque performance of the PMa-SynRM but the experimental result shows less torque developed in the PMa-SynRM. The PMa-SynRM with NdFeB magnets generate 38% more torque compared to the reference induction machine with the same excitation. The

output torque is less than the simulation results (48.5Nm), which is because different reasons such as slight difference between steel and NdFeB material characteristic of the simulation and the one used in the rotor fabrication, rotor fabrication tolerance resulting in bigger air gap, accuracy of the FEA calculation, and presence of the friction and wind load on both PMa-SynRM and the dynamometers rotors. The test results show that the PMa-SynRM with Ceramic magnets show higher torque compared to the induction machine (about 14%), which can be increased by optimization of the rotor core for this type of magnet. Finally the low harmonic content of the voltage and current of the NEMA frame PMa-SynRM shows on this type of machine the sensorless algorithms can be used effectively to eliminate the shaft encoder sensor.

CHAPTER V

EFFECT OF THE MAGNET QUANTITY AND TYPE ON THE PERFORMANCE AND ENERGY CONSUMPTION OF THE PMA-SYNRM*

VA. Introduction

In this chapter, the effect of the Magnet type and quantity on the performance of a NdFeB based PMa-SynRM, presented in this work is studied. Two major types of loads, which are fan type and constant speed, are applied to the machine with different rotor variations. The PMa-SynRM uses a stator of a NEMA frame induction machine and the original rotor is optimized for that specific stator. By replacing the original magnets with the same size ferrite magnets, the performance is compared with the original PMa-SynRM. Also more ferrite is added to the rotor to study the effect of the extra ferrite on the power factor and efficiency of the machine. The power factor and efficiency of the PMa-SynRM machines are compared to the magnet-less machine, forming SynRM, to show the effect of the magnets on the performance of the SynRM machine and all results are compared with the standard NEMA frame induction machine as a reference. Finally, by comparing the energy savings of the PMa-SynRMs using NEMA frame stator; this

chapter presents the PMa-SynRM as a suitable candidate for replacement of VFD fed induction motor.

VB. PMa-SynRMs Performance Study with Constant Speed and Fan Load

Two different types of load are applied to the machines in the experiment and the performances are observed. Fig. 5-1 shows the load profile applied to the machines. The first load profile is a fan type load with 30 N.m rated torque at 1800 rpm and shown in Fig. 5-1(a). The other load is variable torque at constant speed of 600 rpm shown in Fig. 5-1(a). The same loads are also applied to the induction machine for performance comparison. The VFD drive is used to run the induction machine. In each operating point, the voltage is optimized in order to reduce the power consumption of the machine.

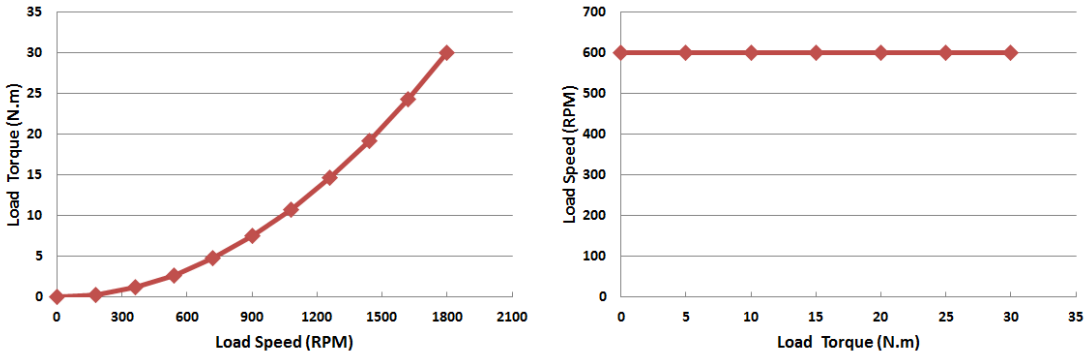

(a) (b)

Fig 5-1: Load profiles applied to the machines: (a) Fan load profile, (b) Constant speed load profile.

Fig. 5-2(a) shows the power factor of each machine under a fan load running below 65% of the rated speed for safety. Again, the SynRM has the lowest and the PMa-SynRM-NdFeB has the highest power factor for this load condition. The power factors

of all PMa-SynRMs have a flat form and stay higher than the induction machine at the most operating points.

Fig. 5-2(b) shows the efficiency comparison of the machines. The induction machine shows the lowest efficiency because of the existence of the higher losses. The SynRM and PMa-SynRM machines show high efficiency comparing to the induction machine, which means that these machines are proper replacement candidates for fan type load applications.

The PMa-SynRM with NdFeB magnets operates with less efficiency compared with the ferrite one and the reason is that the current angle was advanced about 5 degrees to maintain the power factor above 0.9 and this change increased the current slightly and the copper loss increased.

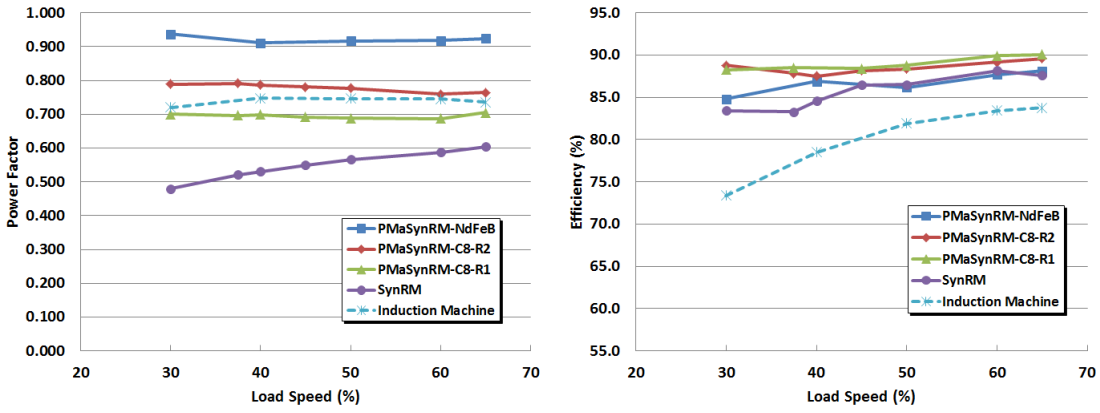

(a) (b)

Fig 5-2: Performance comparison of the machines driving fan load: (a) Power factor, (b) Efficiency.

Input power to the machines is compared in Fig. 5-3(a). As it is expected, the power is exponentially increasing when the speed increases and the induction machine is absorbing more power since has more power loss and less efficiency. The excitation current comparison is shown in Fig. 5-3(b). To drive the same load in each speed, the PMa-SynRM-NdFeB needs less current since its torque density is the highest and comparing the PMa-SynRM and the induction machine, the induction machine needs more current. In light loads (lower speeds) the current of the PMa-SynRM-NdFeB reaches to the half of the induction machine current, which means 75% less copper loss in the stator.

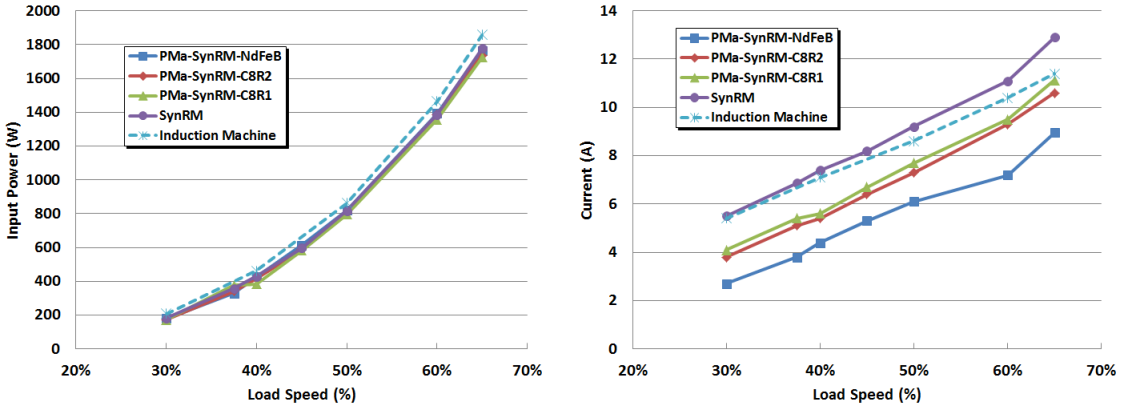

(a) (b)

Fig 5-3: Performance comparison of the machines driving fan load: (a) Input power, (b) Input current.

Apparent power of the machines is compared in Fig 5-4. It can be observed that for each load condition the PMa-SynRM-NdFeB needs less apparent power, which is

because of the better power factor compared to the induction machine and it will need smaller inverter circuit.

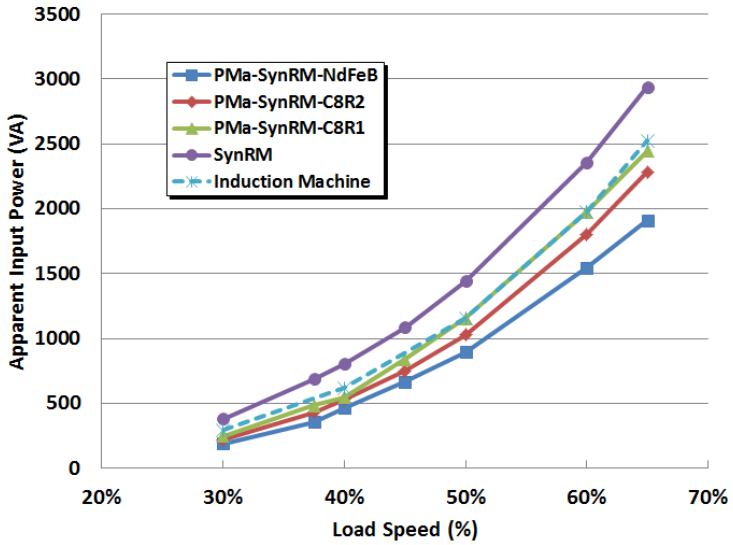

Fig 5-4: Apparent power supplied by inverter for each machine under a fan load.

VC. Energy Consumption Comparison under the Fan and Pump Loads

The efficiency of an electric machine is affected by the design of the machine and results on the energy consumed by the machine. In selecting a motor for a certain application, a slight difference between efficiency of the candidates can make a big difference in the total energy price paid in the lifetime of the machine. In this section, the energy saving opportunity is studied for the presented options. In order to estimate the energy saving opportunity, the duty cycle of the machine has to be considered. A typical duty cycle for variable speed drive is selected according to Fig. 5-5. Based on the power

consumption data, obtained from the experiments ans simulations shown in Table 5-1, the energy consumption of each machine is calculated for the given duty cycle.

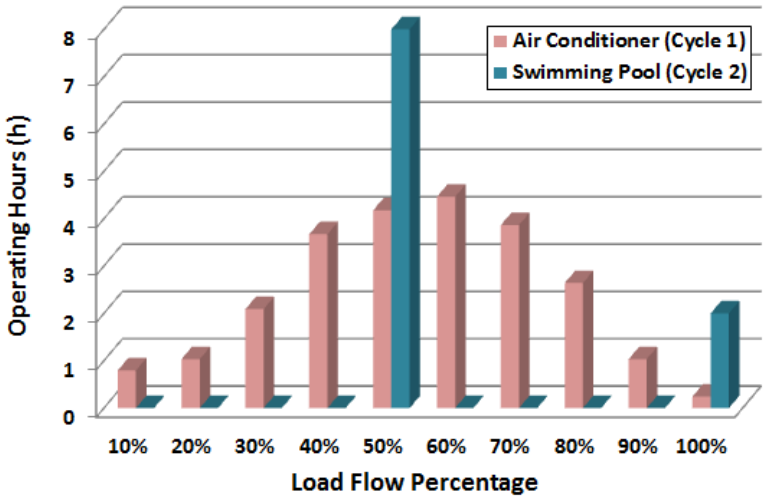

Fig 5-5: Typical duty cycle for time variant loads.

Table 5-1: Load and power consumption data of each machine based on the fan load profile.

Flow (%)	Speed (RPM)	Torque (N.m)	IM	SynRM	PMaSyRM		
					C8-R2	C8-R1	NdFeB
10	180	0.3	60	9	9	9	10
20	360	1.2	65	59	54	55	47
30	540	2.7	208	183	173	180	168
40	720	4.8	461	428	384	417	418
50	900	7.5	863	817	796	800	820
60	1080	10.8	1464	1385	1358	1370	1323
65	1117	12.7	1858	1776	1737	1724	1766
70*	1260	14.7	2450	2137	2122	2112	2090
80*	1440	19.2	3205	3193	3167	3150	3113
90*	1620	24.3	4610	4556	4515	4488	4428
100*	1800	30	6546	6269	6206	6164	6073

*Calculated based on simulation

Fig. 5-6 shows the annual energy consumed by each machine for the fan and constant speed loads. It can be seen that the induction machine has the most energy consumption rate and the PMa-SynRM-NdFeB has the least. The comparison with the induction machine is shown in Fig. 5-7. The PMa-SynRM presents significant energy savings up to 11% for fan load and for the constant speed it reaches up to 10%. Considering 10 cents per kWh average energy price for 10 years, the savings compared to the induction machine running for 10 years is shown in Fig. 5-8. The calculations are based on the power consumed by the machines and the energy loss in the inverter is not considered. Because the current level of the PMa-SynRM machines are less than the induction machine, the power loss in drive will be less for the PMa-SynRMs and the energy savings will be increased even more. Even the SynRM, which is not optimized for the stator, shows significant energy savings. Comparing the PMa-SynRM-C8-R1 with C8-R2 the energy savings increment is noticeable while the added magnet is only 160 gr. With an optimized design based on ferrite magnets this machine can be a suitable option for replacing with induction machine. Table IV includes the material consumption of each machine. Since the stator and the winding are the same, the only difference is the magnet and aluminum in the rotor. The NdFeB magnet mass used in the original design is about 470 gr. The comparison of energy savings of the PMa-SynRM-NdFeB with other options justifies the use of rare earth magnet in these applications.

The operating temperature of the reference induction machine is 40°C and the recorded temperature of the winding at the end windings are 55°C at rated current. Since the induction machine has service factor higher than one, the current density in the stator

conductors are not significantly high (about 4 A/mm^2 in this machine); therefore, rare earth magnet with low operating temperature (80°C-regular or 100°C-grade M) can be considered.

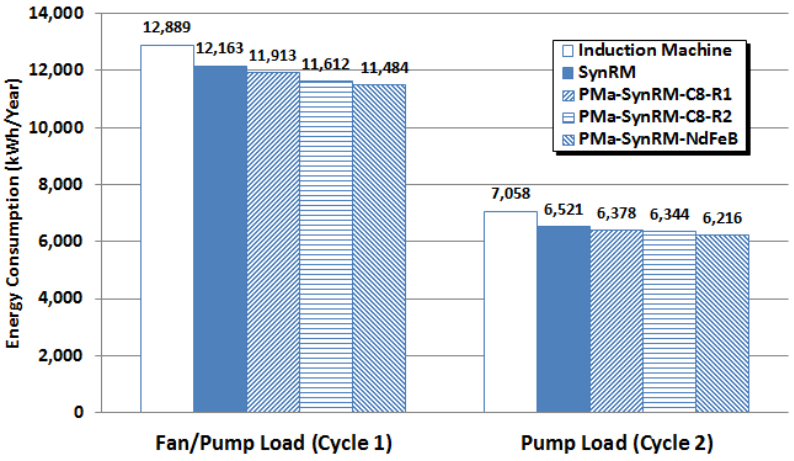

Fig 5-6: Annual electric energy consumption of the machines operating under the typical cycles.

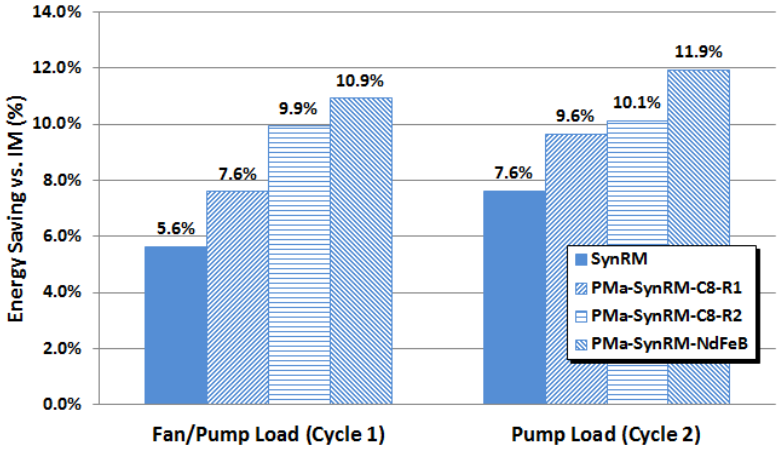

Fig 5-7: Electric energy saving of each machine operating under the typical cycles compared to the induction machine.

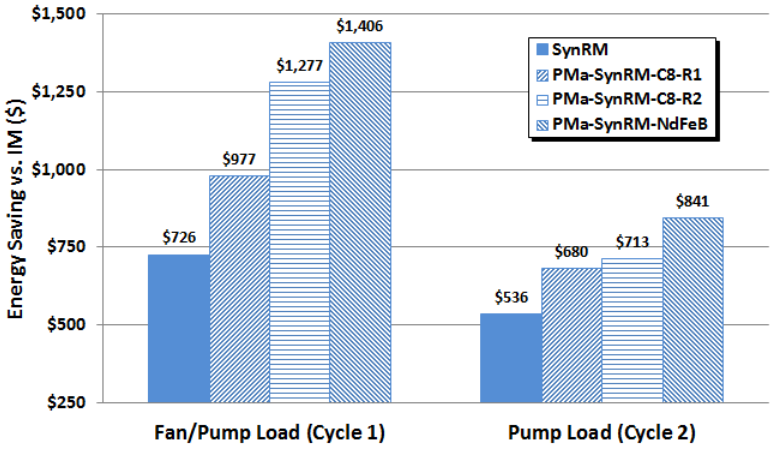

Fig 5-8: Capital saving of each machine operating under the typical cycles for ten years compared to the induction machine (10 cents/kWh).

VD. Performance Comparison for Constant Load Condition

Another load profile applied to the machines is constant load profile. This profile is an example for elevator or escalator load, which runs at constant speed but the load torque is variable. Fig. 5-9(a) shows the measured power factor of the studied machines under this condition. The results show that the SynRM has the lowest and the PMa-SynRM-NdFeB has the highest power factor. Adding ferrite magnets to the SynRM increases the power factor of the machine slightly, but adding extra magnets (C8-R2 rotor case) increases the power factor of SynRM from 0.6 to 0.7 under the full load condition. Rare earth magnet (NdFeB) increases the power factor of the machine to 0.88 (about 47% improvement of power factor in the SynRM).

Fig. 5-9(b) shows the measured efficiency of the machines. Among the studied synchronous machines, the SynRM has the lowest efficiency because of the higher current needed in the stator to generate the required torque, which is all reluctance

torque. The PMa-SynRM-NdFeB has the highest efficiency because of developing more magnet torque in comparison with the others. In the induction machine case, although the voltage-frequency ratio of the VFD drive is adjusted to minimize the losses; the induction machine has the lowest efficiency because of the rotor copper and iron losses. Due to the extra loss in induction machine, the power consumption of the induction machine is higher, which can be seen in Fig. 5-10(a). The excitation current of each machine is compared in Fig. 5-10(b). It is obvious that the induction machine needs more exciting current to drive the load in compare with the PMa-SynRMs, which is because of the lower torque density of the induction machine. Fig. 5-11 compares the apparent power entering to each machine for constant speed condition. Since the power factor and torque density of the PMa-SynRM-NdFeB is the highest, the apparent power of this machine is the least. The apparent power of PMa-SynRM-C8R2 is very close to the induction machine even though its torque density is higher than the induction machine. Although its torque density is higher than the induction machine but its lower power factor cancels the benefit of the higher torque density factor.

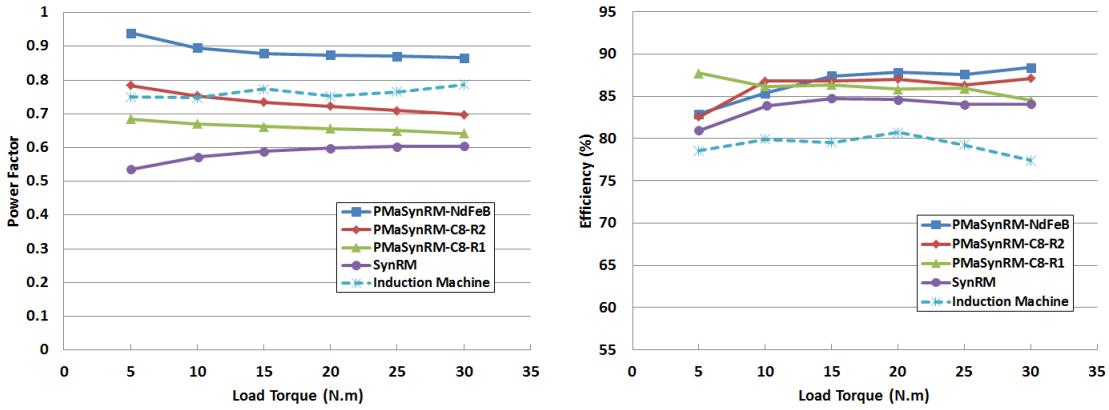

(a) (b)

Fig 5-9: Performance comparison of the machines under a constant speed load: (a) Power factor and, (b) Efficiency.

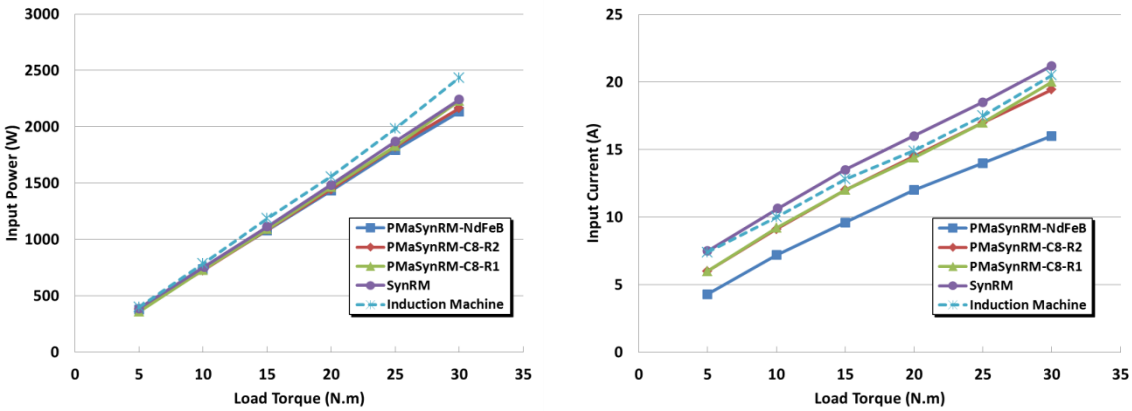

(a) (b)

Fig 5-10: Performance comparison of the machine under a constant speed load condition: (a) Input power, (b) Input current.

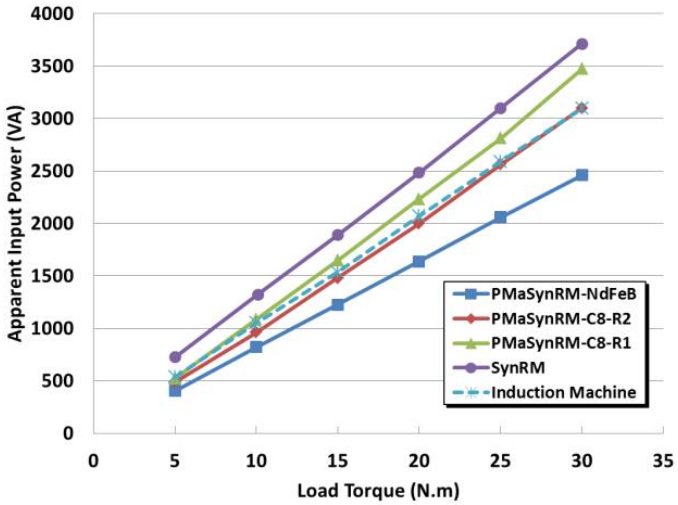

Fig 5-11: Apparent power entering to the machines under a constant speed load.

VE. Energy Consumption Comparison under the Fan and Constant Speed Loads

The performance of the machines is compared in the previous sections and the PMa-SynRM-NdFeB shows the highest power factor and the least power loss in constant speed-variable torque load condition. Induction machine shows highest power loss among the compared machines under this type of load. In this section the energy consumption of the machines are calculated and compared to the same results obtained from fan load profile, assuming the load profile according to the cycle 1 shown in Fig. 5-5. Fig. 5-12 shows the annual energy consumption of the machine and again the induction machine has the highest energy consumption and the PMa-SynRM-NdFeB has the least. The energy savings are compared to the induction machine in Fig. 5-13 and the capital savings are shown in Fig. 5-14. As it was expected in the constant load condition the PMa-SynRM-NdFeB shows more energy saving compared to other machines but it is noticeable that the energy saving of the PMa-SynRM-C8R2 is very close to PMa-

SynRM-NdFeB. This means that with optimization of the PMa-SynRM for Ceramic base magnets it is possible to achieve a very high efficient PMa-SynRM for fan and pump and constant speed-variable torque applications but it needs larger size in the inverter drive circuit.

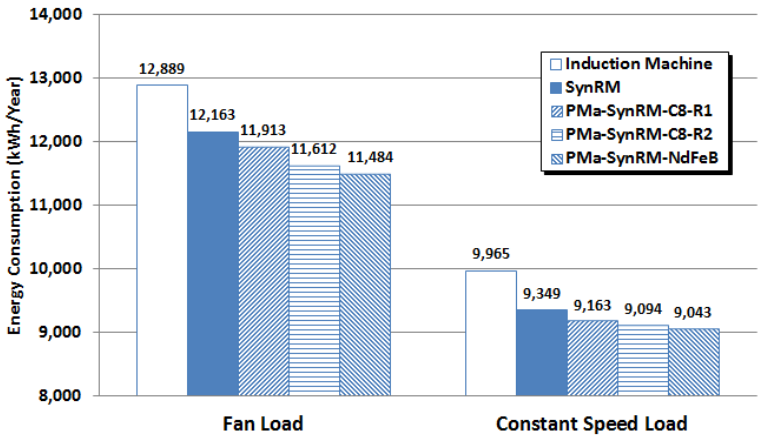

Fig 5-12: Annual electric energy consumption of the machines operating under the typical cycle.

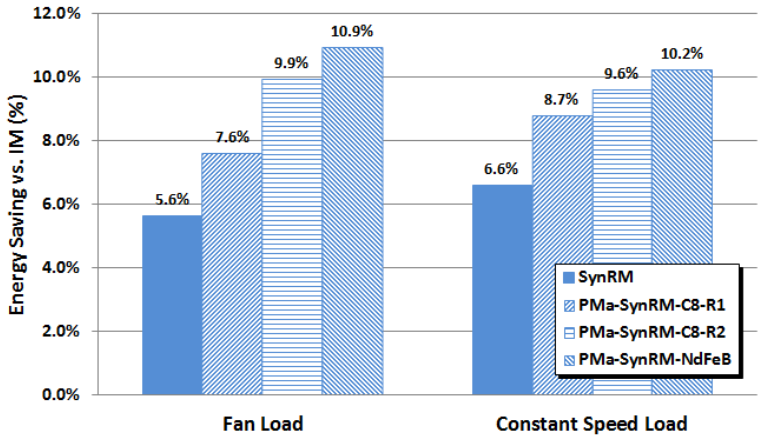

Fig 5-13: Electric energy saving of each machine operating under the typical cycle compared to the induction machine.

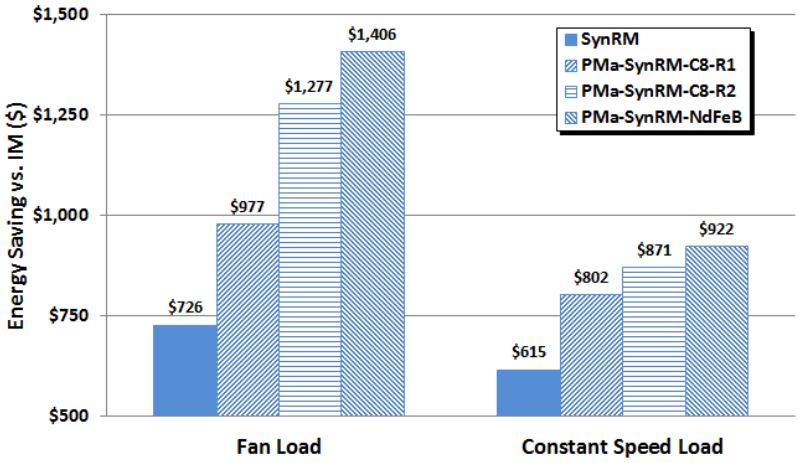

Fig 5-14: Capital saving of each machine operating under the typical cycle for ten years compared to the induction machine (10 cents/kWh).

VF. Conclusion

The performances of the PMa-SynRMs are studied by operating two common type loads and comparing them with the reference induction machine. The induction machine has the least efficiency among the studied machines and in each type of load the efficiency of the induction machine remains lower than the other machines; this is attributed to the rotor copper loss of the induction machine resulting in more power consumption than SynRM and PMa-SynRMs.

Ferrite magnets increase the power factor and efficiency of the SynRM, which was expected, but adding more ferrite (50% more) shows a noticeable improvement compared to the PMa-SynRM with less ferrite. The energy saving capability of PMa-SynRM with ferrite is noticeable and it suggests that a ferrite based optimized PMa-SynRM can have a significant energy cost reduction during the life time of the machine

and it is a suitable candidate to drive fan and constant speed-variable torque loads instead of induction machine with VFD drive without significant extra cost.

In the studied cases, PMa-SynRM-NdFeB has the highest power factor, which will result in smallest drive for the machine. Energy saving calculation shows that the PMa-SynRM with NdFeB magnets is a proper option for driving variable speed loads and fan type loads and using rare earth magnet will still be justified considering the energy saving capability. Moreover, because of less copper loss in the PMa-SynRM especially with NdFeB permanent magnet the operating temperature of the machine is lower than the induction machine therefore a longer life is expected for this machine compared to the induction machine.

For constant speed load, the comparison of the machines shows that the PMa-SynRM with NdFeB magnet has the least energy consumption and neglecting the drive size of the machine, it is possible to reach to the same energy saving with Ceramic magnets.

CHAPTER VI

EFFECT OF THE MAGNET QUANTITY ON ENERGY CONSUMPTION OF LOW POWER PMA-SYNRM*

VIA. Introduction

Low power induction machines are common type electric machines widely in service to drive fans and pumps and these types of loads are a significant portion of the loads in industry[1]. In majority of applications, variable speed is required to control the flow. The same as before, Variable Frequency Drives (VFDs) can be used in order to adjust speed to meet the speed requirement in some applications or reduce energy consumption in others. As it is shown in previous chapter, induction machines show low efficiency at lower speed and lighter load especially running fan and pump loads but it is possible to reduce the energy consumption using PMa-SynRM, which is less expensive machine compared to other type of PM machines. In previous chapter the performance of a PMa-SynRM machine with NEMA frame stator was compared with the reference induction machine and it showed that PMa-SynRM machine has less energy consumption compared to the induction machine driven by VFD drive under the fan and pump loads. This chapter presents the performance analysis of a fractional horsepower prototype PMa-SynRM for the same application with different quantity of Ceramic magnets and

---

results are compared with the general purpose induction machine under the same load condition. The original PMa-SynRM rotor core is designed based on Ferrite permanent magnets in [29]. The permanent magnets inside the rotor are block shape therefore it is possible to remove the magnets easily. This changes the machine to a SynRM machine and the effect of the permanent magnets on the SynRM can be observed. Also additional magnets can be added to increase the Back-EMF of the machine. The performance of this machine holding more magnets has been studied under the same load condition and compared with other revision of the PMa-SynRM. Finally, the results are compared with the performance of a general purpose 0.5 Hp induction machine under the same load condition and the energy consumption of the machines are compared.

VIB. Flux Linkage Variation in Studied PMa-SynRM

The geometry of the studied PMa-SynRM has made it possible to remove the block shape magnets from the rotor core (SynRM configuration) or add more magnets to the rotor and increase the flux linkage more than the original design. Fig. 6-1 shows the geometry of the original PMa-SynRM and the information of the machine is included in Appendix.

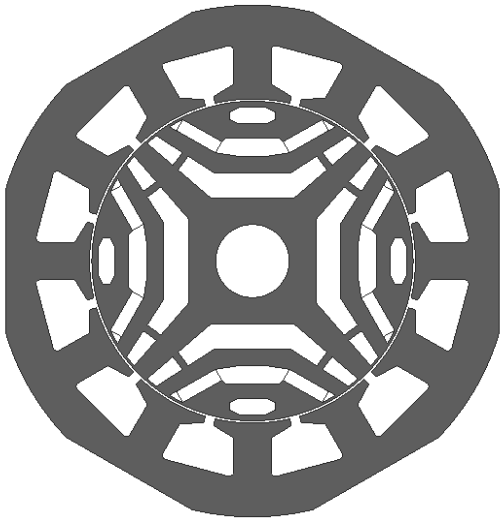

Fig 6-1: Geometry of the prototype PMa-SynRM [29].

Three designs studied in this chapter are: (i) SynRM – with no magnets, (ii) PMa-SynRM-A with two block magnets per pole as shown in Fig. 6-2(a), which is the original design based on [29] and (iii) PMa-SynRM-B with three block magnets per pole as shown in Fig. 6-2(b). These three designs share the same rotor structure but different quantities of hard ferrite (ceramic) magnets with remanent flux Br= 0.38 T (known as grade C5). Table 6-1 includes the magnetic property of the rotors. The PMa-SynRM core designed for Ferrite PMa-SynRM-A is shown in Fig. 6-4(a). By adding more magnets, the second type of PMa-SynRM is prepared, which is shown in Fig. 6-4(b). This version of the rotor will create more flux linkage; therefore, higher torque and power factor performances are expected.

Table 6-1: Magnetic property of the SynRM and PMa-SynRMs.

Machine type	Magnet Type	Magnet Br (T)	Magnet BHmax (MGOe)	Magnet Mass (lb)
SynRM	-	-	-	0
PMa-SynRM-A	Ferrite-C5	0.38	3.4	0.18
PMa-SynRM-B	Ferrite-C5	0.38	3.4	0.27

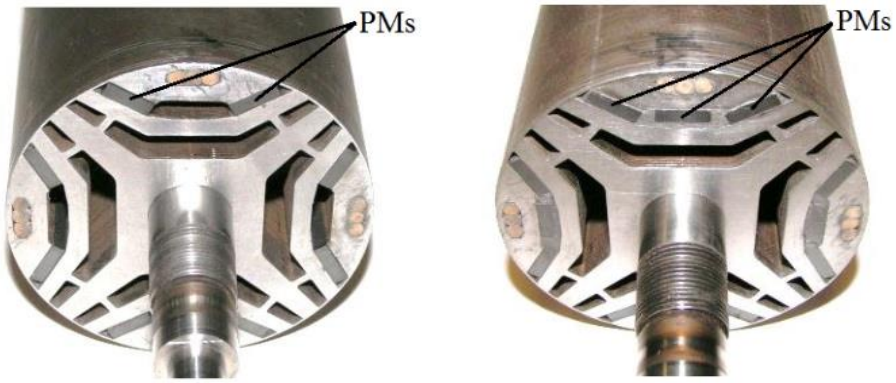

(a) (b)

Fig 6-2: PMa-SynRM different rotor versions: (a) PMa-SynRM-A (original design), (b) PMa-SynRM-B (more magnets).

In each case, the back-EMF of the PMa-SynRMs has been measured and the flux linkage is calculated using (4-7). Fig. 6-3 shows the waveform of the measured back-EMF for the PMa-SynRM-B. In the flux linkage measurement, the fundamental wave of the back-EMF is used. Table 6-2 includes the flux linkage obtained for each machine. As expected, the rotor core with more magnets generates higher back-EMF; therefore, it produces higher flux linkage, which can further improve the power factor. In this case, the quantity of additional magnet is 50% and the increased flux linkage is about 33% (based on back-EMF waveform) as compared to PMa-SynRM-A.

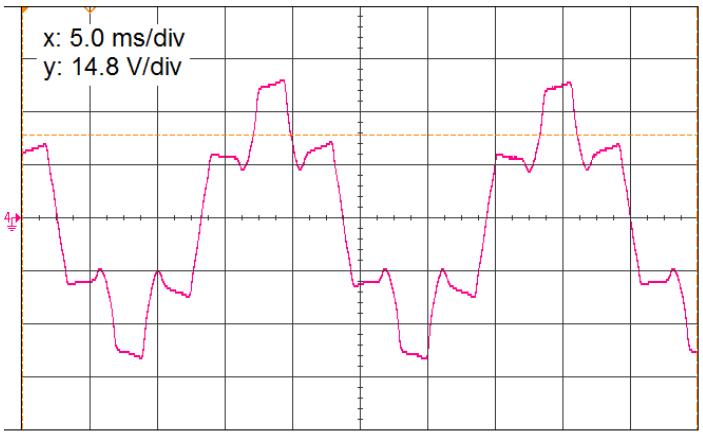

Fig 6-3: Line-to-line back-EMF of the PMa-SynRM-B at 1440 RPM.

Table 6-2: Flux source in the SynRM and PMa-SynRMs.

Machine type	Line Back-EMF (V)	Speed (RPM)	λPM (wb)
SynRM	0	0	0
PMa-SynRM-A	17.3	1440	0.0468
PMa-SynRM-B	23.0	1440	0.0623

VIC. Load Profile

To evaluate the performance of the PMa-SynRM under the fan load, a load profile is selected according to Fig. 6-4. The rated torque is selected to match with the rated torque of a general purpose 0.5hp 4-pole induction machine (included in the Appendix). Fig. 6-5 shows the test bed with the PMa-SynRM machine. The voltage applied to the Hysteresis brake controls the load torque and the speed is controlled by DSP with closed loop control implemented for the SynRM and PMa-SynRMs. The control is based on the MTPA used with vector control applied to the machine. In each case study the controller minimizes the current by controlling the current angle using the angle calculated by (3).

The induction machine, selected for comparison with the studied synchronous machines, is shown in Fig. 6-6. The same load profile is applied to the induction machine using the hysteresis brake.

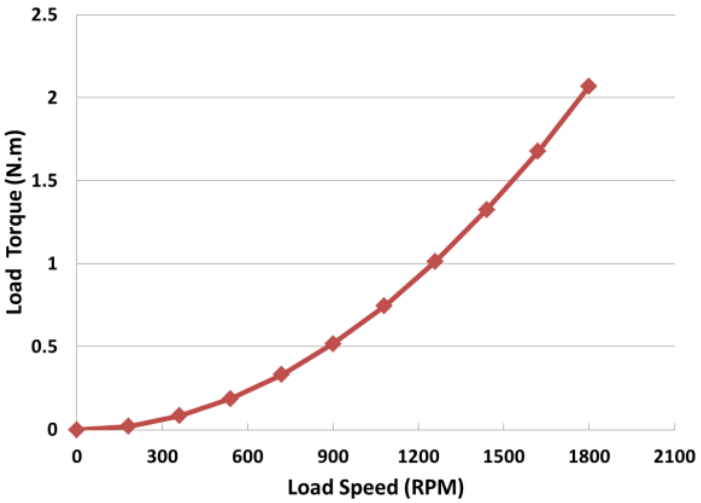

Fig 6-4: Load profile applied to the machine.

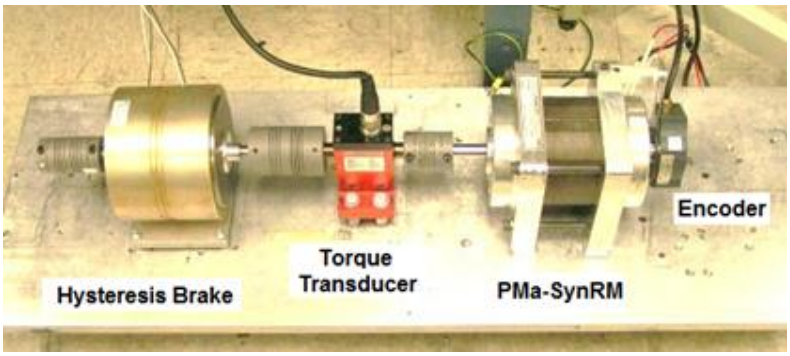

Fig 6-5: Experiment test bed with PMa-SynRM.

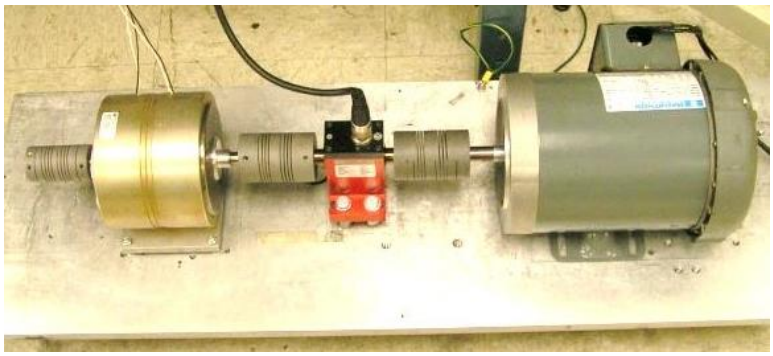

Fig 6-6: Experiment test bed with Marathon induction machine.

A variable speed drive is used to adjust the speed of the induction machine. In each operating point, the applied voltage and frequency of the machine has been adjusted in order to minimize the machine power consumption.

VID. Experimental Results

The power factor and input power of the machines are measured using power analyzer and the output power of the machine is calculated using the shaft speed and the torque measured from the torque transducer. For all machines, the power factor, efficiency, active power, and apparent power provided for the machines are measured.

Fig. 6-7 shows the power factor of each machine operating the fan load. Low power factor was expected for the SynRM in comparison with the other machines since the magnetizing current is higher. PMa-SynRM-A has higher power factor in comparison with the SynRM because of existence of the flux linkage, which reduces the magnetizing current and improves the power factor. This effect is more significant when extra magnets are added to the rotor (PMa-SynRM-B case). In this case, the power factor improves further by about 9%. The power factor of the upgraded PMa-SynRM is

increased by over 30% in comparison with the SynRM. Further improvement of the power factor can be achieved by using available higher energy density grades of ferrite magnets.

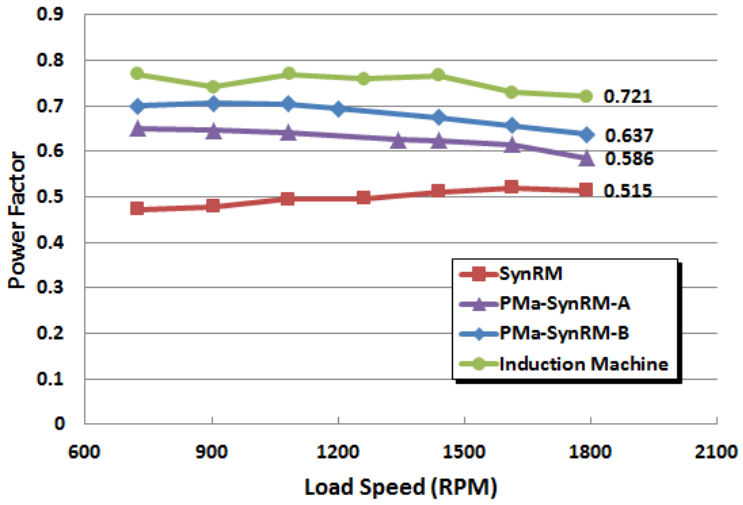

Fig 6-7: Power factor comparison of the machines in different load condition.

Induction machine operates with high power factor because of the optimization done on the voltage level of the VFD drive manually during the test. This reduces the magnetizing current of the induction machine and increasing the power factor in each operating point. As a result, if the drive employs an effective algorithm then the induction machine can operate in better power factor in wide load-speed range.

The efficiencies of the machines are compared in Fig. 6-8. PMa-SynRM-B has the highest efficiency in all operating range and the SynRM has the least. PMa-SynRM-A has higher efficiency than the induction machine and the SynRM since the magnet torque results in lower current needed to drive the same load compared to SynRM.

Therefore, the copper loss in the stator is reduced. Adding the extra magnets to PMa-SynRM-A increases the efficiency of the machine by 2% (PMa-SynRM-B case). Compared to the SynRM, the efficiency of the upgraded PMa-SynRM is increased by 5.3% at full load. It is obvious that the PMa-SynRMs have higher efficiency over a wider range of operating conditions compared to the induction machine, which has copper loss in the rotor.

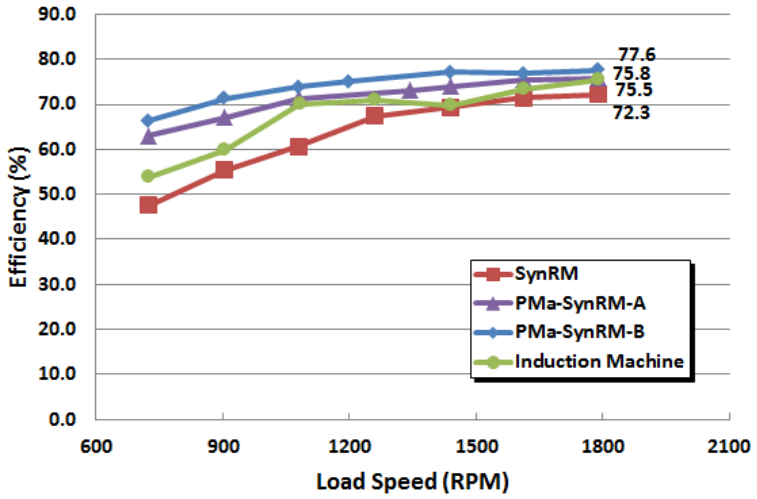

Fig 6-8: Efficiency comparison of the machines in different load condition.

The active power consumption of each machine is compared in Fig. 6-9. Because of the fan load characteristics, the power consumption is exponential. The SynRM machine has more power consumption because of lacking the magnet torque, which PMa-SynRMs utilize that. The induction machine has more power consumption than the PMa-SynRMs because of the rotor losses (including copper and iron losses) but it stays below the SynRM. More current is needed an equivalent torque in SynRM as compared to the

PMa-SynRM due to absence of magnet torque in SynRM. This generates higher copper loss in the SynRM stator windings and reduces the efficiency as it was shown in Fig. 6-8. To have a better comparison, the power consumption at full speed (full load) and half speed (25% load) are compared in Fig. 6-10. At the full fan speed the induction machine has less power consumption compared with the SynRM (about 4.5%); but the power consumption of the PMa-SynRM-B is less than the other machines. At the half fan speed, the power consumption of the PMa-SynRM-B is still the least in comparison with the other machines and has dropped to 13.8% of its full power. In this case, the induction machine has higher losses in comparison with the other PM machines and the input power of the induction machine has dropped to 16% of the full power condition.

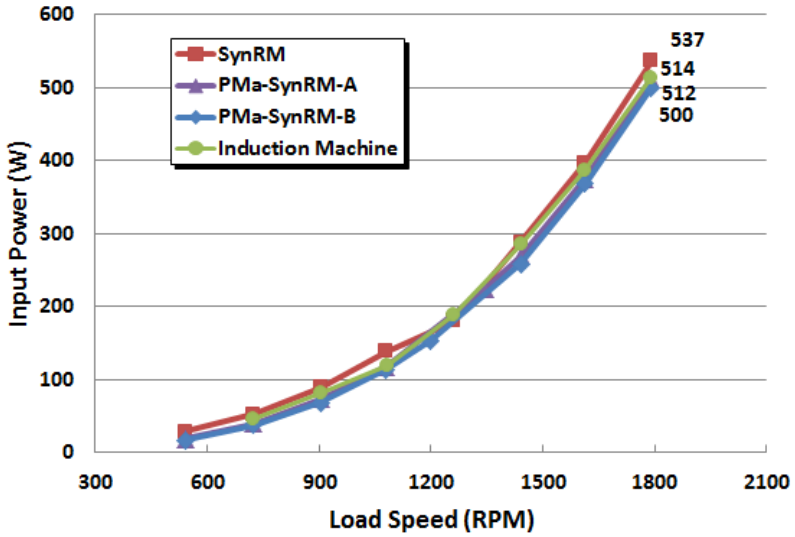

Fig 6-9: Input power comparison of the machines in different load condition.

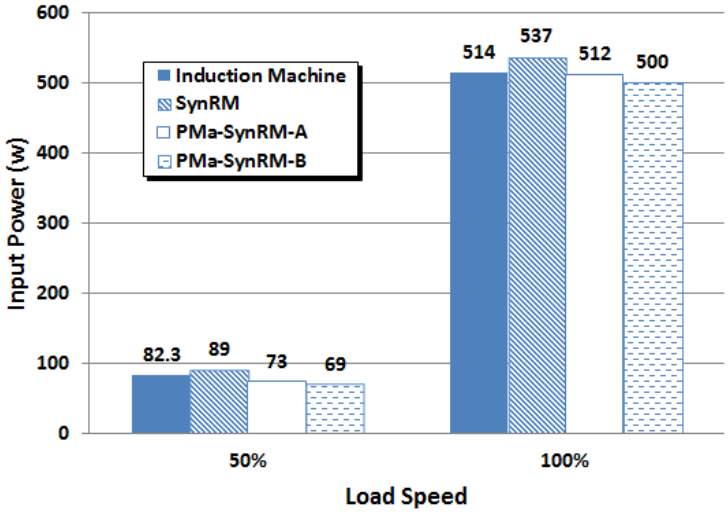

Fig 6-10: Power consumption of the machines at full and half load speeds.

Fig. 6-11 shows the excitation current and Fig. 6-12 shows the apparent power supplied by the inverter to the machines. Because of the low power factor of the SynRM, the higher Volt-Ampere was expected and by adding the permanent magnets to the rotor the power factor increases and the needed Volt–Ampere for the machine is decreased. Using the PMa-SynRM-A as the Volt-Ampere comparison base and comparing at full load condition, the SynRM needs 20% bigger whereas PMa-SynRM-B needs 10% smaller drive circuit while needing only 0.1 lbs. more ferrite. Finally, The PMa-SynRM-B shows a close Volta-Ampere performance to the induction machine, which can result in a same size drive circuit. It should be noticed that the induction machine performance was optimized by changing the VFD drive setting manually in each operating point, which cannot be done in practice unless the drive employs a very high performance drive algorithm. Also using a higher energy product ferrite magnet will improve the PMa-SynRMs performance to reach to the induction machine.

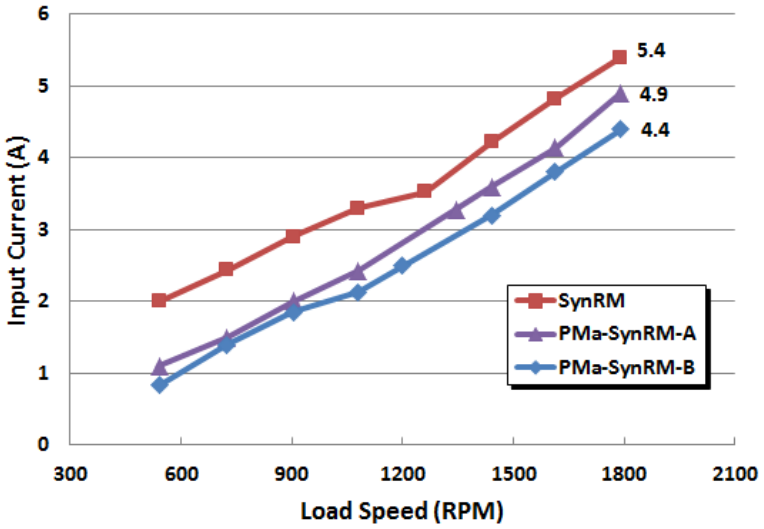

Fig 6-11: Input current comparison of the machines in different load condition.

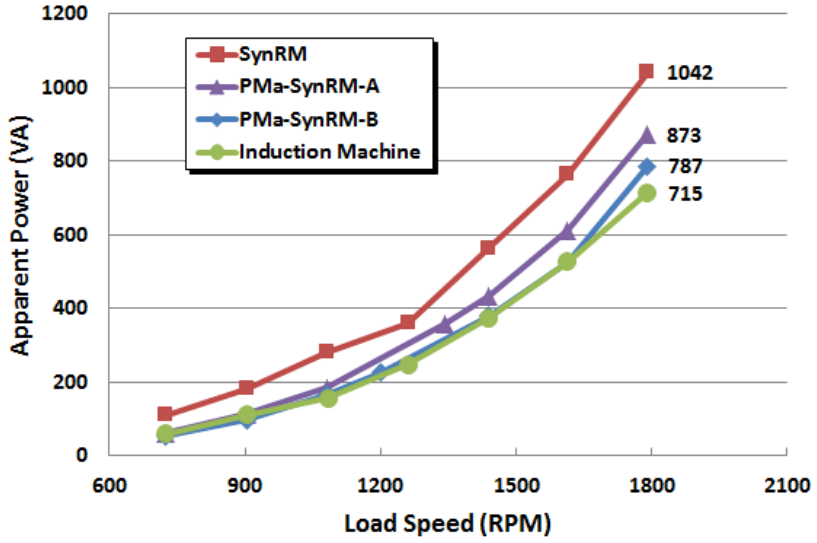

Fig 6-12: Apparent power provided by drive in different load condition.

VIE. Energy Consumption Comparison

Since the energy consumption of the machine is determined by the load cycle, some typical load cycles are chosen. The first operating cycle is a typical air conditioning cycle and the second cycle is a swimming pool pump, assumed that the pump operates at half speed for eight hours to circulate the water and two hours (circulating and cleaning), which was shown in Fig. 5-5.

Using these cycles and the power consumption data, obtained from the experiment, the energy input for each machine for each cycle is computed. Table 6-3 shows the daily energy taken from grid of each machine for each driving cycle. The results show that in each driving cycle the PMa-SynRM-B consumes less energy compared with all the other studied machines. In the other hand, the SynRM has higher losses due to the lack of magnet torque.

Table 6-3: Energy consumed by machines.

Energy Consumption (kWh/day)	Cycle 1	Cycle 2
Induction Machine	3.16	1.69
SynRM	3.25	1.79
PMa-SynRM-A	3.12	1.61
PMa-SynRM-B	2.77	1.55

Table 6-4 shows the comparison of the energy entered to the machines using the induction machine as the base. This comparison shows that using magnets has reduced the energy loss of the PMa-SynRM-A and it is very close to the induction machine. Adding more magnets has significant effect and it has reduced the energy loss up to 10% in compare with the induction machine.

The additional magnet will add the cost of the magnet used in the machine by 50% but according to the Fig. 6-12, the apparent power supplied to upgraded PMa-SynRM will drop from 873VA to 787VA, which is about 10%. This will result in a smaller drive, which can justify the cost of the extra Ferrite magnets (40 grams more Ferrite in this case). In addition, the energy saving will be another compensation for the extra magnet.

Table 6-4: Comparison of the energy consumption of the synchronous machines with the induction machine.

Energy Consumption Ratio	Cycle 1	Cycle 2
SynRM	+2.53%	+5.91%
PMa-SynRM-A	-1.27%	-4.73%
PMa-SynRM-B	-12.34%	-8.28%

VIF. Conclusion

In this chapter, the performance of a fractional horsepower ferrite-based PMa-SynRM is analyzed and compared with a general purpose induction machine for fan and pump applications. The results show that a significant power factor improvement for the SynRM is achievable by using low cost ferrite magnets. Also, using ferrite magnets will improve the torque performance of the machine, allowing it to drive the load with lower current and higher power factor, which will reduce the size of the drive circuit. The effects of adding extra magnets to the original PMa-SynRM are studied, which shows about 30% power factor improvement and the efficiency is added by 5% in comparison with the SynRM. More improvement can be achieved by selecting ferrite magnets with higher energy density grades.

Depending on the load cycle, the PMa-SynRM with more magnets shows a significant energy saving compared to the induction machine and SynRM. For some fan application, in which the load operates in half speed, the efficiency drop in the induction machine is large comparing with the PMa-SynRM with extra magnet. The upgraded PMa-SynRM shows at least 10% energy saving happens in comparison with the induction machine. The results show that in the cycles that the load has to work in lower speed, the PMa-SynRM has a better performance. Moreover, the PMa-SynRM with extra magnets shows a noticeable energy saving in comparison with the induction machine and the original PMa-SynRM. Considering the drive size reduction and the energy saving, the cost of extra magnet will be negligible.

CHAPTER VII

CONCLUSION AND EXTENSIONS

VIIA. Conclusion

A significant portion of the operation cost of an electric machine is the cost of the electric energy consumed by the machine; therefore, using energy efficient motors has become more important in recent years in order to save more energy and money.

Fan and pump loads are a large category of the loads in industry and according to the Affinity laws, reducing the load speed can reduce the energy consumption significantly. Usually these loads are driven by induction machines, which can be replaced by more efficient motors, or those can be equipped with VDF drives to lower the load speed and reduce the energy consumption.

On the other hand, using synchronous machines can offer less energy loss and better torque density compared to the induction machine. Permanent Magnet assisted Synchronous Reluctance Machine, which is investigated in this dissertation, is one of the synchronous machines that can be used for fan and pump application.

In Chapter II the performance of a general purpose NEMA frame induction machine and its stator and winding is investigated in order to evaluate to use in the PMa-SynRM machine design. It is shown that PMa-SynRM can benefit the maximized MMF in the air gap due to the distributed winding form in the stator (designed for the high performance induction machine) therefore a machine with high torque density can be designed using

induction machine stator and it will make the performance comparison easier by selecting the original induction machine as the reference.

Chapter III presents the PMa-SynRM computer aid design procedure using 2D FEA tool based on the fact that the stator of the machine is selected from the NEMA standard induction machine. During the design procedure, it is always considered that in order to have a PMa-SynRM with high performance, the SynRM rotor core itself should have high performance such as low ripple torque and high torque density. After achieving a high performance SynRM rotor core, adding a permanent magnet in proper locations in the geometry of the rotor is investigated and it is shown that placing the permanent magnets in the first air barrier of two barrier SynRM rotor has the best back-EMF performance such as lower harmonics and higher fundamental harmonics while the quantity of magnets are kept the same.

To improve the back-EMF, cogging torque, and ripple torque of the PMa-SynRM rotor skewing is investigated, and it shows that even step skewing of the rotor, which is a practical solution, will improve those factors.

In addition, due to the lower current in the stator and less rotor weight, a longer life and less maintenance cost is expected for NEMA PMa-SynRM machines.

Also, using other types and quantities of magnets such as ferrite ceramic magnet in the same optimized rotor is investigated and the results show that the PMa-SynRM rotor optimized with NdFeB magnets can generate more torque than the reference induction machine since the SynRM rotor torque was close to the induction machine with the same excitation current.

Chapter IV presents the development of the hardware and control software for evaluation of the design. Field oriented control is selected to control the machine in speed closed loop form using Maximum Torque per Ampere method (MTPA). Also the method used to measure the parameters of the machine used in the control development is presented. Experimental results are obtained and compared with the induction machine using all NdFeB and ferrite ceramic magnets and the results show that the PMa-SynRM machine generates a noticeable high torque compared to the induction machine, which promises a lower loss while driving a certain load such as fans and pumps.

In Chapter V the effect of the magnet quantity and type on the performance and energy consumption of the designed PMa-SynRM under the fan and pump load is investigated. The electric power consumption of the PMa-SynRM machines is compared with the reference induction machine under a simulated fan and pump type load. It is shown that the designed PMa-SynRM machine has less power loss, and considering a typical operating cycle of operation, the energy consumption of the PMa-SynRM machine is less than the induction machine significantly. Also, using ferrite ceramic magnets shows that the PMa-SynRM machine has higher efficiency and less energy consumption compared to the induction machine. Moreover, the results show that with optimization of the PMa-SynRM with more ferrite magnets will improve the energy consumption of the machine since it is optimized for NdFeB magnets and performance of the ferrite based PMa-SynRM can be improved more with optimization based on ferrite type magnets. Although the energy consumption with less expensive ferrite can be improved but the drive circuit will be larger since the power factor of the PMa-SynRM machine shows

better improvement with magnets with higher remanent flux density such as NdFeB magnets. Finally, NEMA frame PMa-SynRM with both ferrite and NdFeB magnets shows better performance than the induction machine for variable speed application such as fan load.

Chapter VI investigates the effect of the magnet quantity on the performance and energy consumption of low power PMa-SynRM. It is shown that the magnet quantity of the PMa-SynRM has a significant impact on the performance of the machine such as improving the power factor and reducing its energy consumption by increasing its torque density. The cost of the additional magnets can be negligible compared to the savings on the energy and the potential drive size reduction due to the improved power factor and torque density.

VIIB. Suggestions and Extensions

In this work, a four-pole induction machine is selected as the reference machine for the design comparison purposes. Another option is selecting two-pole machine, which can be studied for PMa-SynRM design and leads to a two-pole PMa-SynRM design running at synchronous speed or four-pole machine running two times faster, which can reduce the efficiency of the machine due to the higher iron loss in the stator and rotor cores. Continued design and studying these cases and comparing with the reference induction machine will increase the knowledge of using PMa-SynRM for fan and pump applications.

Another work extension is to develop sensorless control methods for NEMA frame based PMa-SynRM, which can eliminate the shaft encoder sensor and make it easier to replace the induction machine with PMa-SynRM type machine.

In this work, the results shows that a low cost magnet based PMa-SynRM has significant energy saving opportunity for fan and pump drive application. Optimization of this type of PMa-SynRM is another step to keep the cost of the machine low even though the quantity of magnets is significant.

The power loss of the drive circuit should be added to the energy saving investigation by studying the power loss of the machines and drive together. When permanent magnets with higher flux remanent are used in the PMa-SynRM, the torque density of the machine is higher; therefore, the power loss in the inverter will be less and it should be studied. In this case study, the reference induction machine should be driven by the same drive circuit to make it possible to compare the energy consumption side by side.

REFERENCES

[1] Xenergy Inc., "United States Industrial Electric Motor Systems Market Opportunities Assessment," Washington, DC, Dec. 2002,.Available at: https://www1.eere.energy.gov/manufacturing/tech_assistance/pdfs/mtrmkt.pdf

[2] S. Chun-Lien, C. Wei-Lin, and Y. Kuen-Tyng, "An energy-savings evaluation method for adjustable-frequency drives on sea water cooling pumps on ships," in *Industrial & Commercial Power Systems Technical Conf (I&CPS), 2013 IEEE/IAS 49th*, pp. 1-10, Stone Mountain, GA ,2013,.

[3] J. Maxwell, "How to Avoid Overestimating Variable Speed Drive Savings," 2005. Proceedings of the Twenty-Seventh *Industrial Energy Technology Conference*, New Orleans, LA, May 10-13, 2005 Available at: http://repository.tamu.edu/bitstream/handle/1969.1/5621/ESL-IE-05-05-05.pdf

[4] ABB Ltd. "Technical guide No4, Guide to Variable Speed Drives" REVC, 2011.,Available at : http://www05.abb.com/global/scot/scot201.nsf/veritydisplay/d3c711ec2acddb18c125788f002cf5da/$file/ABB_Technical_guide_No_4_REVC.pdf

[5] T. Ristimäki, "Energy efficiency through Variable Frequency Drives," Honeywell International Inc., 2008. Available at: http://inverter.ecc.emea.honeywell.com/Download/h-energy-VDF-en.pdf

[6] J. G. Cleland, V. E. McCormick, and M. W. Turner, "Design of an efficiency optimization controller for inverter-fed AC induction motors," in *Industry*

Applications Conference, 1995. Thirtieth IAS Annual Meeting, IAS '95., Conference Record of the 1995 IEEE, 1995, pp. 16-21 vol.1.

[7] H. Murakami, Y. Honda, H. Kiriyama, S. Morimoto, and Y. Takeda, "The performance comparison of SPMSM, IPMSM and SynRM in use as air-conditioning compressor," in *Industry Applications Conference, 1999. Thirty-Fourth IAS Annual Meeting. Conference Record of the 1999 IEEE*, 1999, pp. 840-845 vol.2.

[8] N. Bianchi and S. Bolognani, "Interior PM synchronous motor for high performance applications," in *Power Conversion Conference, 2002. PCC-Osaka 2002. Proceedings of the*, 2002, pp. 148-153 vol.1.

[9] Y. Honda, T. Nakamura, T. Higaki, and Y. Takeda, "Motor design considerations and test results of an interior permanent magnet synchronous motor for electric vehicles," in *Industry Applications Conference, 1997. Thirty-Second IAS Annual Meeting, IAS '97., Conference Record of the 1997 IEEE*, 1997, pp. 75-82 vol.1.

[10] Z. Jun, M. F. Rahman, and C. Grantham, "A New Scheme to Direct Torque Control of Interior Permanent Magnet Synchronous Machine Drives for Constant Inverter Switching Frequency and Low Torque Ripple," in *Power Electronics and Motion Control Conference, 2006. IPEMC 2006. CES/IEEE 5th International*, 2006, pp. 1-5.

[11] W. L. Soon, D. A. Staton, and T. J. E. Miller, "Design of a new axially-laminated interior permanent magnet motor," in *Industry Applications Society Annual Meeting, 1993., Conference Record of the 1993 IEEE*, 1993, pp. 27-36 vol.1.

[12] J. Wai and T. M. Jahns, "A new control technique for achieving wide constant power speed operation with an interior PM alternator machine," in *Industry Applications Conference, 2001. Thirty-Sixth IAS Annual Meeting. Conference Record of the 2001 IEEE*, 2001, pp. 807-814 vol.2.

[13] T. M. Jahns and V. Caliskan, "Uncontrolled generator operation of interior PM synchronous machines following high-speed inverter shutdown," *Industry Applications, IEEE Transactions on,* vol. 35, pp. 1347-1357, 1999.

[14] T. M. Jahns, G. B. Kliman, and T. W. Neumann, "Interior Permanent-Magnet Synchronous Motors for Adjustable-Speed Drives," *Industry Applications, IEEE Transactions on,* vol. IA-22, pp. 738-747, 1986.

[15] E. C. Lovelace, T. M. Jahns, and J. H. Lang, "A saturating lumped-parameter model for an interior PM synchronous machine," *Industry Applications, IEEE Transactions on,* vol. 38, pp. 645-650, 2002.

[16] S. Morimoto, M. Sanada, and Y. Takeda, "Wide-speed operation of interior permanent magnet synchronous motors with high-performance current regulator," *Industry Applications, IEEE Transactions on,* vol. 30, pp. 920-926, 1994.

[17] G. Pellegrino, A. Vagati, P. Guglielmi, and B. Boazzo, "Performance Comparison Between Surface-Mounted and Interior PM Motor Drives for Electric Vehicle Application," *Industrial Electronics, IEEE Transactions on,* vol. 59, pp. 803-811, 2012.

[18] M. A. Rahman, D. M. Vilathgamuwa, M. N. Uddin, and T. King-Jet, "Nonlinear control of interior permanent-magnet synchronous motor," *Industry Applications, IEEE Transactions on,* vol. 39, pp. 408-416, 2003.

[19] W. L. Soong and N. Ertugrul, "Field-weakening performance of interior permanent-magnet motors," *Industry Applications, IEEE Transactions on,* vol. 38, pp. 1251-1258, 2002.

[20] I. Boldea, Z. X. Fu, and S. A. Nasar, "Performance evaluation of axially-laminated anisotropic (ALA) rotor reluctance synchronous motors," *Industry Applications, IEEE Transactions on,* vol. 30, pp. 977-985, 1994.

[21] A. J. O. Cruickshank, A. F. Anderson, and R. W. Menzies, "Theory and performance of reluctance motors with axially laminated anisotropic rotors," *Electrical Engineers, Proceedings of the Institution of,* vol. 118, pp. 887-894, 1971.

[22] A. J. O. Cruickshank, R. W. Menzies, and A. F. Anderson, "Axially laminated anisotropic rotors for reluctance motors," *Electrical Engineers, Proceedings of the Institution of,* vol. 113, pp. 2058-2060, 1966.

[23] P. Guglielmi, B. Boazzo, E. Armando, G. Pellegrino, and A. Vagati, "Permanent-Magnet Minimization in PM-Assisted Synchronous Reluctance Motors for Wide Speed Range," *Industry Applications, IEEE Transactions on,* vol. 49, pp. 31-41, 2013.

[24] J. Yun-Ho, K. Kwangdeok, K. Yong-Jae, P. Byung-Sup, and J. Sang-Yong, "Design characteristics of PMa-SynRM and performance comparison with

IPMSM based on numerical analysis," in *Electrical Machines (ICEM), 2012 XXth International Conference on*, 2012, pp. 164-170.

[25] A. Vagati, B. Boazzo, P. Guglielmi, and G. Pellegrino, "Ferrite assisted synchronous reluctance machines: A general approach," in *Electrical Machines (ICEM), 2012 XXth International Conference on*, 2012, pp. 1315-1321.

[26] P. Guglielmi, B. Boazzo, E. Armando, G. Pellegrino, and A. Vagati, "Magnet minimization in IPM-PMASR motor design for wide speed range application," in *Energy Conversion Congress and Exposition (ECCE), 2011 IEEE*, 2011, pp. 4201-4207.

[27] B. Jeihoon, M. M. Rahimian, and H. A. Toliyat, "Optimal design and comparison of stator winding configurations in permanent magnet assisted synchronous reluctance generator," in *Electric Machines and Drives Conference, 2009. IEMDC '09. IEEE International*, 2009, pp. 732-737.

[28] S. Talebi, P. Niazi, and H. A. Toliyat, "Design of Permanent Magnet-Assisted Synchronous Reluctance Motors Made Easy," in *Industry Applications Conference, 2007. 42nd IAS Annual Meeting. Conference Record of the 2007 IEEE*, 2007, pp. 2242-2248.

[29] P. Niazi, H. A. Toliyat, C. Dal-Ho, and K. Jung-Chul, "A Low-Cost and Efficient Permanent-Magnet-Assisted Synchronous Reluctance Motor Drive," *Industry Applications, IEEE Transactions on,* vol. 43, pp. 542-550, 2007.

[30] S. Morimoto, M. Sanada, and Y. Takeda, "Performance of PM-assisted synchronous reluctance motor for high-efficiency and wide constant-power

operation," *Industry Applications, IEEE Transactions on,* vol. 37, pp. 1234-1240, 2001.

[31] S. Morimoto, M. Sanada, and Y. Takeda, "Performance of PM/reluctance hybrid motor with multiple flux-barrier," in *Power Conversion Conference - Nagaoka 1997., Proceedings of the*, 1997, pp. 649-654 vol.2.

[32] A. Vagati, "The synchronous reluctance solution: a new alternative in AC drives," in *Industrial Electronics, Control and Instrumentation, 1994. IECON '94., 20th International Conference on*, 1994, pp. 1-13 vol.1.

[33] V. B. Honsinger, "The Inductances Ld and Lq of Reluctance Machines," *Power Apparatus and Systems, IEEE Transactions on,* vol. PAS-90, pp. 298-304, 1971.

[34] P. J. Lawrenson and L. A. Agu, "A new unexcited synchronous machine," *Electrical Engineers, Proceedings of the Institution of,* vol. 110, p. 1275, 1963.

[35] P. J. Lawrenson and L. A. Agu, "Theory and performance of polyphase reluctance machines," *Electrical Engineers, Proceedings of the Institution of,* vol. 111, pp. 1435-1445, 1964.

[36] P. J. Lawrenson and L. A. Agu, "Low-inertia reluctance machines," *Electrical Engineers, Proceedings of the Institution of,* vol. 111, pp. 2017-2025, 1964.

[37] P. J. Lawrenson, "Two-speed operation of salient-pole reluctance machines," *Electrical Engineers, Proceedings of the Institution of,* vol. 112, pp. 2311-2316, 1965.

[38] P. J. Lawrenson, S. K. Gupta, and S. R. Murthy Vamaraju, "Multispeed performance of segmental-rotor reluctance machines," *Electrical Engineers, Proceedings of the Institution of,* vol. 115, pp. 695-702, 1968.

[39] B. J. Chalmers and A. S. Mulki, "New reluctance motors with unlaminated rotors," *Electrical Engineers, Proceedings of the Institution of,* vol. 117, pp. 2271-2272, 1970.

[40] W. Fong and J. S. C. Htsui, "New type of reluctance motor," *Electrical Engineers, Proceedings of the Institution of,* vol. 117, pp. 545-551, 1970.

[41] V. B. Honsinger, "Steady-State Performance of Reluctance Machines," *Power Apparatus and Systems, IEEE Transactions on,* vol. PAS-90, pp. 305-317, 1971.

[42] P. J. Lawrenson and S. R. Bowes, "Stability of reluctance machines," *Electrical Engineers, Proceedings of the Institution of,* vol. 118, pp. 356-369, 1971.

[43] B. J. Chalmers and A. S. Mulki, "Design and Performance of Reluctance Motors with Unlaminated Rotors," *Power Apparatus and Systems, IEEE Transactions on,* vol. PAS-91, pp. 1562-1569, 1972.

[44] V. B. Honsinger, "Inherently Stable Reluctance Motors Having Improved Performance," *Power Apparatus and Systems, IEEE Transactions on,* vol. PAS-91, pp. 1544-1554, 1972.

[45] R. M. Mathur, H. W. Lee, and R. W. Menzies, "Theory and Operation of Reluctance Motors with Magnetically Anisotropic Rotors II - Synchronous Performance," *Power Apparatus and Systems, IEEE Transactions on,* vol. PAS-91, pp. 42-45, 1972.

[46] R. W. Menzies, "Theory and Operation of Reluctance Motors with Magnetically Anisotropic Rotors Part I Analysis," *Power Apparatus and Systems, IEEE Transactions on,* vol. PAS-91, pp. 35-41, 1972.

[47] S. Chandrasekhara Rao, "Dynamic performance of reluctance motors with magnetically anisotropic rotors," *Power Apparatus and Systems, IEEE Transactions on,* vol. 95, pp. 1369-1376, 1976.

[48] E. A. Klingshirn, "DC Standstill Torque Used to Measire Lq of Reluctance and Synchronous Machines," *Power Apparatus and Systems, IEEE Transactions on,* vol. PAS-97, pp. 1862-1869, 1978.

[49] M. Ramamoorty and P. J. Rao, "Optimization of Polyphase Segmented-Rotor Reluctance Motor Design: A Nonlinear Programming Approach," *Power Apparatus and Systems, IEEE Transactions on,* vol. PAS-98, pp. 527-535, 1979.

[50] D. A. Staton, T. J. E. Miller, and S. E. Wood, "Maximising the saliency ratio of the synchronous reluctance motor," *Electric Power Applications, IEE Proceedings B,* vol. 140, pp. 249-259, 1993.

[51] P. Niazi, "PERMANENT MAGNET ASSISTED SYNCHRONOUS RELUCTANCE MOTOR DESIGN AND PERFORMANCE IMPROVEMENT," Texas A&M University, 2005.

[52] K. Won-Ho, K. Kwang-Soo, K. Seung-Joo, K. Dong-Woo, G. Sung-Chul, C. Yon-Do*, et al.*, "Optimal PM Design of PMA-SynRM for Wide Constant-Power Operation and Torque Ripple Reduction," *Magnetics, IEEE Transactions on,* vol. 45, pp. 4660-4663, 2009.

[53] E. Armando, P. Guglielmi, G. Pellegrino, M. Pastorelli, and A. Vagati, "Accurate Modeling and Performance Analysis of IPM-PMASR Motors," *Industry Applications, IEEE Transactions on,* vol. 45, pp. 123-130, 2009.

[54] M. Barcaro, N. Bianchi, and F. Magnussen, "Permanent-Magnet Optimization in Permanent-Magnet-Assisted Synchronous Reluctance Motor for a Wide Constant-Power Speed Range," *Industrial Electronics, IEEE Transactions on,* vol. 59, pp. 2495-2502, 2012.

[55] T. A. Lipo, *Introduction to AC Machine Design*: Wisconsin Power Electronics Research Center, University of Wisconsin, 2004.

[56] N. Mohan, *Electric Drives: An Integrative Approach*: MNPERE, 2003.

[57] B. K. Bose, *Modern Power Electronics and Ac Drives*: Prentice Hall, 2002.

[58] T. Matsuo and T. A. Lipo, "Rotor design optimization of synchronous reluctance machine," *Energy Conversion, IEEE Transactions on,* vol. 9, pp. 359-365, 1994.

[59] T. J. E. Miller, *Brushless permanent-magnet and reluctance motor drives*: Clarendon Press, 1989.

[60] T. J. E. Miller, A. Hutton, C. Cossar, and D. A. Staton, "Design of a synchronous reluctance motor drive," *Industry Applications, IEEE Transactions on,* vol. 27, pp. 741-749, 1991.

[61] "Ansys Maxwell," 17.0 ed: Ansys.

[62] R. Lohninger, H. Grabner, G. Weidenholzer, S. Silber, and W. Amrhein, "Modelling, Simulation and Design of a Permanent Magnet Assisted

Synchronous Reluctance Machine," *Industry Applications, IEEE Transactions on,* vol. PP, pp. 1-1, 2014.

[63] A. K. Chakali, H. A. Toliyat, and H. Abu-Rub, "Observer-based sensorless speed control of PM-assisted SynRM for direct drive applications," in *Industrial Electronics (ISIE), 2010 IEEE International Symposium on*, 2010, pp. 3095-3100.

[64] D. W. Novotny and T. A. Lipo, *Vector Control and Dynamics of AC Drives*: Clarendon Press, 1996.

[65] A. Quntao and S. Li, "On-line parameter identification for vector controlled PMSM drives using adaptive algorithm," in *Vehicle Power and Propulsion Conference, 2008. VPPC '08. IEEE*, 2008, pp. 1-6.

[66] P. Niazi, H. A. Toliyat, and A. Goodarzi, "Robust Maximum Torque per Ampere (MTPA) Control of PM-Assisted SynRM for Traction Applications," *Vehicular Technology, IEEE Transactions on,* vol. 56, pp. 1538-1545, 2007.

[67] T. Matsuo and T. A. Lipo, "Current sensorless field oriented control of synchronous reluctance motor," in *Industry Applications Society Annual Meeting, 1993., Conference Record of the 1993 IEEE*, 1993, pp. 672-678 vol.1.

[68] N. Bianchi and S. Bolognani, "Influence of Rotor Geometry of an IPM Motor on Sensorless Control Feasibility," *Industry Applications, IEEE Transactions on,* vol. 43, pp. 87-96, 2007.

[69] M. G. Jovanovic and R. E. Betz, "Maximum torque control of a sensorless synchronous reluctance motor drive," in *Industry Applications Conference, 1997.*

Thirty-Second IAS Annual Meeting, IAS '97., Conference Record of the 1997 IEEE, 1997, pp. 637-644 vol.1.

[70] K. Matsumoto, H. Gao, Y. Yu, and S. Cheng, "Sensorless control of SynRM based on PWM inverter carrier frequency component," in *Vehicle Power and Propulsion Conference, 2008. VPPC '08. IEEE*, 2008, pp. 1-4.

[71] M. G. Jovanovic, R. E. Betz, and D. Platt, "Sensorless vector controller for a synchronous reluctance motor," *Industry Applications, IEEE Transactions on,* vol. 34, pp. 346-354, 1998.

[72] K. Hyunbae, J. Hartwig, and R. D. Lorenz, "Using on-line parameter estimation to improve efficiency of IPM machine drives," in *Power Electronics Specialists Conference, 2002. pesc 02. 2002 IEEE 33rd Annual*, 2002, pp. 815-820 vol.2.

[73] N. Bianchi and S. Bolognani, "Sensorless-Oriented Design of PM Motors," *Industry Applications, IEEE Transactions on,* vol. 45, pp. 1249-1257, 2009.

[74] Q. Zhaowei, S. Tingna, W. Yindong, Y. Yan, X. Changliang, and H. Xiangning, "New Sliding-Mode Observer for Position Sensorless Control of Permanent-Magnet Synchronous Motor," *Industrial Electronics, IEEE Transactions on,* vol. 60, pp. 710-719, 2013.

[75] P. Guglielmi, M. Pastorelli, G. Pellegrino, and A. Vagati, "Position-sensorless control of permanent-magnet-assisted synchronous reluctance motor," *Industry Applications, IEEE Transactions on,* vol. 40, pp. 615-622, 2004.

[76] J. Chung, M. Dolen, K. Hyunbae, and R. D. Lorenz, "A continuous-time observer to estimate electrical parameters of induction machines," in *Industry*

Applications Conference, 2001. Thirty-Sixth IAS Annual Meeting. Conference Record of the 2001 IEEE, 2001, pp. 259-265 vol.1.

[77] R. D. Lorenz, "A simplified approach to continuous on-line tuning of field-oriented induction machine drives," *Industry Applications, IEEE Transactions on,* vol. 26, pp. 420-424, 1990.

APPENDIX A

INDUCTION MOTOR DATA

The name plate information, general information, stator and rotor dimension, winding configuration, and material used in the reference induction machine are presented in this section.

Table A-1: Induction machine name plate.

Machine Parameters	Measurement
Frame	C213T
Power	7.5 (HP)
Current	21(A)
Voltage	230(V)
Speed	1730(RPM)
Temperature	40 (°C)
Service factor	1.15

Table A-2: Induction machine parameters.

Machine Parameters	Measurement
Number of poles	4
Rated Power	7.5 (HP)
Rated Speed	1730(RPM)
Rated Torque	30 (N.m)
Rated Current	21(A)
Rated Efficiency	89.1(%)
Rated PF	0.81
Minimum Air Gap	0.016(inch)
Rotor Inner Diameter	1.551(inch)
Rotor Outer Diameter	4.968(in)
Stator Inner Diameter	5.00 (in)
Rotor Inner Diameter	1.551(in)
Stator Outer Diameter	9 (in)
Number of Stator Slots	36
Stator Winding Coil Pitch	8
Number of Winding Layers Per Slot	2
Number of Winding Turns per Slot	60

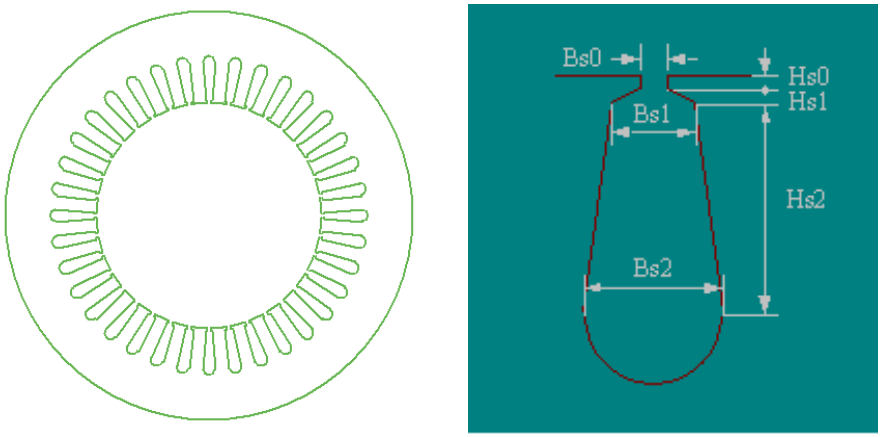

(a) (b)

Fig A-1: Induction machine stator cross section: (a) Stator geometry, (b) Stator slot dimension.

Table A-3: Stator slot and tooth dimensions.

Stator Slot and Tooth Dimensions			
Hs0 (inch)	0.031	Top Tooth Width (inch)	0.270973
Hs1 (inch)	0.0184	Bottom Tooth Width (inch)	0.307395
Hs2 (inch)	0.8376		
Bs0 (inch)	0.095		
Bs1 (inch)	0.174		
Bs2 (inch)	0.284		

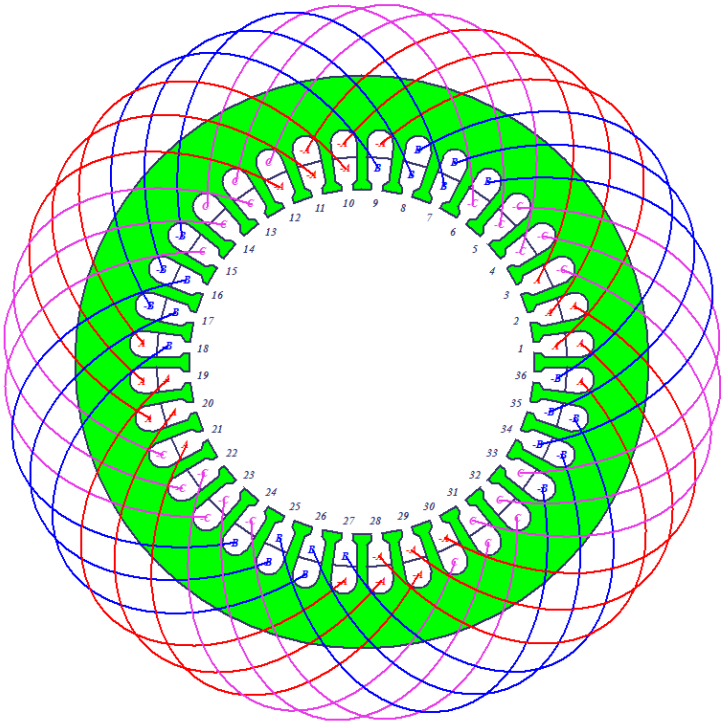

Fig A-2: Winding layout.

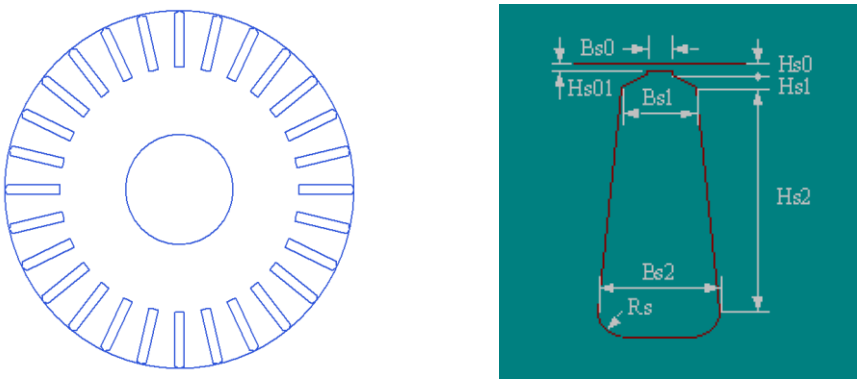

(a) (b)

Fig A-3: Induction machine rotor cross section: (a) Rotor geometry, (b) Rotor slot depiction.

Table A-4: Rotor slot and bar dimensions.

Rotor Slot and Bar Dimensions	
Hs0 (inch)	0.012
Hs01 (inch)	0.012
Hs1 (inch)	0.025
Hs2 (inch)	0.75
Bs0 (inch)	0.032
Bs1 (inch)	0.135
Bs2 (inch)	0.135
Rs (inch)	0
Bar End Length (inch)	0.75
End Ring Height (inch)	1
End Ring Width (inch)	0.438
Air Gap (inch)	0.016

Table A-5: Induction machine material data.

Materials Used		
Stator Core	Steel	M-45
	Gage	26
	Stacking Factor	0.95
Rotor Core	Steel	M-45
	Gage	26
	Stacking Factor	0.95
Stator Winding	Copper	Gage 19
	Wire Diameter (inch)	0.03589
	Parallel Branches	2
	Conductors Per Slot	60
	Coil Sides Per Slot	2
	Strands Per Conductor	2
Rotor Bar	Aluminum	Cast
	Number of Bars	28

APPENDIX B

INDUCTION AND PMA-SYNRM MATERIAL CONSUMPTION

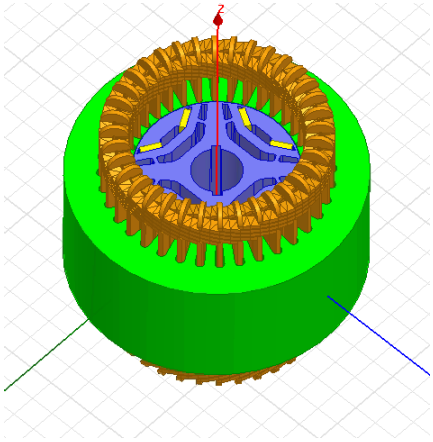

Fig B-1: 3D Model of the PMa-SynRM.

Table B-1: Machine component cross section and weight.

item	IM	PM-SynRM NdFeB	PM-SynRM C8-R1	PM-SynRM C8-R2
Stator cross section(mm^2)	23061	23061	23061	23061
Rotor cross section(mm^2)	9420	9420	9420	9420
Stator weight(kg)	24.3	24.3	24.3	24.3
Rotor core weight(kg)	8.24	6.28	6.11	6.27
Shaft weight~(kg)	4.2	4.2	4.2	4.2
Rotor total weight(kg)	12.4	10.5	10.3	10.5

Table B-2: Material density.

Material	Density (kg/m^3)	Density (lb/in^3)
Aluminum	2689	0.097
Steel (MG45)	7700	0.278
NdFeB	7550	0.273
Ferrite	4900	0.177

APPENDIX C

FRACTIONAL HORSEPOWER INDUCTION AND PMA-SYNRM DATA

Table C-1: Induction machine parameters.

Machine Parameters	**Measurement**
Number of poles	4
Brand	Marathon
Model	56T17F5321J
Catalog No.	G581
Rated Power	0.5 (HP)
Rated Speed	1725(RPM)
Rated Torque	2.1(N.m)
Rated Current	2.07(A)
Rated Efficiency	72(%)
Rated PF	0.53

Table C-2: PMa-SynRM characteristic with full pitch stator.

Machine Parameters	**Measurement**
Number of poles	4
Stator slot number	12
Stator OD	112(mm)
Rotor OD	70(mm)
Air Gap	0.5(mm)
Stack length	70(mm)
Rated Torque	2.1(N.m)
Rated Current	5(A)
R_s	0.95(ohm)
L_d @ 5A	38(mH)
L_q @ 5A	16(mH)